

AD-A269 578



Annual Progress Report

June 1, 1992 to May 31, 1993

Visible Light Emitting Materials and Injection Devices

ONR/ARPA URI

Grant Number N00014-92-J-1895

DTIC ELECTE
SEP 13 1993
S E D

Prepared by:

Paul H. Holloway
Department of Materials Science and Engineering
University of Florida
Gainesville, FL 32611
Ph: 904/392-6664; FAX: 904/392-4911
E-Mail: Internet-PHOLL@MAILGATE.ENGNET.UFLEDU

Participants:
University of Florida
Kevin Jones
Robert Park
Joe Simmons
Dept. of Materials Science and Engineering
Tin Anderson
Dept. of Chemical Engineering
Peter Zory
Dept. of Electrical Engineering
University of Colorado
Jacques Pankove
Dept. of Electrical Engineering
Columbia University
Gertrude Neumark
Dept. of Materials Science and Engineering
Oregon Graduate Institute of Science and Engineering
Reinhart Engelmann
Dept. of Electrical Engineering

Accession For	
NTIS CRA&I	<input checked="" type="checkbox"/>
DTIC TAB	<input type="checkbox"/>
Unannounced	<input type="checkbox"/>
Justification	
By	
Distribution /	
Availability Codes	
Dist	Avail and/or Special
A-1	

Statement A per telecon Dr. Alvin Goodman
ONR/Code 1114
Arlington, VA 22217-5000

NW 9/8/93

Approved for public release
Distribution is unlimited

93 8 10 207

93-18463



TABLE OF CONTENT

(I)	Molecular Epitaxial Growth	3
	Widegap II-VI/GaAs Activities	3
	MBE Growth of GaN	4
(II)	MOCVD Growth of II-VI Materials	4
(III)	Ohmic Contact Formation	7
(IV)	Characterization of Column III Nitrides	9
	AlN, GaN, InN on InP	9
	AlN on Sapphire	9
	GaN on GaAs	10
	GaN on GaP	10
(V)	Optical Studies	11
(VI)	Transport Studies in n-Type ZnSe	11
	Free Carrier Concentration	11
	Mobility	13
	Hopping Conduction	13
(VII)	Development of Blue Diode Lasers	14
	Photopumped Lasing	14
	Wafer Process Development	14
	Diode Laser Modelling	15
(VIII)	Theoretical Calculations for Dopants in ZnSe	16
(IX)	Gain Modelling in II-VI Strained Layer QW Structures	18
(X)	MOCVD Growth of Column III Nitrides	25
	Second Year Plans	25
	Post Doctoral Associates, Graduate and Undergraduate Research Assistants	29
	Industrial Collaborators	30
	Publications	31
	Presentations	32
	Tables and Figures	35

(I) Molecular Beam Epitaxial Growth (Robert Park)

Widegap II-VI/GaAs Activities

- (1) GaAs substrate cleaning for II-VI epitaxy using a remotely generated atomic hydrogen beam.

In situ GaAs surface cleaning prior to molecular beam epitaxy using a combined thermal/H-atom treatment, the H-atom flux being derived from an Oxford Applied Research RF (13.56MHz) plasma discharge, hydrogen free-radical source, has been compared and contrasted to conventional thermal treatment of GaAs surfaces. Surface quality, *i.e.* morphology, was monitored *in situ* in real-time using conventional reflection high energy electron diffraction and a diffuse optical reflectivity technique (see Fig. I.1) employed simultaneously.

GaAs surfaces were found to clean readily at temperatures below 400°C using the combined thermal/H-atom treatment as opposed to the conventional thermal treatment which requires temperatures in the vicinity of 600°C. The atomically-clean GaAs surfaces were also found to be specular when prepared using the combined thermal/H-atom treatment in contrast to conventional thermally-treated GaAs surfaces which are considerably rough on the atomic scale, surface roughening in the conventional case being associated with the oxide desorption process (see Fig. I.2).

- (2) Real-time in-situ monitoring of defect evolution at widegap II-VI/GaAs heterointerfaces during epitaxial growth.

We have developed a real-time *in situ* monitoring technique employing an optical probe during molecular beam epitaxial (MBE) growth which is capable of monitoring the evolution of dislocations at widegap II-VI/GaAs heterointerfaces. Specifically, we have measured using the apparatus illustrated in Fig. I.3 the intensity of elastically scattered HeNe laser light incident on a slightly lattice-mismatched ZnSe/GaAs heterointerface as a function of deposition time. In addition to providing critical thickness data, the real-time monitoring scheme also revealed that the degree of light scattering, resulting from dislocation multiplication and propagation, mirrors the strain relaxation process in the ZnSe/GaAs system as a function of increasing film thickness, saturating in intensity at a ZnSe film thickness around 0.5 μ m (see Fig. I.4). We postulate, based on theoretical analysis, that the microelectric fields present around dislocations are responsible for the index perturbations necessary to account for the observed laser light scattering.

- (3) Real-time in-situ monitoring of CL intensities during MBE growth of p-type ZnSe:N

We have developed an experimental apparatus (see Fig. I.5) for the detection and quantification of the cathodoluminescence emission which is observed during the MBE

growth of doped (either n- or p-type) ZnSe epilayers as a consequence of the impinging electron beam normally employed for RHEED analysis. In the case, specifically, of p-type doping of ZnSe using the Oxford Applied Research rf plasma discharge nitrogen free-radical source, we have discovered that the CL intensity recorded during growth at the growth temperature is a strong function of the remote plasma intensity. The CL intensity as shown in Fig. I.6 appears to go through a peak as the plasma intensity is increased monotonically. We have also observed the CL intensity to be a function of substrate temperature having corrected for the temperature dependence of the CL emission intensity. The dependence of CL intensity on other parameters such as film growth rate and II-VI ratio is currently being examined. We are also in the process of correlating CL intensity recorded at the growth temperature with the electrical properties of the p-type ZnSe:N material.

MBE growth of GaN

We have successfully grown zincblende-GaN epitaxial films on β -SiC coated (001) Si substrates using a molecular beam epitaxy approach in which the reactive nitrogen species are generated in a remote 13.56 MHz rf plasma discharge, nitrogen free-radical source. We postulate, based on optical emission spectroscopy studies of the remote plasma, that nitrogen atoms having purely thermal energy are the species responsible for efficient nitridation in our case. The zincblende nature of the GaN films was confirmed by *in situ* reflection high-energy electron diffraction, *ex situ* X-ray diffraction and *ex situ* low-temperature photoluminescence analyses. Fig. I.7 shows a wide scan x-ray rocking curve spectrum recorded from a 1.4 μm thick GaN film grown on a 3.5 μm thick β -SiC epilayer on (001) Si. The spectrum is indicative of a purely cubic system. A rocking curve spectrum of the (004) reflection is shown in Fig. I.8, illustrating an x-ray linewidth of 48 arc. mins. Fig. I.9 shows a 7.5K PL spectrum recorded from the same 1.4 μm thick zincblende-GaN layer. As can be seen from the figure, the PL spectrum is dominated by a rather broad peak having a peak energy of 3.23 eV at 7.5K.

Our zincblende-GaN film growth rates ($\sim 0.3 \mu\text{m/hr}$) are higher than those reported to date involving the use of electron cyclotron resonance type reactive nitrogen sources. Table I.1 compares our zincblende-GaN properties to those reported in the literature as produced using various modified MBE approaches. As the table indicates, we are presently growing state-of-the-art zincblende-GaN films.

(II) MOCVD Growth of II-VI Materials (Tim Anderson) }

Recent advances in II-IV semiconductor laser diodes have been demonstrated with ZnSe/CdZnSe separate confinement structures that lase in the blue-green. To reach true blue, or even UV wavelengths, and to achieve improved optical and carrier confinements, wider bandgap materials are needed. In particular, work in the US and

Japan has been directed towards the quaternary $MgZn_{1-x}S_ySe_{1-y}$. Another candidate system is the pseudoternary $Mg_xZn_yCd_{1-x-y}S$ system that can be lattice matched to either GaAs or GaP. From a growth perspective, this material should be easier since it contains only 3 compounds (MgS, CdS, and ZnS) as compared to 4 compounds in the quaternary (MgS, MgSe, ZnS, ZnSe). Furthermore, composition variation occurs only on the Group II sublattice and these species are the mass transfer limited ones. Therefore, the composition should vary in a linear fashion with reactant input; a condition that permits good composition control (e.g., compare the growth of $Al_xGa_{1-x}As$ with $GaAs_xP_{1-x}$). Importantly, the growth of this pseudoternary material avoids the use of highly toxic Se precursors (e.g., H_2Se). For these reasons, a research program has been initiated towards achieving laser structures based on this pseudoternary material.

Unfortunately, no reports of previous work could be located for the growth of $Mg_xZn_yCd_{1-x-y}S$ films. It was thus decided to first approach the growth of the Zn-Cd-S pseudobinary material, focusing on the composition lattice matched to GaAs. A study was performed to establish the influence of growth conditions on the composition and growth rate of ZnCdS and the crystal structure.

The substrates used in the growth of ZnCdS were semi-insulating (100) $\pm 0.5^\circ$ or (100) 2° GaAs. GaAs was chosen as the substrate due to its wide availability and high quality. With a lattice constant of 5.654\AA , GaAs makes a suitable substrate to which ZnCdS can be lattice matched. The reactants were diethylzinc (DEZn), dimethylcadmium (DMCd), and hydrogen sulfide (H_2S). The two common choices for the Zn precursor are DEZn and dimethylzinc (DMZn). Since the ethyl ligand is reported to minimize carbon contamination compared to the methyl ligand, DEZn was selected for the Zn source. The metalorganics are highly reactive with the hydride gas even at room temperature. To prevent parasitic gas-phase reactions, the group II metalorganics and H_2S were introduced into the reactor through two separate ports.

Five parameters were investigated in the growth of ZnCdS: (1) growth temperature, (2) reactor pressure, (3) VI/II molar ratio, (4) substrate baking procedure, and (5) ratio of gas velocities in the carrier gas to MO lines.

To grow a high quality film with good morphology, the epilayer should be of uniform thickness. The main parameter that affects the uniformity of the epilayer thickness was found to be the ratio of gas velocities in the carrier gas to MO lines. In varying this ratio from 0.2 - 10.6, epilayers of uniform thickness were observed with values of this ratio in the range of 7.3 and 8.7. The uniformity was maintained in this range regardless of the growth temperature which was varied over the range 250 to 450°C . Apparently, natural convection does not greatly affect the thickness uniformity.

The growth process is usually better controlled if it is mass transfer limited rather than kinetically limited. Measurement of the growth rate as a function of temperature showed that the growth rate was constant in the temperature range 300 to 450°C (Figure II.1). This indicates that the growth rate is independent of temperature in this range and therefore the growth process is mass transfer limited. In the mass transfer limited region, the growth rates for the (100) $\pm 0.5^\circ$ and the (100) 2° GaAs substrates were $5.5 \mu\text{m/hr}$ and $6.8 \mu\text{m/hr}$, respectively. The conditions for these runs were: reactor pressure = 70 Torr, VI/II = 117, [DMCd] = 42.8 mmol/min., and [DEZn] =

28.6 mmol/min.

At a 400°C, with mass transfer limit growth conditions, the growth rate was measured as a function of the molar flow rate of DMCd + DEZn. Since the VI/II ratio was always much greater than one, the group II organometallics were the limiting reactants at these growth conditions. As expected, a linear relationship between growth rate and group II molar flow rate was observed.

To better understand and better control the growth process, the solid composition of $Zn_{1-x}Cd_xS$ was measured as a function of growth temperature. The incorporation of Cd into solid ZnCdS varied with growth temperature. The results showed that the films were Cd-rich at lower growth temperature in the range 250 to 450°C. As the temperature approaches 450°C, the solid composition nearly matched the inlet mole fraction. For a gaseous Cd composition of 0.6 ($[DMCd]/\{[DMCd] + [DEZn]\} = 0.6$), the solid composition of Cd (x of $Zn_{1-x}Cd_xS$) at 250 and 450°C was 0.715 and 0.645, respectively (Figure II.2). The data showed an exponential decay between these two bounds. In the lower temperature range, ZnCdS was Cd-rich possibly because the DEZn had not fully decomposed. In addition, the sticking coefficient could be higher at lower temperatures for Cd thereby producing a Cd-rich epilayer. More studies need to be performed to determine the reasons for this observed behavior.

The lattice constant of ZnCdS was determined as a function of solid composition (EMPA) for the first time (Figure II.3). The data indicates that Vegard's Law is followed assuming that the binary materials of ZnS and CdS have the cubic structures. The FWHM of X-ray diffraction peaks is one of the measures of the quality of the epilayer. A plot of the FWHM versus solid composition showed a local minima where ZnCdS is lattice-matched to GaAs at the solid composition of $x = 0.55$. The FWHM at the lattice matching conditions is approximately 700 arc-seconds. Photoluminescence data indicate that the maximum peak is near 2.85 eV at 18 K. Although the luminescence position is slightly smaller than the expected bandgap energy, its near bandgap energy does suggest that ZnCdS is a viable candidate for blue-light emitting optoelectronic devices. A plot of the bandgap energy (PL) as a function of composition (X-ray) is shown in Figure II.4.

Of the five growth parameters examined, the baking procedure was the most important to the quality of the surface morphology. Of the baking parameters examined, temperature was the most important for producing consistently smooth epilayers. At 550°C about half the films were smooth. At 600 to 750°C, the films always showed good morphology. The baking times were varied from 10 to 20 minutes. The optimal baking condition was at a temperature of 620°C and pressure of 50 Torr for a time of 15 minutes.

The growth pressure was found not to be an important factor in determining the film properties. The crystallinity also was independent of the VI/II ratio as long as the ratio was much greater than one.

The cross sectional TEM and TEM diffraction patterns of the lattice matched sample (Figure II.5) indicated a single phase zinc blende crystal structure (first time ever observed for the MOCVD grown ZnCdS) with a large density of stacking faults visible along (111) facets of the crystal. For a sample that is Cd rich ($x=0.81$), the patterns

provided inconclusive evidence to suggest a particular crystal structure. At best, the patterns seem to suggest a tetragonal structure or a two phase system composed of both sphalerite and wurtzite. However, the crystal structure is definitely not zinc-blende. From X-ray diffraction, the lattice parameter is stretched out from that of the zinc-blende structure and is perpendicular to the (100) face of the GaAs substrate. This deviation of the lattice parameter may be due to the strain caused by incorporating more Cd, a larger atom as compared to Zn, into the crystal lattice, or because with Cd-rich samples, the wurtzite structure is thermodynamically stable and the c-axis is evidently aligned along the (100) direction with respect to the GaAs substrate. Interestingly, this indicates a critical composition where a transition occurs from the zinc blende at $x=0.55$ to a non-cubic structure at $x=0.81$. More studies need to be done to determine this structural transition composition.

For good quality, single-phase zinc-blende epilayers, the layer thickness was found to be uniform as indicated by the SIMS depth profile at different locations of the layer. As shown in Figure II.6, the PL spectra gives maximum peaks at 2.78 eV for room temperature and 2.83 eV (strong blue to violet luminescence for 10K measurements. The FWHM is 57 meV and 95 meV for 10K and room temperature measurements, respectively. There is also minimal deep level peaks indicating low contamination. Work is in progress to improve the quality of the zinc blende ZnCdS epilayers both structurally and optically by performing growths at lower growth rates.

In summary, we have identified growth conditions for the production of high quality epitaxial layers of ZnCdS on GaAs. Importantly, we have shown that single crystal cubic material can be grown that is clean with respect to deep levels. The next benchmark that must be achieved is the reduction in the density of stacking faults.

(III) Ohmic Contact Formation (Paul Holloway and Kevin Jones)

Our work in ohmic contact work has focused on obtaining an ex-situ process for the formation of ohmic contacts to nitrogen doped p-type ZnSe with carrier concentrations $\approx 3 \times 10^{17}$. Initial efforts included studies of as deposited and heat treated metal/alloy contacts formed by evaporation and sputter deposition. The evaporated materials which were studied included Au, In, Sn, and In-Sn, while the sputter deposited materials include Au, Ag, Cu, and Ag-Cu. In addition to the characterization of metal/alloy contacts, the use of elemental semiconductors, including chalcogenide Se and Te, was also studied. This work led to the investigation of the mercury chalcogenide, HgSe, as a contact material, which has resulted in electrical contacts with pseudo-ohmic behavior.

In the as deposited condition, all of the metal/alloy contacts studied were found to be rectifying with low currents (nanoamps) and breakdown voltages in excess of 5V. The effect of sintering on the electrical characteristics of the metal contacts was studied for temperatures between 100 and 400°C. The sputter deposited Au contacts showed the greatest reduction in breakdown voltages for all of the sintered metal contacts. After 90 minutes at a temperature of 350°C, the breakdown voltage of the Au contacts decreased to $\approx 3.5V$. Auger depth profiles were performed on the metal contacts but failed to

indicate any diffusion or compound formation. SIMS data suggest that Au diffuses into the ZnSe at these temperatures. Based on this work, we concluded that metal and alloy depositions were unlikely to produce low resistance ohmic contacts to p-type ZnSe.

As a result, efforts were redirected to study semiconductor contacts of Se and Te. The materials were deposited by evaporation and characterized in the as deposited condition as well as following heat treatments at temperatures ranging from 100 to 400°C. The as deposited films were again found to be rectifying, but the breakdown voltage for Te was reduced to $\approx 2.5V$ by heat treating for 30 min. at 200°C. The current transport through the sintered contacts, however, did not increase linearly with respect to applied voltage, therefore the contacts were still rectifying.

Based on this work and results reported by Schetzina, et al [Appl. Phys. Lett. 61 (1992) 2554], we began developing a process to form HgSe contacts on p-type ZnSe by reacting a Se layer with Hg vapor. The process was designed to be a simple *ex situ* method of producing HgSe contacts at atmospheric pressure, in contrast to using MBE growth as demonstrated by Schetzina. At the current stage of refinement, the process begins with in situ capping of the ZnSe surface with Se, prior to its removal from the MBE growth chamber. The capping layer acts as a protective barrier preventing contamination and oxidation of the ZnSe upon removal from the MBE system. Next, the sample is heated in the presence of Hg vapor, resulting in the formation of HgSe.

The electrical characteristics of HgSe contacts using the previously described method have resulted in a significant reduction of breakdown voltage, as compared to the metal/alloy contacts, yielding pseudo-ohmic behavior. However, the current transport through the contacts is low (0.01mA at 2V). TEM and x-ray diffraction data indicate that crystalline HgSe has formed and appears to be orienting, even epitaxed, to the underlying ZnSe during formation. Auger depth profiles indicate that an excess of Se may be present at the HgSe/ZnSe interface suggesting that the kinetics of HgSe formation are limited by a diffusion process. Subsequent reductions in the Se capping layer thickness, from 10,000 Å to 3000 Å, has resulted in less excess interfacial Se as observed by Auger depth profiles. Thinner Se layers resulted in improved electrical performance. Following this trend, further reductions in the Se capping layer thickness, leading to complete reaction of the Se, should yield good electrical performance.

The optimal results to date for HgSe contacts formed by this process were obtained from a 3000 Å Se capping layer deposited by MBE immediately following growth of the p-type ZnSe. The sample was then heated *ex situ* to 150°C for 45 min. in Hg vapor. The Hg vapor was generated by heating liquid Hg to 100°C in a separate chamber. Atmospheric pressure N₂ gas flowed through the chamber containing liquid Hg to a second chamber which contained the heated sample. The N₂ gas transported the Hg vapor through an entrainment process to the sample surface, resulting in the formation of HgSe.

The current vs voltage for the HgSe/p-ZnSe interface is plotted in Figure III.1. For comparison, the results obtained for sputter deposited Au annealed at 350°C for 90 min. are also shown. The data shows that the breakdown voltage of the HgSe contacts has been reduced to $\approx 0.2V$. Due to the high resistance of the HgSe contacts, however, the current transport through the Au contacts will exceed that of the HgSe for voltages

$> \approx 4V$. As discussed above, it is believed that further reduction of the Se capping layer will improve the electrical properties of the HgSe contacts, reducing their resistance and increasing their current transport. The second area of research has focused on contacts to ZnSe, specifically assisting in the TEM characterization of HgSe contacts. A HgSe contact to p-type ZnSe has been processed by heating Se capped p-type ZnSe samples in the presence of Hg vapor at atmospheric pressure. The effect of varying the thickness of the Se capping on the final HgSe/ZnSe microstructure was studied using cross-section TEM.

(IV) Characterization of Column III Nitrides (K.S. Jones, UF, and C. Abernathy, S.J. Pearton and A. Katz, AT&T Bell Laboratories)

We have been working with AT&T Bell Laboratories (Drs. C.Abernathy, A.Katz and S.J.Pearton) in Murray Hill, NJ on the MOMBE growth of GaN, InN, and AlN. The III-V nitrides - GaN, AlN and InN - form a continuous alloy system with direct band gaps ranging from 1.9eV for InN, to 3.4eV for GaN to 6.2eV for AlN. Thus the III-V nitrides could potentially be fabricated into optical devices which are active at wavelengths ranging from the red well into the UV. In addition the large bandgaps, especially of GaN, make these semiconductors excellent prospects for high temperature microelectronic devices. A variety of substrates and growth conditions have been investigated and detailed characterization by cross-sectional TEM, x-ray diffraction, SIMS and other methods have been done. Dr.Abernathy is growing III-V nitrides by MOMBE modified with a RF nitrogen source, while Drs. Katz and Pearton have been involved with electrical characterization. To date films of AlN, GaN and InN have been grown on InP, Sapphire, GaAs and GaP substrates. The goal is to grow high quality single crystal films (both hexagonal and cubic films are being investigated) with a stoichiometry suitable for doping. Results of our characterization of these films are summarized below:

1) AlN, GaN and InN layers grown on (001) InP

X-ray results and transmission electron diffraction results indicate the films are highly oriented. The hexagonal basal plane (0001) of AlN, GaN or InN is parallel to the (001) surface of the InP substrate. Plan view and cross-sectional TEM diffraction data indicate that the films are polycrystalline in nature with columnar grains. The diameter of the grains was 100-200 Å for AlN, 300-500 Å for GaN and 1000-1200 Å for InN. The samples were subsequently annealed for 30 minutes at temperatures between 300 and 600°C. There was no significant difference in crystal structure between the as deposited sample and those annealed. This experiment successfully indicated that III-V nitride films can be grown in this MOMBE system.

2) GaN layers grown on (0001) sapphire

A second series of samples were grown in order to explore methods of growing hexagonal and cubic single crystal films. An AlN buffer layer is expected to improve the crystallography and morphology of GaN grown on sapphire by grading the mismatch. It

has been demonstrated that it is possible to grow high quality GaN layers on a strained low temperature buffer layer. The epitaxial growth on this low temperature buffer layer is expected to lead to a good quality single-crystal GaN film (hexagonal) with a smooth surface morphology.

Initial results from X-ray diffraction indicate that the samples grown might be single crystal, however because of the strong tendency of the basal plane to orient itself parallel to the surface, it is not possible by X-ray alone to determine if the films are single crystal. Cross-sectional TEM studies show growth of wurtzite GaN with a high density of vertical defects which extend from the interface to the surface.

The orientation relationship was determined to be as follows:

$$\begin{array}{l} (0001)_{\text{GaN}} // (0001)_{\text{substrate}} \\ [1010]_{\text{GaN}} // [1120]_{\text{substrate}} \end{array}$$

3) GaN layers grown on (001) GaAs

Literature has shown that cubic GaN can be epitaxially grown on (001) GaAs substrates, however a high density of planar defects, mostly {111} microtwins and stacking faults are observed. Attempts have been made to force growth of cubic GaN on (001) GaAs substrates. An initial direct growth led to highly defective hexagonal GaN. However cubic material was successfully nucleated and grown using several methods including low temperature buffer layers, GaAs to GaN gradation or a 15 minute intermediate anneal under N₂ atmosphere. The structural characterization of the GaN films was carried out by X-ray diffraction and TEM.

The orientation relationship from XTEM is as follows:

$$\begin{array}{l} (001)_{\text{GaN}} // (001)_{\text{GaAs}} \\ [001]_{\text{GaN}} // [001]_{\text{GaAs}} \end{array}$$

The x-ray results indicate the film may revert to hexagonal structure with increasing thickness. The growth conditions are being changed in order to maximize the cubic growth.

4) GaN layers grown on (001) GaP

In an experiment similar to the growth of cubic GaN on (001) GaAs, cubic GaN has been epitaxially grown on (001) GaP substrates. Since the lattice mismatch between GaN and GaP (17%) is less than that between GaN and GaAs (20%) it is hoped that films having better structural quality will be grown on GaP.

X-ray diffraction and TEM showed growth of cubic GaN on GaP, having the following orientation relationship:

$$\begin{array}{l} (001)_{\text{GaN}} // (001)_{\text{GaP}} \\ [001]_{\text{GaN}} // [001]_{\text{GaP}} \end{array}$$

Again however the films appear to change to the hexagonal structure at greater thicknesses and changes in the growth conditions similar to those for the GaAs substrates are being tried.

This work has resulted in the first demonstrated growth of cubic GaN on GaP by any technique. In addition cubic GaN has also been grown on GaAs (for the first time by MOMBE). These cubic layers tend to change to hexagonal with increasing thickness.

Future work is aimed at improving the growth of the cubic phase to thicker layers by decreasing the growth rate and increasing the growth temperature. The goal of this research is to develop the best method of growing GaN on commercially available GaP and GaAs substrates. In addition to improving the crystal quality it is also important to develop dopants in these materials. Dr. Abernathy at AT&T, as part of this project, has demonstrated for the first time the p-type doping of GaN using carbon. Future work will focus on comparing the carbon (as well as other elemental) doping efficiency in hexagonal versus cubic GaN. Finally the growth of lattice matched InGaN on ZnO may be addressed if a promising source of material successfully delivers the ZnO (0001) substrates.

(V) Optical studies (Joe Simmons)

We have supported the development of p-type ZnSe fabricated by MBE by conducting PL measurements for quality evaluation in heavily doped films. We have also supported the development of $Cd_xZn_{1-x}S$ films made by MOCVD. Research has begun on PL measurements in GaN films.

We have recently acquired a short pulse laser and high speed detection equipment, and are currently assembling apparatus for conducting mode mixing measurements on PL relaxation. These measurements will allow an estimate of both the majority and minority photo-excited carrier lifetimes. Such measurements will lead to an evaluation of the processes which interact with photo-excited carriers to induce trapping or recombination. These results can be used to evaluate the role of excitons and defects in estimating the quantum efficiency of optical devices.

(VI) Transport Studies in n-Type ZnSe (Joe Simmons)

We have studied measurements of Hall Effect on partially compensated n-type ZnSe (doped with Cl_2) films produced by MBE, and having room temperature free carrier densities ranging from 10^{16} to 10^{19} carriers/cm³. A consistent temperature-dependent analysis over this range of carrier densities has not been successfully produced in the past. The problem is that the dopant densities cover the range from light doping to such heavy doping as to produce metallic behavior.

A. Free carrier concentration

While the extremes of light doping and the metallic behavior are well understood, there is a great deal of debate regarding what happens in the intermediate region. The variation in temperature dependent behavior in the transition between light and heavy doping gives the key to the analysis as follows:

(1) lightly doped samples ($10^{16} - 10^{17} \text{ cm}^{-3}$)

At room temperature, carriers are thermally excited from the donor states into the conduction band according to simple excited carrier calculations.

As the temperature is decreased, carrier freeze out occurs, as the excited carrier concentration decreases and the carriers repopulate the donor state.

The decrease in carrier concentration with temperature can be easily calculated with and without taking into account the occupation of various excited states. (See Table VI.1, "Models for Free Carrier Density".)

(2) heavily doped samples ($5 \times 10^{18} - 10^{19} \text{ cm}^{-3}$)

At these dopant densities in partially compensated n-ZnSe, the carrier concentration is above the Mott density, which means that the Bohr diameter of the individual dopant states overlap. Consequently, the impurity (donor) levels make up a continuous impurity band. The carrier density is divided between the conduction and the impurity bands. Since both contribute to carrier conduction, the free carrier density measured from the Hall Effect shows no temperature dependence.

So far, the data and the models agree very well and are based on well established theories of behavior. Figure VI.1 depicts these results. In the figure, the data from 2 samples with room temperature free carrier concentrations below 10^{17} cm^{-3} were fitted with the single donor equation from Table VI.1, while the data from the 2 samples with room temperature free carrier concentrations above 10^{18} cm^{-3} were assumed to have a constant free carrier density as would be expected for the combination of impurity and conduction band conduction. (The data from the 2 intermediate samples were fitted using a 2-donor sstate model to be discussed below.)

(3) intermediate dopant levels ($10^{17} - 5 \times 10^{18} \text{ cm}^{-3}$)

In this dopant range, the temperature dependence of the free carrier concentration exhibits a reduced decrease with temperature. Near the upper end of the range, the free carrier density reaches a constant asymptotic behavior between about 50 and 30K. Studies with doped Ge and Si semiconductors exhibit a marked drop in the Hall coefficient occurring at temperatures below 20K. Several models have been presented to account for this behavior, including (a) temperature dependent donor ionization energy, (b) the presence of a doubly ionized state (upper Hubbard band), (c) the presence of two separate donor levels, and (d) activated hopping conduction.

We have conducted an analysis of the behavior of samples in this range and have obtained the following conclusions. A paper is in preparation.

(a) The change in ionization energy with temperature required by the observed behavior is very much larger than expected from proposed models, therefore, it can only be a second order modification of the primary cause of the intermediate behavior.

(b) The doubly ionized defect state was taken into account and only shows a minor modification of the singly ionized defect model. If the state is localized, then its addition increases the freeze out behavior and is contrary to observations. If the level

is non-localized (upper Hubbard band), it only contributes a second order modification of the intermediate behavior.

(c) The presence of two donor states provides the experimental behavior when the second donor state has a small ionization energy. However, we have not yet found any other experimental verification of this structure. Far IR absorption measurements are being planned to determine the defect ionization energies. The two-defect model also fits well the temperature dependence of the mobility. This is shown in Figs. VI.2 and VI.3.

(d) Hopping conduction has been suggested in Ge and Si studies to explain the low temperature behavior of the Hall Coefficient in the intermediate dopant range. Hopping conduction, however, includes several separate processes. Activated hopping, normally postulated in the variable range hopping model, proposes that free carrier behavior is observed when carriers are activated between localized defect states. All activated processes, however, exhibit the wrong temperature dependence. This leaves tunnelling between adjacent localized defect sites. We are currently evaluating this process and have made encouraging progress. This transport process, however, will have a strong effect on the measured mobility, and we are currently examining the effect to determine agreement with experimental data.

B. Mobility

A program has been developed for numerical calculation of the mobility by solving the Boltzmann equation using generalized Fermi-Dirac statistics including the full screening and scattering terms. The program was based on earlier work by Gobba and others in HgTe. The program is written in FORTRAN and runs easily on a computer workstation.

We have used this program to calculate the Hall mobility of the same partially compensated n-ZnSe films discussed above. The fits were conducted as in Fig. VI.1, using a single defect model for the 2 lightly-doped samples, a metallic model for the two heavily-doped samples and a two-defect model for the 2 intermediate samples. In the lightly-doped and the heavily-doped samples, an accurate fit of the experimental mobility was obtained over most of the temperature range (see Fig. VI.4). The fits obtained for the two-defect model are also quite good, except for the low temperature region where impurity scattering seems to be overestimated in the model. We are reviewing these results to help address the issue of tunnelling conduction in the intermediate dopant range.

C. Hopping conduction

The question of hopping conduction for the low temperature free carrier density and mobility has been examined, as noted above. We have discarded all activated processes, since they give the wrong temperature dependence. We are currently examining a tunnelling approach which appears very promising. We expect to fit the free carrier density using the two competing models of tunnelling and two-donor states, then determine the appropriate model using the mobility data and far IR absorption data - the latter to be taken in the continuation of these studies.

(VII) Development of Blue Diode Lasers (Peter Zory)

Work done during the year can be categorized as follows:

- A. Photopumped Lasing - Experiment and Theory
- B. Wafer Process Development - CdZnSe single quantum well (QW) diode laser material
- C. Diode Laser Modelling - CdZnSe, single QW lasers

Summaries of work done in each of the above areas are given below.

A. Photopumped Lasing

1. A number of ZnSe epitaxial films of different thickness were grown on GaAs substrates by MOCVD (B. Pathangey and T. J. Anderson). Photopumped lasing experiments were carried out and the data analyzed. A paper has been written which summarizes the results.¹ A strong dependence of the laser threshold pump intensity (I_{th}) on pump photon energy ($h\nu$) and film thickness (t) was found and successfully modeled. The main conclusion is that one must understand how to select t and $h\nu$ if one is to utilize I_{th} as a measure of the potential of such films to be used as active layers in diode light emitting devices.

2. Photopumped lasing was achieved in CdZnSe/ZeSe multiquantum well (MQW) material grown by MBE (L. Calhoun and R. M. Park). Threshold pump intensities as low as 35 Kw/cm^2 were found for devices made with $100 \mu\text{m}$ widths and $500 \mu\text{m}$ cavity lengths (work done by F. Ihren under the supervision of Y. Guan and P. Zory). This value compares favorably with the best data reported in the literature for such structures. Far field measurements were made and used to determine the effective refractive index difference, Δn , between the MQW active layer and the ZnSe cladding layers. The result, $\Delta n = 0.09$ for beam divergence of 33 degrees, combined with the low threshold pump intensity indicates that this structure is a potentially good one for making quasi-DH diode lasers provided good injection efficiency into the MQW active region and degradation resistance can be achieved. Photopumped lasing over several hours did not produce any noticeable degradation although the duty cycles used were quite small. A master's degree thesis² summarizing these results has been completed.

B. Wafer Process Development

As reported by 3M at the October '92 Workshop, CdZnSe QW material demonstrated to date has the following properties:

1. Free hole densities in contacting cap layers grown at 150°C , will be reduced significantly during processing and packaging if temperatures higher than 150°C are encountered.
2. Dark-line defect nuclei and/or dark-line defect growth rates may be increased due to the wafer thinning procedures usually done to simplify cleaving into bars.

In order to process/package both 3M and UF diode materials, so as to minimize the

above problems, we have developed a processing/package procedure where temperatures were kept below 100°C and "thick" wafers could be cleaved into high quality bars (non-striated facets) with high yield. A scribe and break procedure for separating bars into chips has also been developed.

Using these techniques, a standard single QW AlGaAs laser wafer was processed in parallel with a single QW CdZnSe laser wafer provided by 3M. While the AlGaAs 100 μm wide stripe devices worked perfectly, the CdZnSe devices showed complete loss or radiative efficiency except near the edges of the 100 μm stripes. We believe we understand the origin of the failure and are attempting to demonstrate this fact by processing a new piece of the 3M CdZnSe single QW material.

C. Diode Laser Modelling

The fundamental relationship between peak optical gain, g , and current density, J (the g vs J relation), for strained CdZnSe quantum well/ZnSeS laser configurations has been derived assuming strict k -selection and valence band mixing. This relation allows one to predict the temperature dependence of threshold current density of diode lasers incorporating such structures. Good agreement with 80K to 300K experimental data measured at Phillips Labs (see Appl. Phys. Lett. 62, 2462, 1993) is obtained with no adjustable parameters other than an intraband relaxation time of 60fsec. While not conclusive, this agreement indicates that optical gain in CdZnSe QW lasers is derived from stimulated processes between free electrons and holes rather than between bound electrons and holes (excitons) as suggested in Phys. Rev. Lett. 69, 1707, 1992. A paper discussing our results has been accepted for presentation at the IEEE/LEOS Annual Meeting.³

References:

1. "Photopumped Lasing of Variable Thickness ZnSe Thin Films", by Y. Guan, P. S. Zory, B. Pathangay and T. J. Anderson, submitted for publication.
2. "Photopumped ZnSe/CdZnSe MQW Lasers" by F. Ihren, Master of Science Thesis, Dept. of Electrical Engineering, Univ. of Florida.
3. "Temperature Dependence of Threshold Current Density in CdZnSe Single QW Lasers", by Y.S. Park, P.S. Zory, and G. Lim, to be presented at the IEEE/LEOS Annual Meeting, Nov. 1993, San Jose, CA.

(VIII) Theoretical Calculations for Dopants in ZnSe (Subcontract to Gertrude Neumark, Columbia University)

Objective and Rational

The objective was to determine the role of dopant solubility limits and of self-compensation in equilibrium doping in wide-gap materials, with emphasis on ZnSe. It can be noted that, aside from doping aspects, levels introduced by self-compensation provide alternate recombination paths to the desired luminescence one, and thus degrade the efficiency. As regards the relevance of equilibrium doping, there is a strong possibility that the doping at the growing MBE interface is at, or close to equilibrium conditions, in view of the high ionic mobilities of Zn vacancies and Zn interstitials.

The two specific primary first-year objectives of the work, were:

- 1) To evaluate the cause of orders-of-magnitude differences in calculated solubility limits of ZnSe (N), one from a first-principles treatment [Van de Walle, Laks, Neumark, and Pantelides, Phys. Rev. B47, 9425 (1993)] and the other from a thermodynamic approach [Neumark, Phys. Rev. Lett. 62, 1800 (1989)]
- 2) To determine whether solubility limits and self-compensation were separate phenomena or were related.

Progress

Both primary objectives have been met. It was shown that the thermodynamic analysis, which assumed that one could compare the doped material to intrinsic material, neglected the energy required to introduce defects to provide, the intrinsic material. Thus the first principles results are more reliable. These predict a room temperature hole concentration for ZnSe (N) of $\sim 10^{18}/\text{cm}^3$. If the dominant compensating defect is a simple native defect (such defects are included in the calculation) this result is expected to be accurate to about an order of magnitude; however this treatment neglects complex defects, which may also be playing a role.

It was also shown that solubility limits and self-compensation are related, being different facets of the same physics.

To better highlight the insight gained over the past year, we now discuss the results in more detail. First, we consider the self-compensation aspect.

The driving force towards self-compensation can be understood readily. Thus, for shallow donors, the electrons, and the Fermi level, are located close to the band-edge (i.e. approximately at E_G); if a compensating species were now provided, an electron would have a lower-energy state available and, for equal numbers of donors and compensating species, the Fermi level would be at approximately mid-gap (i.e. $E_G/2$). The system would thus gain an electronic energy of $E_G/2$ per electron. Obviously, this energy gain increases with band-gap, and thus becomes more pronounced in wide-gap materials. To obtain this gain, the material must however "introduce" such compensating levels, i.e. native defects (vacancies, interstitials, or anti-sites) or complexes with these. Thus the electronic gain is not "free": one must pay the energy of formation of the compensating defects, and this mostly seemed relatively high. The recent work has now

given an improved understanding of the energy "trade-off".

The important aspect of recent work on defect energies is emphasis on the role of chemical potentials of the system. The formation energy of a native defect can be represented as e.g. Van de Walle et al.)

$$E_{\text{form}} = \epsilon \pm \mu_{\text{M(X)}}$$

where ϵ is the calculated supercell energy, $\mu_{\text{M(X)}}$ is the chemical potential of the metal (anion) constituent of the material, and where the \pm denotes whether the defect energy is increased or decreased by the particular μ . The relation between the μ 's, for a binary compound, is:

$$\mu_{\text{M}} + \mu_{\text{X}} = \mu_{\text{MX}} = \mu_{\text{M(bulk)}} + \mu_{\text{X(bulk)}} + H_{\text{f}}(\text{MX}) \quad ,$$

where $H_{\text{f}}(\text{MX})$ is the heat of formation of compound MX. What must now be realized is that usually one obtains the maximum solubility of a desired dopant at - or close to (subject to constraints of second phases of host/dopant compounds) - the maximum (or minimum) value of one of the host chemical potentials. For example, for N doping in ZnSe, one wants a low μ_{SE} (high μ_{Zn}) for easier incorporation of N on the Se site. Our recent work under the present grant has led to the realization that this same value for the chemical potential is the one of relevance for defect incorporation, rather than the energy at stoichiometry, which was the one usually considered previously. E_{form} is thus reduced appropriately. Moreover, there will always be at least one native defect (or complex with one) which is favored under the conditions for maximum doping (e.g. Zn interstitial in the case of N in ZnSe). Thus the required formation energies will be lower than had previously been realized, and self-compensation becomes far more likely. It must however still be noted that a key word in the last sentence was likely; it does not follow that one will get this self-compensation, or at least strong self-compensation, in all cases. The relative energy gain depends on relatively small differences between large numbers, namely on $E_{\text{G}}/2$, the defect formation energy (at stoichiometry), and the proper chemical potential. The numbers will thus be favorable to good dopant incorporation in some cases, and unfavorable in others. This can thus account for the observation that good conductivity has been fairly readily obtained in some cases, but has been very difficult in others (there is, to our knowledge, still no report of good conductivity in n-ZnTe).

As regards the tendency towards low solubilities, the recent (grant) work has shown that this results basically from the compensating defects. This has thus clarified the relation between self-compensation and solubility limits, and shows that the two are merely different facets of the same physics.

Lastly, we have also carried out a literature survey under the grant, to evaluate experimental evidence of self-compensation and low solubility. This has confirmed the prevalence of these tendencies. This work has been included in a review article, "Defects in II-VI Compounds" written for the "Encyclopedia of Advanced Materials"

(IX) Gain Modeling in II-VI Strained-Layer QW Structures (Subcontract to Reinhart Engelmann, Oregon Graduate Institute of Science and Technology)

Objective

To provide a comprehensive design tool for separate confinement heterostructure (SCH) QW lasers in the expanded wide band gap II-VI material system that is fast and easy to use.

Approach

Use simplified physical models for band structure in order to elucidate trends in a large parameter space including the incorporation of IIa(Mg, Ca) elements.

Progress

1. A data base for relevant material parameters of the wide band gap II-VI compounds and alloys has been established

1.1 Band gap vs. lattice constant

Band gap and lattice constant are the most important parameters in diode laser design and modeling. We have established a collection of relevant high band gap semiconductors including IIa(Be, Mg, Ca)-VI, IIb-VI and III-V(Nitride) from literature survey and theoretical calculations. A simple method to estimate the lattice constant based on covalent radii¹ for a new zinc-blende material system is available on line. The temperature dependence of band gap and lattice constant have also been studied². Band gap versus lattice constant diagrams were generated for the IIa(Mg, Ca)-VI, IIb-VI and III(Al, Ga, B)-V(Nitride) material systems at room temperature. In the diagrams of II(Mg, Zn, Cd)-VI(S, Se, Te), the band gap versus lattice constant of the ternary alloys has also been determined according to the following approach.

For ternary alloys, $A_xB_{1-x}C$, band gap and lattice constant is obtained from the respective binary values. The lattice constant follows from Vegard's law

$$a(x) = xa_{AC} + (1-x)a_{BC}$$

and the band gap E_g can be described by the equation

$$E_g(x) = [xE_{gAC} + (1-x)E_{gBC}] - bx(1-x),$$

where b , the so-called bowing parameter, can be calculated from³

$$b = (Ze/8\pi\epsilon_0) (1/r_F - 1/r_G)^2 (r_F + r_G) \exp(-s d_M/2).$$

Here, Z is the valence number and r_F and r_G are Pauling's covalent radii of the two substitutional elements (e.g. A and B above), e is the electron charge, ϵ_0 the permittivity of free space, $s=0.25$ ($1/\text{\AA}$ a screening constant, and d_M the tetrahedral bond length at mid-composition).

The data for the quaternaries are obtained by interpolation from the corresponding ternaries.

Based on above consideration, a FORTRAN code to calculate the bowing parameter as well as the band gap and lattice constant of ternary or quaternary alloys has been generated. The band gap vs. lattice constant diagrams are plotted in Fig. IX.1 and IX.2.

1.2 Strain effect

From Fig. IX.1, one can see that it is very hard to get a large band gap difference between QW and barrier in standard lattice matched IIb-VI heterostructures. So, incorporation of strained, rather than unstrained QWs in II-VI alloy systems is inevitable. In addition, both biaxial compressive and tensile strain in the QW is expected to reduce lasing threshold current, which has already been demonstrated in III-V devices. The critical thickness is an important parameter which determines how much strain could be incorporated in the QW⁴. The strain tensor is given by⁵

$$\epsilon = 1 - (a_{Ba}/a_{QW}),$$

where a_{QW} and a_{Ba} are the lattice constants of QW and barrier, respectively. The hydrostatic- and shear-components of the strain-induced band gap shift are

$$\delta E_{hy} = -2a\epsilon ((C_{11} - C_{12})/C_{11}),$$

and

$$\delta E_{sh} = +b\epsilon ((C_{11} + 2C_{12})/C_{11}),$$

respectively, where a and b are the deformation potentials, and C_{11} and C_{12} are the elastic constants. For zinc-blende CdSe, the numerical values of elastic constants are estimated following Ref. 6 and applied to ZnCdSe.

1.3 Band offset

The band offset is still a controversial issue in both theory and experiments. For estimating purposes, we adopt the common anion/cation rules in our calculations. The strain effect on the band alignment is obtained following the discussion in Ref. 5.

2. Optical waveguide modeling studies were performed for several QW structures with ZnCdSe QW's.

Wave guide modeling of specialized II-VI device structures is of particular interest for determining the optical confinement factor Γ , an important parameter in diode laser design. As an example, we performed calculations for a MQW $\text{Cd}_{0.23}\text{Zn}_{0.77}\text{Se}/\text{ZnSe}$ device structure (100Å/130Å, 10.5 periods, embedded in ZnSe) as described by Ref. 7. The gain confinement factor Γ for the entire MQW layer is 0.74 (summing over all the Γ 's of each individual QW layer), which is somewhat higher than the value of a GaAs/AlGaAs laser with the same structure. Fig. IX.3 and IX.4 show the near field and far field intensity distribution of this device.

3. Gain spectra were modeled as a function of carrier injection for several strained SCH SQW structures

3.1 Simplified approach to the gain/current calculations

The goal of our studies is to arrive at a flexible modeling program that allows to elucidate trends in a large parameter space and that can be easily applied to a variety of different material systems, rather than a sophisticated procedure that generates highly accurate data for specialized situations. Hence, we adopted a simplified theoretical approach to the gain/current calculations^{8,9}.

In this simplified approach, k selection rules are taken into account as well as the polarization effect for stimulated transition (i.e. TE vs. TM) due to the anisotropy of the QW structure, and intraband scattering of the injected carriers. Band-mixing effects are neglected and effective masses are assumed to be energy independent. Space charge induced electrostatic carrier confinement^{9,10} could be considered when the injection level becomes very high for those SCH structures with unbalanced carrier confinement.

3.2 Gain modeling results on SCH structures with a $\text{Zn}_{0.8}\text{Cd}_{0.2}\text{Se}$ QW and three different barriers: I. ZnSe , II. $\text{ZnS}_{0.06}\text{Se}_{0.94}$, and III. $\text{Mg}_{0.05}\text{Zn}_{0.95}\text{S}_{0.1}\text{Se}_{0.9}$

Three types of GaAs lattice matched SCH structures have been studied, as shown in Fig. IX.5. All of the three structures are using $\text{Cd}_{0.2}\text{Zn}_{0.8}\text{Se}$ as the QW layer. The first structure (SCH1) corresponds to the first demonstrated blue-green diode laser¹¹ using ZnSe as the barrier and $\text{ZnS}_{0.06}\text{Se}_{0.94}$ as cladding. The second structure (SCH2) uses $\text{ZnS}_{0.06}\text{Se}_{0.94}$ as the barrier and a $\text{Mg}_{0.1}\text{Zn}_{0.9}\text{S}_{0.1}\text{Se}_{0.9}$ as cladding, this structure is very similar to the one recently described by the Philips group¹². The third one (SCH3) uses $\text{Mg}_{0.05}\text{Zn}_{0.95}\text{S}_{0.1}\text{Se}_{0.9}$ as the barrier and $\text{Mg}_{0.2}\text{Zn}_{0.8}\text{S}_{0.3}\text{Se}_{0.7}$ as cladding; this structure has been designed by us based on the largest Mg content used in real devices thus far¹³. The band offset ratio was evaluated relying on the common anion/cation rules plus the strain effect on the band gap shift and valence band splitting. A simplified modeling program as described in 3.1 has been applied to calculate the gain-carrier injection relations. Figs. IX.6-IX.8 are the gain spectra of these structures under a variety of injection levels and Fig. IX.9 is the peak gain vs. carrier density of the three device structures. Fig. IX.9 clearly shows that the best results for blue-green diode lasers currently obtained with SCH2 can be improved by adding more Mg into the barrier and the claddings. The carrier densities in QW and barrier are also plotted in Fig. IX.10-IX.12 for the three structures. The improvement of the carrier confinement of SCH2 and SCH3 over the SCH1 are the main reason for the increasing gain in those structures containing the Mg. (Note: the cladding compositions are quoted above for completeness; they will be used for waveguide modeling in the future.)

3.3 Gain modeling on SCH structures with ZnSeTe QW and compare with the one with ZnCdSe QW

From Fig. IX.1, one can see that, just like ZnCdSe , ZnSeTe can be used also as the strained QW layer for the ZnSe based structures. Although the ZnSe/ZnTe heterojunction has been reported in type II alignment, due to the space charge induced

confinement effect¹⁰, substantial electron confinement is still possible. By incorporation of a simplified approach, which is based on local charge neutrality control⁹ for this space charge induced confinement effect, we obtained the gain spectra of a SCH with a $\text{ZnSe}_{0.8}\text{Te}_{0.2}$ QW and ZnSe barrier. Compared with the $\text{Zn}_{0.8}\text{Cd}_{0.2}\text{Se}/\text{ZnSe}$ structure, it showed somewhat higher gain than the ZnCdSe QW device under the same injection. This follows from the fact that a large valence band offset tends to give better carrier confinement. This is consistent with what we have observed in the III-V system and results mainly from the large density of states available in the valence band of the barrier material as compared with the corresponding values in the conduction band.

4. Two novel SCH-QW laser structures have been proposed

4.1 Novel diode laser structure based on MgZnSeTe alloys

A SCH SQW diode laser can be obtained by choosing the appropriate quaternary composition of the MgZnSeTe alloy for each of the active, barrier and cladding layers. It is well known that ZnTe is the only binary of the wide bandgap II-VI semiconductors with a p-type residual conductivity, and it was found that the $\text{ZnSe}_{1-y}\text{Te}_y$ alloy could be doped both p-type and n-type in the composition range of $0.5 < y < 0.614$. Good quality ZnSeTe material has been grown by MBE^{15,16} and MOCVD (metalorganic chemical vapor deposition)¹⁷ on various substrates (GaAs, InP, InAs and ZnTe). Mg introduction opens up the band gap energy of the standard II-VI compounds for diode laser design. Compared with MgSe and MgS, MgTe has less ionicity (Fig. IX.13) and can be grown more easily in zinc-blende structure¹⁸. Notice that $\text{MgSe}_{1-y}\text{Te}_y$ has a similar bowing characteristic as $\text{ZnSe}_{1-y}\text{Te}_y$, as shown in Fig. IX.14. Also, the doping property of $\text{Mg}_x\text{Zn}_{1-x}\text{Te}$ is very similar to that of ZnTe for x as high as 0.719. Hence, we expect that the engineered zinc-blende $\text{Mg}_{1-x}\text{Zn}_x\text{Se}_{1-y}\text{Te}_y$ quaternaries ($0.5 < y < 0.6$) between the dotted tieline in Fig. IX.14, have a similar amphoteric doping property as the ternary $\text{ZnSe}_{1-y}\text{Te}_y$ ($0.5 < y < 0.6$). Thus, by choosing $\text{Mg}_{1-x}\text{Zn}_x\text{Se}_{1-y}\text{Te}_y$ cladding layers with y in the range of 0.5 - 0.6 preparation of a pn diode structure should be available. Several lattice matched substrates are available for this composition range, such as InAs, GaSb, and ZnTe.

For blue-green light emission, the band gap of the cladding should be close to 3 eV. A high Mg mole fraction x (about 0.6-0.8 from Fig. IX.14) is needed in this case. Hence, $\text{Mg}_{0.8}\text{Zn}_{0.2}\text{Se}_{0.4}\text{Te}_{0.6}$ is chosen as cladding layer material (C in Fig. IX.14), which is lattice matched to GaSb, a commercially available substrate. For the barrier and active layers, doping is of minor concern, so the band offset is the most important issue. Based on the common anion rule, it is the advantage of the MgZnSeTe system that the Se/Te ratio can be adjusted to provide a reduced valence band offset thus overcoming the type II alignment problem of the ZnSe/ZnTe system, as shown in Fig. IX.15. The barrier can be easily chosen to be lattice matched with the cladding, as B ($\text{Mg}_{0.6}\text{Zn}_{0.4}\text{Se}_{0.3}\text{Te}_{0.7}$, $E_g = 2.8$ eV) in Fig. IX.14. As the first step, in view of reducing the difficulty in control of the quaternary composition, ZnTe could be the choice for an unstrained QW, though the wavelength is 538 nm, as A1 in Fig. IX.14. To obtain blue-green light emission, preferably a compressive strained QW such as A2 ($\text{Mg}_x\text{Zn}_{1-x}\text{Te}$) could be incorporated. With Mg composition about 0.2, blue-green light emission ($\lambda \approx 490$ nm) can be achieved.

Notice also the pronounced hole-barrier lowering for the MgZnSeTe alloys as compared with ZnSe, which is favorable for ohmic contact formation to the p-type cladding layer.

Using a MgZnSeTe quaternary alloy provides several advantages for II-VI diode lasers, such as the possibility for high doping of both p- and n-type, and large band offsets in both conduction and valence band with lattice matched barrier and cladding layers. All these advantages are dependent on very accurate control of the composition of each epitaxial layer. Hence, investigations on the growth conditions for these compounds need to be performed in the future both experimentally (by MBE and MOCVD) and theoretically. Growth simulations in such a system become more important, since a higher degree of complexity is involved as compared with III-V systems.

4.2 A ZnSe/ZnCaCdS/ZnCaS SCH structure lattice matched to GaAs

Besides Mg, Ca might be another choice of group IIa, to give more flexibility for DH structure design. We are not aware of any work on zinc blende structures that contain Ca. We estimated the band gap and lattice constant of zinc blende CaS based on the rock salt structure data of CaS and MgS, and propose a new SCH QW laser structure based on the ZnCaCdS quaternary alloy system lattice matched to GaAs as shown in Fig. IX.16. The advantage of this system would be a better composition control during growth since only one VI constituent is required ("quasi-ternary"). Additionally, the system could be adjusted to provide lattice matching to commercial GaAsP epi-material thereby allowing for larger bandgaps in the active QW layer by incorporation of S into ZnSe to form a ZnSSe QW. This could provide an extension of the available wavelength range into the ultraviolet. The p-type doping of the proposed quaternary alloys, on the other hand, remains an open question.

5. Initial work towards the improvement of our current simplified gain modeling program has been performed

5.1 Accurate model for space charge induced carrier confinement

In most of the II-VI SCH structures, the carrier confinement ability for electrons and holes are quite different due to the different QW depth in conduction and valence bands¹⁰. In case of ZnCdSe/ZnSe, the electrons are easily confined while the holes tend to spill over into the barrier region due to the small valence band offset. As the electron density increases, they attract more and more holes back to the QW, an effect which modifies the band profile. We have developed a simplified model for this space charge induced carrier confinement before that we have applied to InGaAs/GaAs lasers⁹. A more accurate model will now be attempted for calculating space charge induced confinement. This effect can be described by the coupled set of the following equations with the appropriate boundary conditions.

A. Schrodinger Equations for describing the one dimensional quantization for the carriers in the QW :

$$-(\hbar^2 d^2)/(2m_h dz^2) + U_c(z) + V(z) F_{e,i}(z) = E_{e,i} F_{e,i}(z),$$

$$-(\hbar^2 d^2)/(2m_h dz^2) + U_h(z) - V(z) F_{h,i}(z) = E_{h,i} F_{h,i}(z).$$

B. Poisson Equations for describing the space charge effect resulting from the unbalanced carrier spill out of the QW :

$$d^2V(z)/dz^2 = 4\pi\epsilon k_B T [r_h \sum_i \ln(1 + \exp(E_{Fh} - E_{hi})/k_B T) |F_{hi}(z)|^2 - r_e \sum_i \ln(1 + \exp(E_{Fe} - E_{ei})/k_B T) |F_{ei}(z)|^2].$$

Here, $U_c(z)$ and $U_h(z)$ are the built-in potential of conduction and valence band; $V(z)$ is the carrier injection induced potential which modifies the band profile; $F_{e,i}(z)$ and $F_{h,i}(z)$ are the envelope functions for the electron or hole at energy level i .

By solving these equations under the boundary conditions, we can obtain both the modified band profiles and the energy levels. So, solving these equations will providing the energy levels; with these energy levels, the remaining part of the gain calculation can be simply adopted from the previous simplified model.

5.2 User friendly interface of semiconductor modeling program

Since we are going to deal with a large parameter range for trends in diode laser design, it is necessary to have a convenient tools for data input/output control and display. A workstation based diode laser device design environment is being created which utilizes a highly graphical, intuitive and interactive user interface. This would make the modeling program more easy to use and such an environment will be more useful when expanding the one dimensional model currently considered to a two dimensional one in the future. The initial version of the user friendly interface has been developed based on the X-window system (Motif/Xt), which include wave guide modeling and simple gain modeling program with a window/dialog/menu style. The input file currently is still in text form and in the future it will be designed to be capable of drawing a graphic representation of the device structure.

References

1. L. Pauling, "The nature of chemical bond", Cornell University Press, 1960.
2. Landolt-Bonstein, "Data in Science and Technology, Semiconductors Other than Group IV Elements and III-V Compounds", New Series, Springer-Verlag, March 1992
3. R. Hill, J. Phys. C: Solid State Phys., 7, (1974).
4. P. J. Parbrook, B. Henderson, K. P. O'Donnell, P. J. Wright and B. Cockayne, J. Crystal Growth 117, 492 (1992).

5. H. J. Lozykowski and V. K. Shastri, *J. Appl. Phys.* **69**, 3235 (1991).
6. C.G. Van de Walle, *Phys. Rev. B* **39**, 1871 (1989).
7. P. Zory, private communication, July 11, 1992.
8. S.W. Corzine, R.H. Yan and L.A. Coldren, Chapter 1, 'Quantum Well Lasers', ed. P. Zory, Academic Press, 1993.
9. Y. Cai, R. Engelmann, and R. Raghuraman, "Simple model for carrier spill-over in quantum-well lasers consistent with local charge neutrality", OSA'92 Annual Meeting, Albuquerque, NM, Sept. 1992.
10. J. Barrau, T. Amand, M. Brousseau, R. J. Simes and L. Goldstein, *J. Appl. Phys.* **71**, 5768 (1992).
11. M.A. Haase, J. Qiu, J.M. DePuydt, and H. Cheng, *Appl. Phys. Lett.* **59**, 1272-1274 (1991).
12. J.M.Gaines, R. R. Drenten, K. W. Haberern, T. Marshall, P. Mensz, and J.Petruzzello, *Appl. Phys. Lett.* **62**, 2462 (1993).
13. H. Okuyama, T. Miyajima, Y.Morinaga, F. Hiei, Mozawa and K. Akimoto, *Electron. Lett.* **28**, 1798 (1992).
14. M. Aven, *Appl. Phys. Lett.* **7**, 146-148 (1965).
15. T. Yao, Y.Makita and S. Maekawa, *J. Crystal Growth* **45**, 309 (1978).
16. F.S. Turco-Sandroff, R.E. Nahory, M.J.S.P. Brasil, R.J. Martin, R. Beserman, L.A. Farrow, J.M. Worlock and A.L. Weaver, *J. Crystal Growth* **111**, 762 (1991).
17. H. Oguri, K.S. Park, M. Isshiki and Y. Furukawa, *J. Crystal Growth* **117**, 116-118 (1992).
18. Chin-Yu Yeh, Z.W.Lu, S.Froyen, and Alex Zunger, *Phys. Rev. B* **45**, 12130 (1992).
19. S.G. Parker, A.R. Reinberg, J.E. Pinnell, and W.C. Holton, *J. Electrochem. Soc.* **118**, 979 (1971).

(X) MOCVD Growth of Column III Nitrides (Subcontract to Jacques Pankove, University of Colorado)

Many GaN layers were grown on (1102) and (0001) sapphire and on (100) Si. We discovered that the moisture content of ammonia can vary considerably. Thus Matheson "Electronic Grade" is better than their "High Purity" grade. However Scott's ammonia is even better than Matheson gas.

Finally all of the system leaks have been eliminated. The reactor chamber was cleaned by blasting with glass beads, a technique that yields a stainless steel surface one order of magnitude cleaner than that obtained by electrolytic etching. A total pressure in the Torr range was used recently instead of the sub-Torr region used during the first three quarters of this year. As shown in Fig. X.1, GaN of good morphology and uniform nucleation can be obtained. However this layer is still somewhat yellowish. A SIMS measurement of our most recent sample (Fig. X.2) show that the oxygen concentration is lower by more than two orders of magnitude compared to our earlier measurements (Fig. X.3). The residual coloring is tentatively attributed to the presence of carbon, a deep acceptor that makes GaN insulating.

Our strategy for reducing the C concentration is to increase the flow of NH_3 and H_2 . It is hoped that the extra atomic H will leach out the carbon as CH_4 . A higher capacity (1 l/min) mass flow controller has been ordered for the NH_3 line. Also a hot filament will be installed near the substrate to dissociate NH_3 and/or H_2 to increase the concentration of atomic H. In addition, the role of AlN and GaN buffer layers in influencing the subsequent deposits will be assessed.

The cathodoluminescence spectra of our recent GaN samples exhibit a strong yellow emission at 2.2 eV and weak near-gap emission at 3.45 eV (Fig. X.4). The X-ray diffraction spectrum (Fig. X.5) shows a strong peak at 57.7° due to diffraction from the (1120) wurtzite plane of GaN. The small peak at 52.6° corresponds to the (2024) reflection from the sapphire substrate.

A bubbler of CP_2Mg has been installed. It will be used to grow p-type GaN as soon as the O/C contamination is reduced by another order of magnitude.

SECOND YEAR PLANS

Widegap II-VI MBE Growth

- (1) Investigate the dependence of CL intensity recorded in-situ and in real-time on film growth-rate and II-VI incident flux ratio with a view to further optimization of p-type doping of ZnSe using nitrogen.
- (2) Study the relationships between CL intensities measured at the growth temperature and the electrical characteristics of p-type ZnSe:N and the low-temperature PL characteristics of p-type ZnSe:N

- (3) Investigate the growth of lattice-matched quaternary alloys in terms, in particular, of optimizing the conditions for doping these materials both n-type (with Cl) and p-type (with N). CL intensity measurements will be employed in this study to assist with the optimization work.

Zinc Blende-GaN MBE Growth

- (1) Perform a systematic study to determine the influence of growth parameters, principally III-V reactive flux ratio and substrate temperature on the electrical characteristics of unintentionally-doped zincblende-GaN films.
- (2) Investigate n- and p-type doping of zincblende-GaN under optimized growth conditions.
- (3) Investigate the growth of $\text{Al}_x\text{Ga}_{1-x}\text{N}/\text{GaN}$ and $\text{GaN}/\text{In}_x\text{Ga}_{1-x}\text{N}$ heterostructures and quantum well structures.

Electrical Contact Studies:

Emphasis will continue on formation of ohmic contacts using *ex situ* formation of low bandgap, high electron affinity semiconductors like HgSe. The processing will be improved to determine if sufficient current density can be achieved to make *ex situ* grown contacts competitive with *in situ* MBE grown HgSe to ZnTe contacts. With optimization of the conditions, we believe that this process can lead to attractive ohmic contacts. We will also study the amount of voltage drop across the contacts to attempt to determine why diode lasers require such high voltages to operate.

Mechanical Properties of ZnSe: One of our PhD students, J. Kim, will redirect the main focus of his research towards a better understanding of why these II-VI LED's and lasers are degrading so quickly. To accomplish this, it will be necessary to better understand the mechanical properties of ZnSSe and ZnMgSSe compounds. Thus his research will be aimed at understanding how composition affects properties such as hardness, coefficient of thermal expansion, etc. The goal is to provide information that may lead to a better understanding of where strain in these multilayer devices develops, which layers are most likely to plastically deform first and ultimately how II-VI LED's and lasers based on these materials degrade. Dr. Qiu at 3M has agreed to grow the necessary ternary (ZnSSe) and quaternary (ZnMgSSe) films of varying composition by MBE for these studies. The characterization will be conducted both at the University of Florida and Oak Ridge National Laboratories. Parallel studies device degradation using material also grown by Dr. Qiu are being done at 3M by Dr. Guha.

Transport studies: Over the next year we will:

- Support Hall studies with measurements at lower temperatures, and with far R measurements to determine defect ionization energies.
- Evaluate the role of tunnelling in the low temperature behavior of the Hall Coefficient.
- Determine the contribution of low temperature tunnelling to Hall mobility
- Examine the implications of the tunnelling and double defect models regarding the structure of heavily and intermediate level doping of n-ZnSe.
- Conduct the same analysis of Hall Coefficient and Mobility in p-ZnSe.

Optical studies: Over the next year we will:

- Continue to support the materials development efforts in both p-ZnSe and GaN with steady-state PL measurements of defects.
- Assemble and test mode-mixing apparatus for time resolved PL studies to measure majority and minority photo-excited carrier lifetimes.

Development of Blue Diode Lasers: Over the next year we will:

- Continue process development work for DcZnSe QW laser material.
- Continue with modeling and begin experimental work to determine if an excitonic gain model is really required to explain the behavior of CdZnSe single QW lasers.
- Begin photopumping work with GaN-based materials.

Theoretical Calculation of Dopants in ZnSe: We plan to investigate whether impurity incorporation at the growing MBE surface is likely to be close to equilibrium. Specifically, we will consider ZnSe (N). This equilibrium question will depend on the diffusion mechanism of N, and on the concentration and ionic mobility of the defect species involved in the N diffusion (e.g. native vacancies). If the incorporation is close to equilibrium, the achievable N concentration will be constrained by the equilibrium solubility limits.

As a further investigation, we may carry out a re-analysis of literature Hall data on ZnSe (N), for a better evaluation of the extent of observed compensation. This re-analysis would be via the theory of the temperature and concentration dependence of impurity activation energies [Neumark, Phys, Rev. B5, 408 (1972)]

Gain Modeling in II-VI Strained Layer QW Structures:

1. A range of QW sizes and barrier material compositions will be investigated in the gain modeling studies to establish trends. The effort will concentrate on the most advanced material system of MgZnSSe lattice-matched to GaAs, but will explore the other systems we have proposed for comparison. A particular concern is carrier confinement at the injection levels needed for lasing.
2. The waveguide modeling studies will be extended to investigate the role of cladding material compositions and the number of QWs. For modal gain evaluation optical confinement has to be clearly understood. Cladding composition and waveguide size need proper tuning for optimum performance.

3. Implementation and testing of the accurate model for space charge induced carrier confinement (e.g. see 5.2 above). The gain/current calculations will be augmented to include more accurately the effects of space charge induced carrier confinement in those structures with unbalanced primary carrier confinement to the QW. For this purpose solving the coupled Poisson and Schrodinger equations will be pursued.
4. Implementation and testing of user friendly interface (see 5.2 above)

**POST DOCTORAL ASSOCIATES, GRADUATE RESEARCH ASSISTANTS AND
UNDERGRADUATE RESEARCH ASSISTANTS**

Post Doctoral Associates:

Wafaa Gobba with Dr. Simmons
Guan-Jiun Yi (1/2 year) with Dr. Neumark
Christopher Walker with Dr. Pankove

Graduate Research Assistants:

Chris Rouleau with Dr. Park
Bruce Liu with Dr. Park
Austin Frenkel with Dr. Park
C. Kothandaraman with Dr. Neumark
Li Wang with Dr. Simmons
Y. Cai with R. Engelmann
William A. Melton with Dr. Pankove
John Fijol with Dr. Holloway
Jeff Trexler with Dr. Holloway
Steve Miller with Dr. Holloway
Y.S. Park with Dr. Zory
C.L. Young with Dr. Zory
Eric Brettschneider with Dr. Anderson
Joe Cho with Dr. Anderson

Undergraduate Research Assistants:

Julie Sauer with Dr. Simmons
Greg Darby with Dr. Park
Bob Covington with Dr. Anderson
Michael Mui with Dr. Anderson
Brendon Cornwell with Dr. Anderson

INDUSTRIAL COLLABORATORS

- 3M Company** Chris Rouleau to spend Summer 1993 at the 3M Co. (St. Paul, MN) to transfer the real-time in-situ monitoring technologies developed in the MBE group at UF to 3M; material exchanged between 3M and Dr. Zory for packaging/temperature dependence studies.
- Kopin** Phase I SBIR; Development of efficient blue LEDs. Currently working on Phase II proposal.
- AT&T Bell Labs** MOMBE growth of GaN at Bell Labs with characterization of material at UF.

PUBLICATIONS

C.M. Rouleau and R.M. Park, "In-Situ Real-Time Determination of the Free-carrier Density in Doped ZnSe Films During Molecular Beam Epitaxial Growth," *Appl. Phys. Lett.* **60**, 2723 (1992).

R.M. Park, "Low-Resistivity p-type ZnSe:N grown by Molecular Beam Epitaxy Using a Nitrogen Free-Radical Source," *J. Vac. Sci. Technol.* **A10**, 701 (1992).

C.M. Rouleau and R.M. Park, "GaAs Substrate cleaning for Epitaxy Using a Remotely Generated Atomic Hydrogen Beam," *J. Appl. Phys.* **73**, 4610 (1993).

C.M. Rouleau and R.M. Park, "Design and Implementation of a Magnetic Drive Retrofit to the Vacuum Generator's Venetian Style Viewport Shutter Assembly," *J. Vac. Sci. Technol. All*, 464 (1993).

H. Liu, A.C. Frenkel, J.G. Kim and R.M. Park, "Growth of Zincblende-GaN on β -SiC Coated (001) Si by MBE Using a rf Plasma Discharge, nitrogen free-radical Source," submitted to *J. Appl. Phys.* (May, 1993).

C.M. Rouleau and R.M. Park, "Real-Time In-Situ Monitoring of Defect Evolution at Widegap II-VI/GaAs Heterointerfaces During Epitaxial Growth," submitted to *J. Appl. Phys.* (April 1993).

P.W. Wisk, C.R. Abernathy, S.J. Pearton, F. Ren, J.R. Lothian, A.Katz and K.S. Jones "Growth of GaN, AlN, and InN by Electron Cyclotron Resonance Metal Organic Molecular Beam Epitaxy", *MRS Symp. Proc.* **282**, 599, 1993.

G.F. Neumark and G.-J. Yi, "Defects in II-VI Compounds" in "Encyclopedia of Advanced Materials" (Pergamon), in press.

G.F. Neumark, R. Park, and J. DePuydt, "Blue-Green Semiconductor Injection Laser", *Physics Today*, in preparation.

Y. Cai and R. Engelmann, "Design of Novel Blue-Green Diode Laser Based on MgZnSeTe Alloy System," to be submitted for publication.

V. Fischer, P.H. Holloway, E. Ristolainen and D. Schoenfeld, "Formation of ohmic contacts on n-GaAs using $(\text{NH}_4)_2\text{S}$ surface passivation", submitted to *J. Vac. Sci. Technol.*

A. Deneuve, V. Zelezny, D.B. Tanner, C.M. Rouleau, R.M. Park and P.H. Holloway, "Electrical properties of n-type ZnSe/GaAs epilayers deduced from optical (near-infrared) and de Hall-effect measurements: a comparative study", submitted to *Phys. Rev.*

Y.-X. Wang and P.H. Holloway, "Indium ohmic contacts to n-ZnSe", *Vacuum* **43**, 1149 (1992).

PRESENTATIONS

R.M. Park, "Application of an atomic hydrogen source to GaAs wafer cleaning," Fall Workshop on Wide-bandgap II-VI Materials for Lasers, October 27-28, 1992 (St. Paul, MN).

R.M. Park, "P-type doping of widegap II-VI semiconductors," 1993 March Meeting of the American Physical Society, March 22-26, 1993 (Seattle, WA) - INVITED PRESENTATION.

Chris Rouleau and R.M. Park, "In-Situ, Real-Time Monitoring of ZnSe/GaAs Thin Film Parameters During MBE Growth," 39th National Symposium of the American Vacuum Society, Nov. 9-13, 1992 (Chicago, IL).

Lynn Calhoun, C.M. Rouleau and R.M. Park, "Real-time, In-Situ Monitoring of Strain Relief in the Lattice-Mismatched ZnSe/GaAs System During MBE growth," 22nd Annual Applied Vacuum Science and Technology Symposium, Feb. 8-10, 1993 (Clearwater Beach, FL).

G.F. Neumark, "Theory of Dopant Solubility and of Compensation in Wide-Band-Gap Semiconductors", Am. Phys. Soc, Seattle, Mar. 1993, INVITED

Y. Cai and R. Engelmann, "Proposal of novel blue green diode laser based on ZnMgSeTe alloy system," Annual Meeting of the Oregon Academy of Science, Linfield College, McMinnville, OR, 27 Feb 1993.

Y. Cai and R. Engelmann, "Proposal of novel blue-green diode laser based on ZnMgSeTe alloys," LEOS Summer Topical Meeting on Visible Semiconductor Lasers, Santa Barbara, CA, 21-22 July, 1993.

J. Pankove, "Status of Research on Blue Emitters", French-American Midwest Workshop, Chicago, Oct. 4-10, 1992, INVITED TALK.

J. Pankove, "Mitrades for Blue Lasers and Arsenides for Optoelectronic Neurons", University of New Mexico, November 13, 1992, INVITED SEMINAR.

J. Pankove, "Vovel Prospects for EL Displays", SPIE Electronic Imaging Symposium, San Jose, CA, February 1-2, 1993, INVITED TALK.

J. Pankove, "Properties and Applications of GaN", American Physical Society, Seattle, WA, March 21, 1993.

John Fijol, Jeff Trexler and P.H. Holloway, "Ohmic contacts to p-ZnSe", 21st Annual Symposium on Applied Surface and Vacuum Science and Technology, Feb. 8-10, 1993, Clearwater Beach, FL.

H.F. Arlinghaus, M.T. Spaar, N. Thonnard, P.H. Holloway, A.C. Diebold and P. Maillot, "Quantitative and sensitive profiling of dopants and impurities in semiconductors using sputter initiated resonance ionization spectroscopy (SIRIS)", XII National Congress of the Mexican Vacuum Society, Cancun, Sept. 22, 1992, INVITED PAPER.

Y. Darici, J. Marconi, D. Wu, V. Fischer and P.H. Holloway, "Thermal desorption of passivating S from GaAs, 39th National Symp. of the American Vacuum Society, Chicago, Nov. 9-13, 1992.

P.H. Holloway, "Epitaxial growth of compound semiconductors", XII National Congress of the Mexican Vacuum Society, Cancun, Sept. 21, 1992, INVITED TUTORIAL LECTURE.

P.H. Holloway, "Chemical reactions at the Au/GaAs interface", Tampere University of Technology, Tampere, Finland, Oct. 6, 1992, INVITED SEMINARS.

P.H. Holloway, "MOCVD growth of ZnS electroluminescent thin films", Planar Intl. Oy, Espoo, Finland, Oct. 6, 1992; also Helsinki University of Technology, Espoo, Finland, Oct. 7, 1992; INVITED SEMINARS.

P.H. Holloway, "Analysis of solid surfaces", Helsinki University, Helsinki, Finland, Oct. 8, 1992; HELSINKI UNIVERSITY MEDAL AWARD INVITED LECTURE.

Y.-X. Wang and P.H. Holloway, "Metal-MBE grown ZnSe interface and ohmic contacts", National Conference on Condensed Matter Physics, Beijing, PRC, October, 1992.

P.H. Holloway, V. Fischer, W. Lampert, T.W. Haas and J. Woodall, "The role of interfacial reactions and semiconductor regrowth on formation of ohmic contacts", Annual Spring Symposium, Materials Research Society, San Francisco, April 12-16, 1993,

P.H. Holloway, E. Ristolainen, B. Pathangey, M. Puga Lambers, and D. Schoenfeld, "SIMS analysis of widegap semiconductors and insulators", East Coast Workshop on SIMS, IBM, East Fishkill, NY, INVITED PAPER.

P.H. Holloway, "Overview of University of Florida University Research Initiative on Blue Light Emitting Materials and Injection Devices", URI Review and II-VI Workshop, Gainesville, FL, May 26-27, 1993.

P. Zory, "Anomalous Temperature Dependence of Light Emission from CdZnSe MQW LED's", 3M Co., St. Paul, MN, Oct. 1992.

P. Zory, "Visible Semiconductor Lasers", Half day short course at OSA/IEEE sponsored Conference on Lasers and Electron Optics (CLEO), Baltimore, MD, May, 1993.

P. Zory, "Visible Semiconductor Lasers", organized and chaired session at IEEE/LEOS sponsored Semiconductor Laser Workshop, Baltimore, MD, May, 1993.

P. Zory, "II-VI Diode Lasers-Design and Processing", organized and chaired part of II-VI Laser Workshop at URI Review and II-VI Workshop, Gainesville, FL, May 26-27, 1993.

Group	Nitrogen Source	Substrate	β -GaN growth-rate at $T_{\text{sub}} = 600^\circ\text{C}$	β -GaN rocking-curve linewidth (002) reflection
Univ. of Florida Park et al. (1993)	rf plasma	β -SiC/(001)Si	0.3 $\mu\text{m/hr}$	48 mins. (1.4 μm thick film)
Univ. of Illinois Greene et al. (1993)	Single-grid ion source	(001)MgO	Not quoted for β -GaN	43 mins. (≈ 1 μm thick film)
Boston Univ. Moustakas et al. (1992)	Microwave plasma/ ECR with magnetic mirror enhancement	(001)Si	0.2 $\mu\text{m/hr}$	90 mins. (≈ 1 μm thick film)
Univ. of Illinois Morkoc et al. (1991)	Microwave plasma/ ECR	(001)GaAs	150 A/hr	96 mins. (0.3 μm thick films)
N. C. State Univ. Davis et al. (1989)	Microwave plasma	β -SiC/(001)Si	200 A/hr	Not quoted

β -GaN grown by modified MBE approaches.

Table I.1

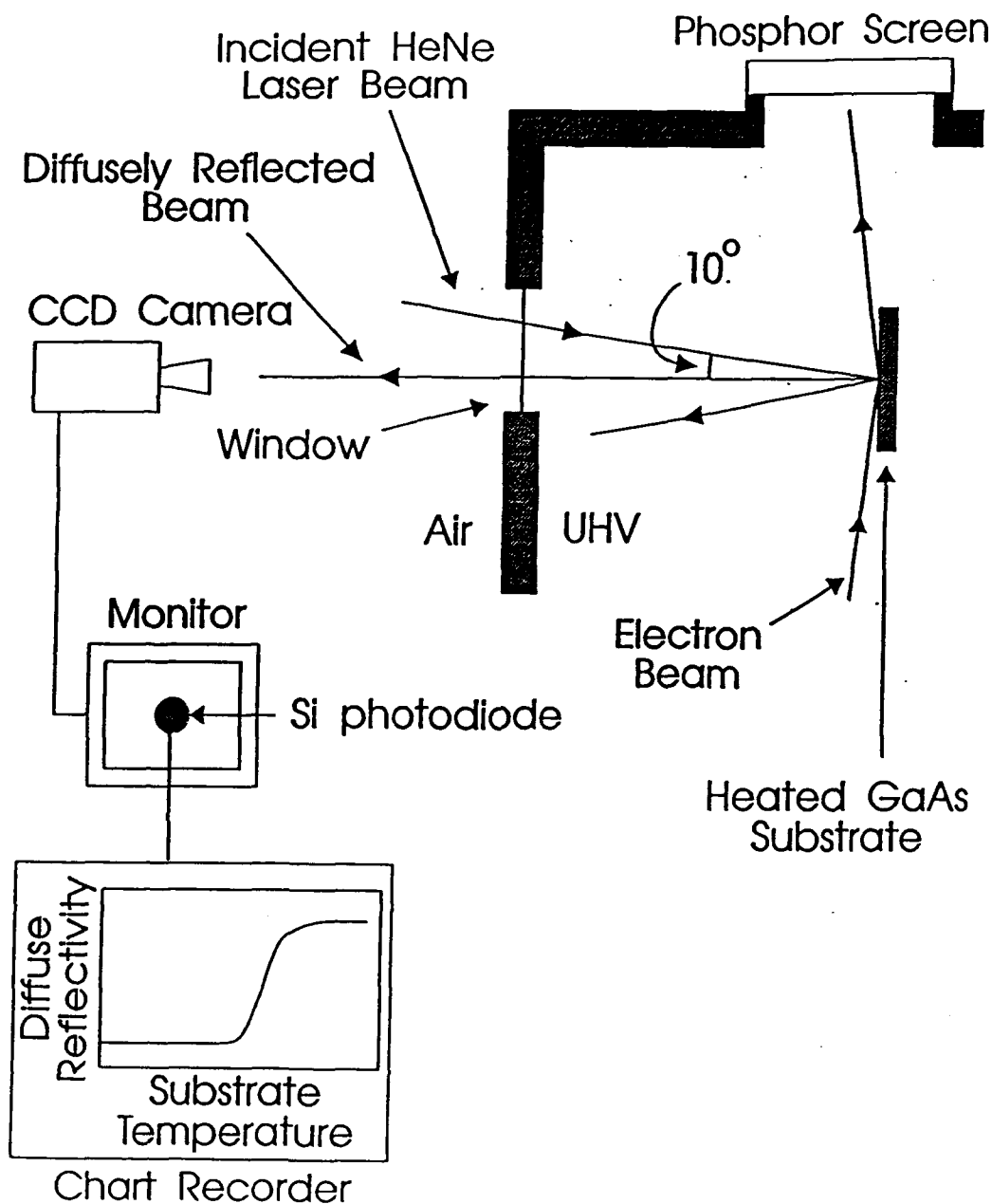


Figure I.1 Schematic of the experimental setup used to characterize the surface morphology of GaAs during cleaning by recording the diffusely reflected HeNe laser light (or lack thereof) generated by virtue of GaAs surface roughening (or lack thereof) during the cleaning procedures discussed in Section III. The geometry indicated in the figure provides for simultaneous reflection high energy electron diffraction analysis as shown.

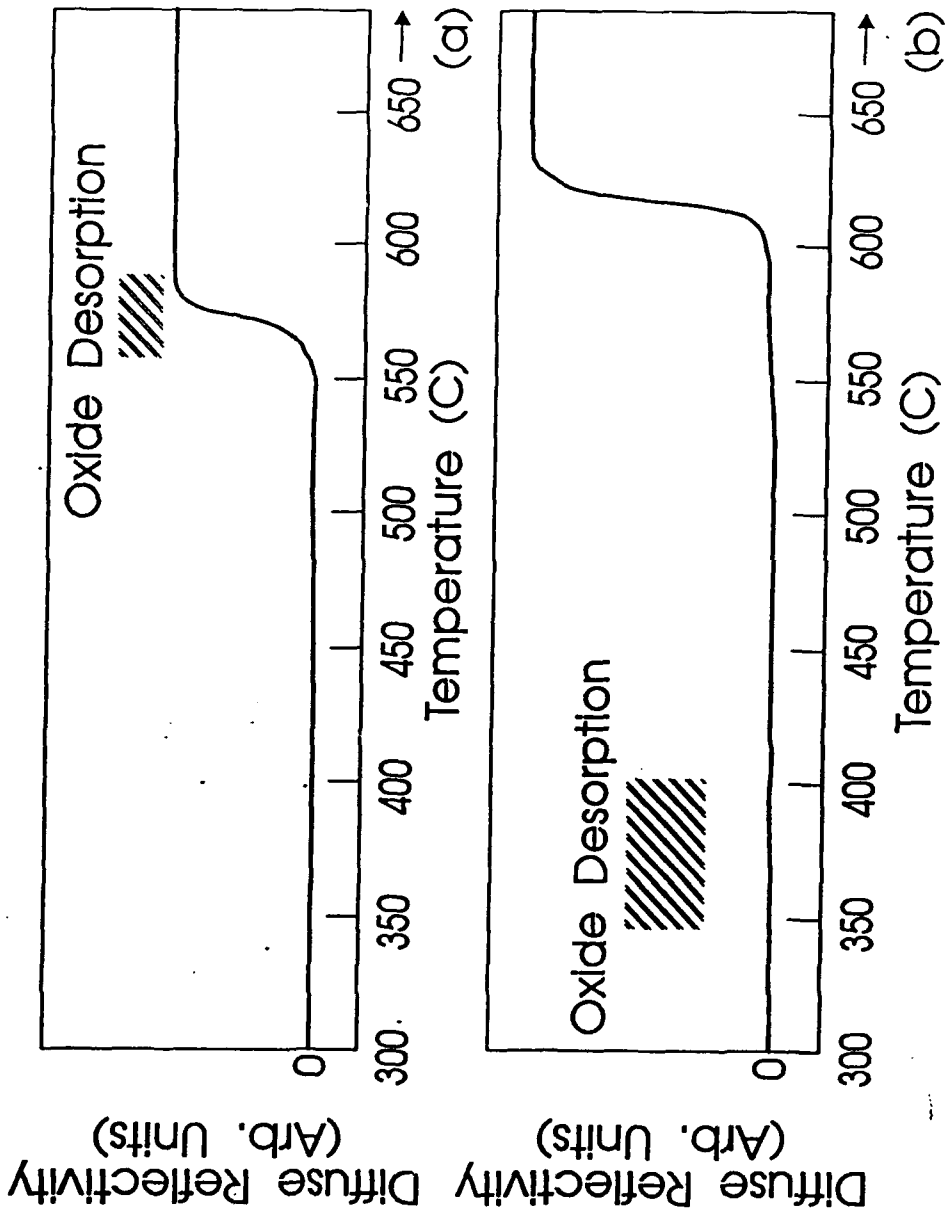
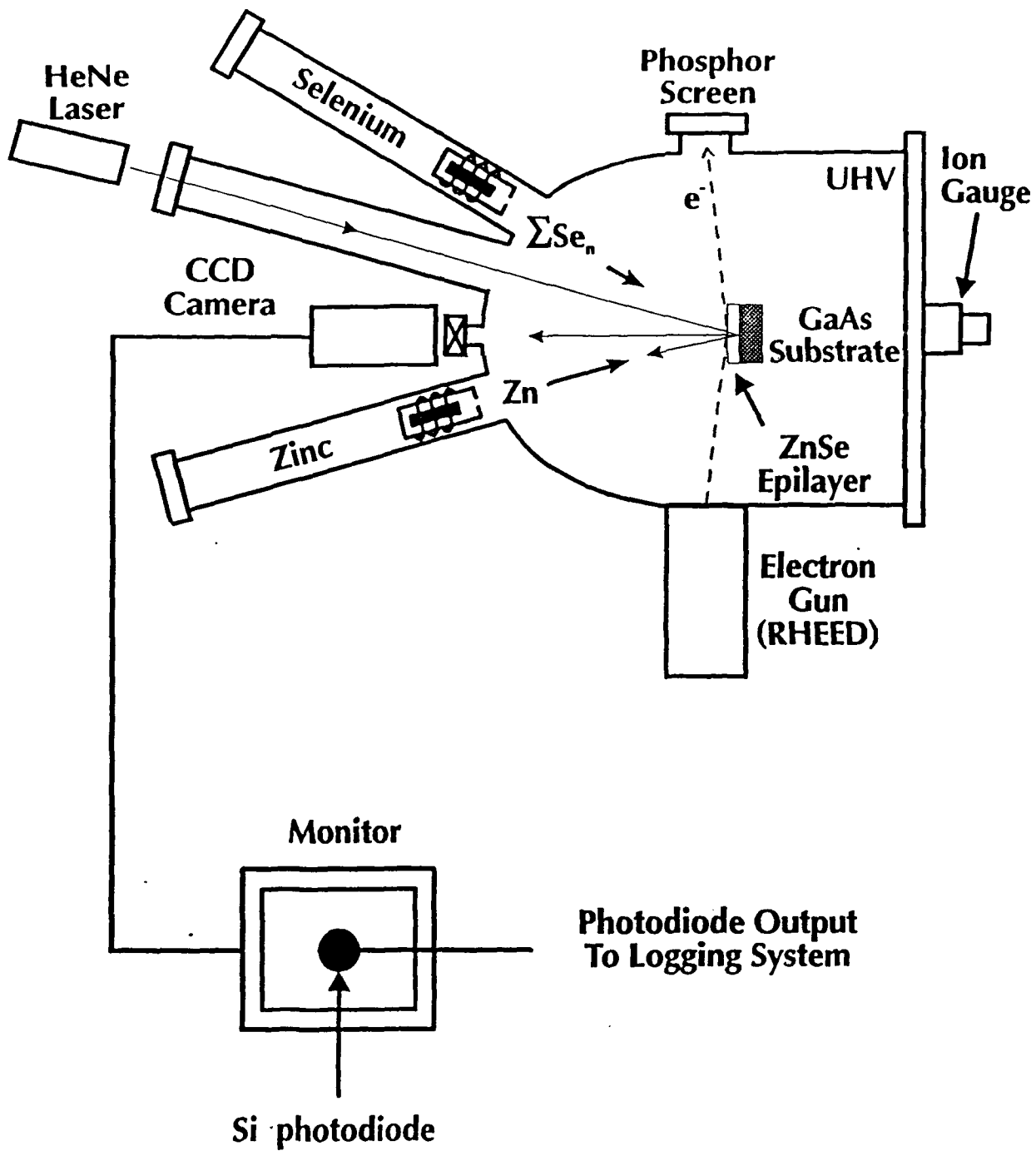


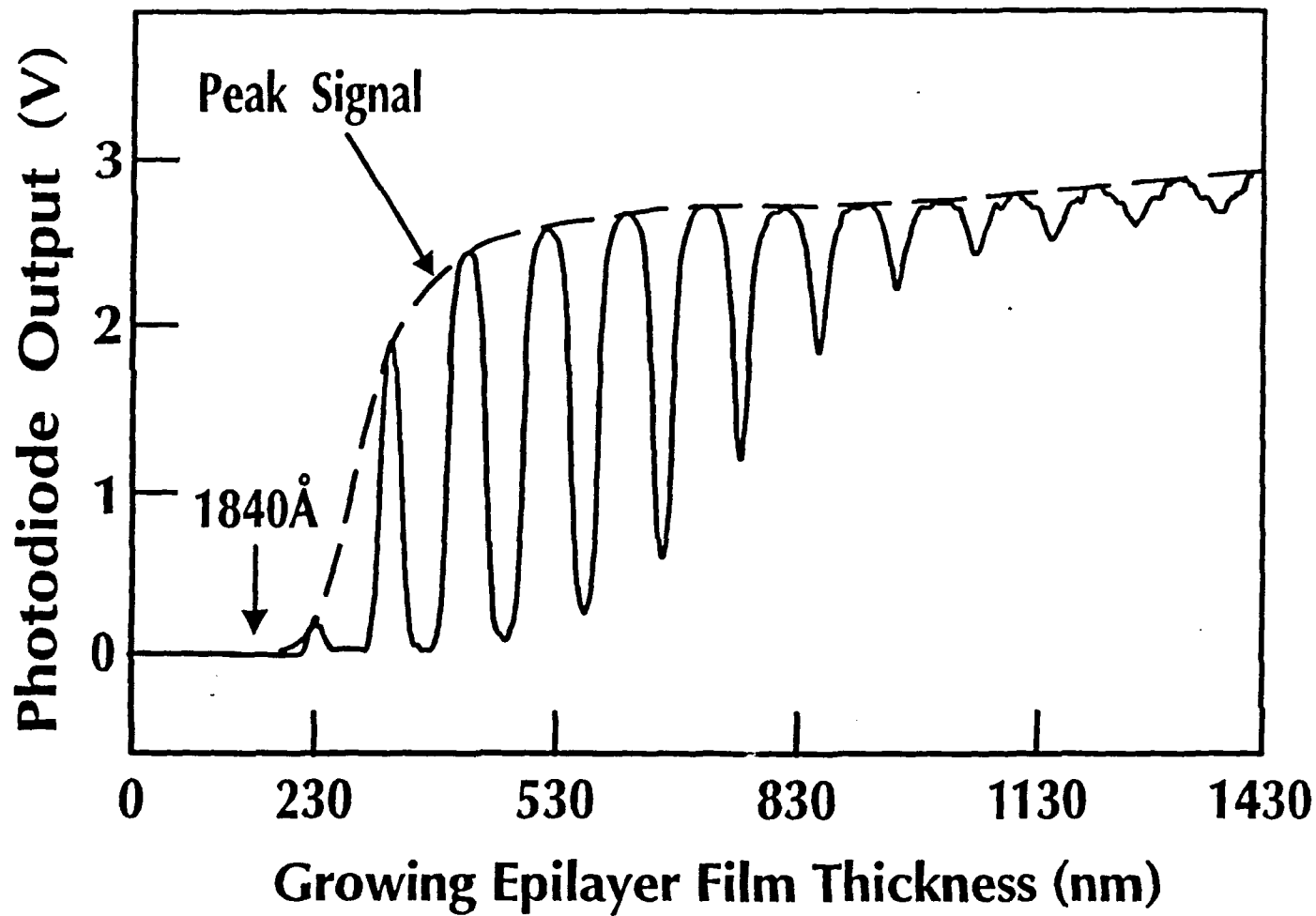
Figure 1.2 Diffuse reflectivity as a function of monitored substrate temperature.

The data was recorded during conventional thermal treatment and during our combined thermal/H-atom treatment of (001)GaAs wafers, (a) and (b) respectively.



Schematic diagram of the experimental setup used to record the elastically scattered HeNe laser light generated by virtue of dislocation evolution upon attainment of the critical thickness ($\sim 1800\text{\AA}$ for ZnSe).

Figure I.3



Intensity of scattering (near the heterointerface) as a function of ZnSe epitaxial layer thickness. Note the optically detectable onset of scattering corresponds to $\sim 1800\text{\AA}$ which is the established critical thickness for ZnSe on GaAs.

Figure I.4

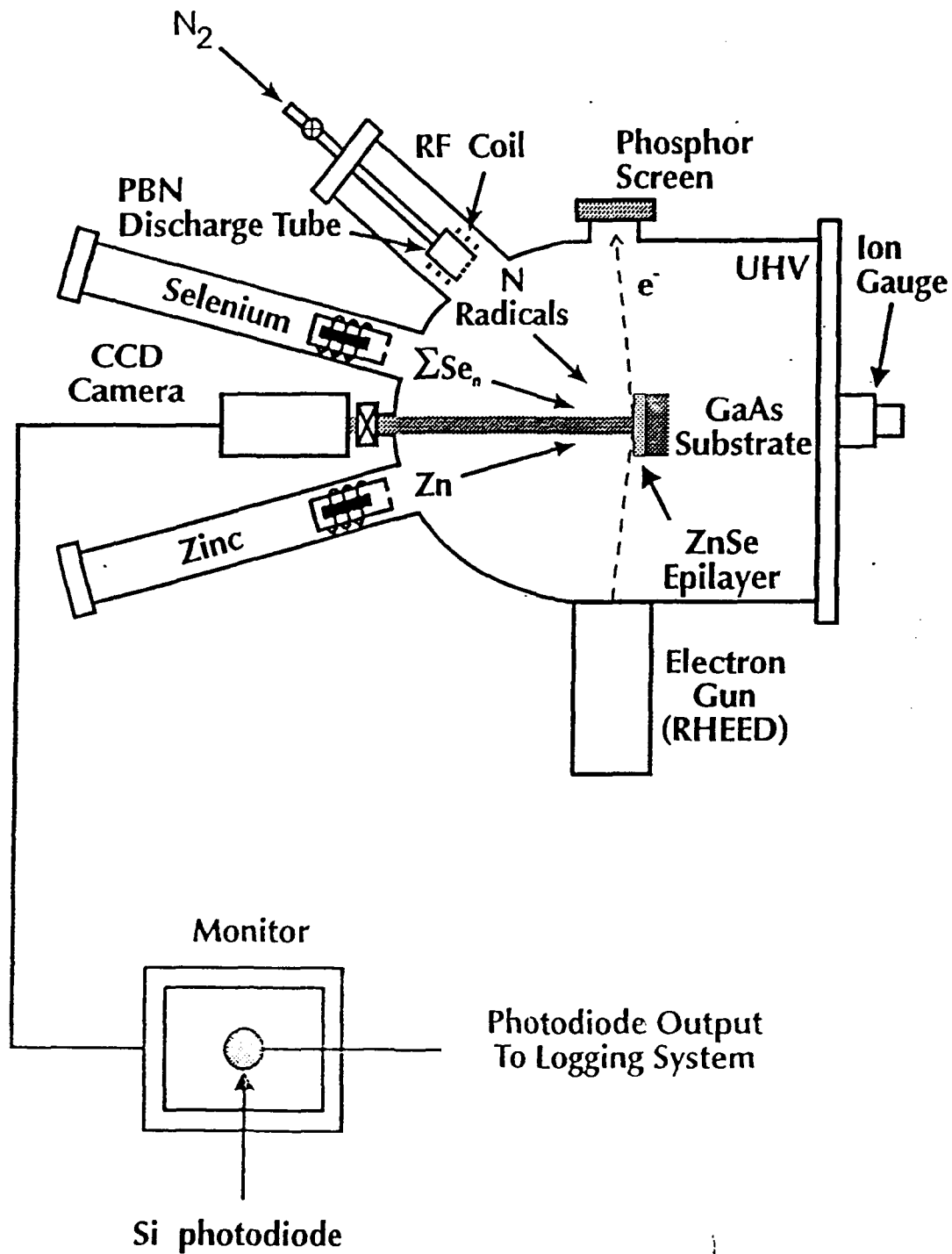
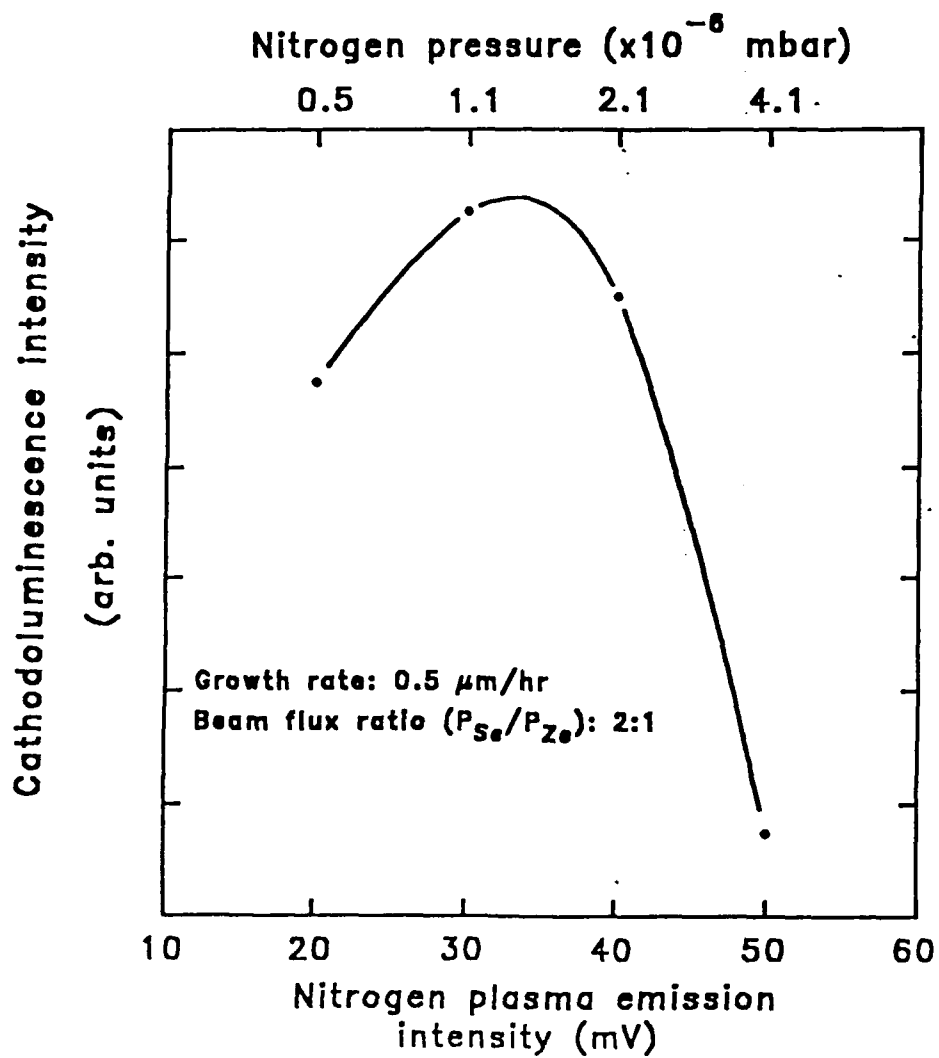
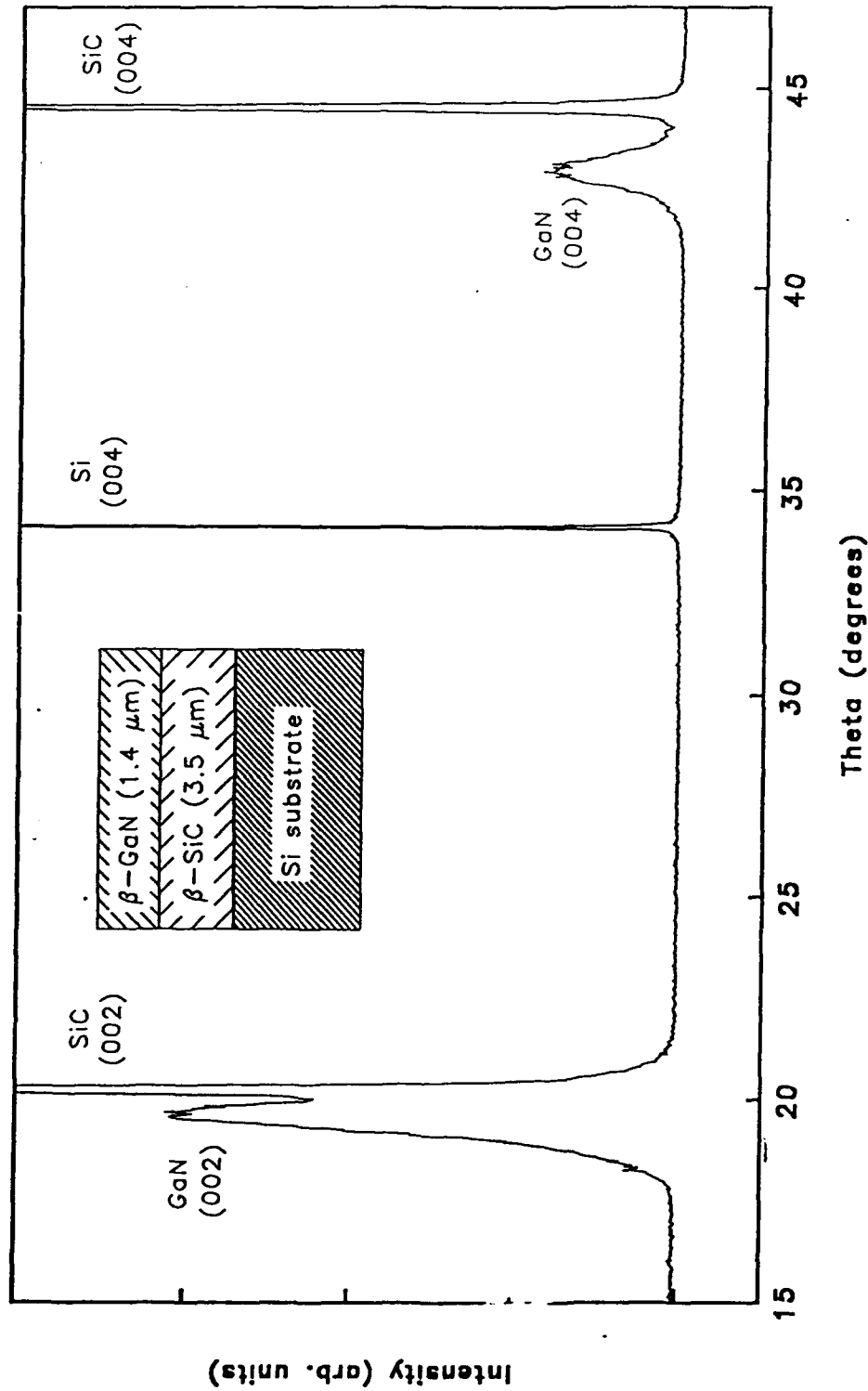


Figure 1.5 Schematic of apparatus used to record in-situ and in real-time the CL emission intensity during the growth of p-type ZnSe:N



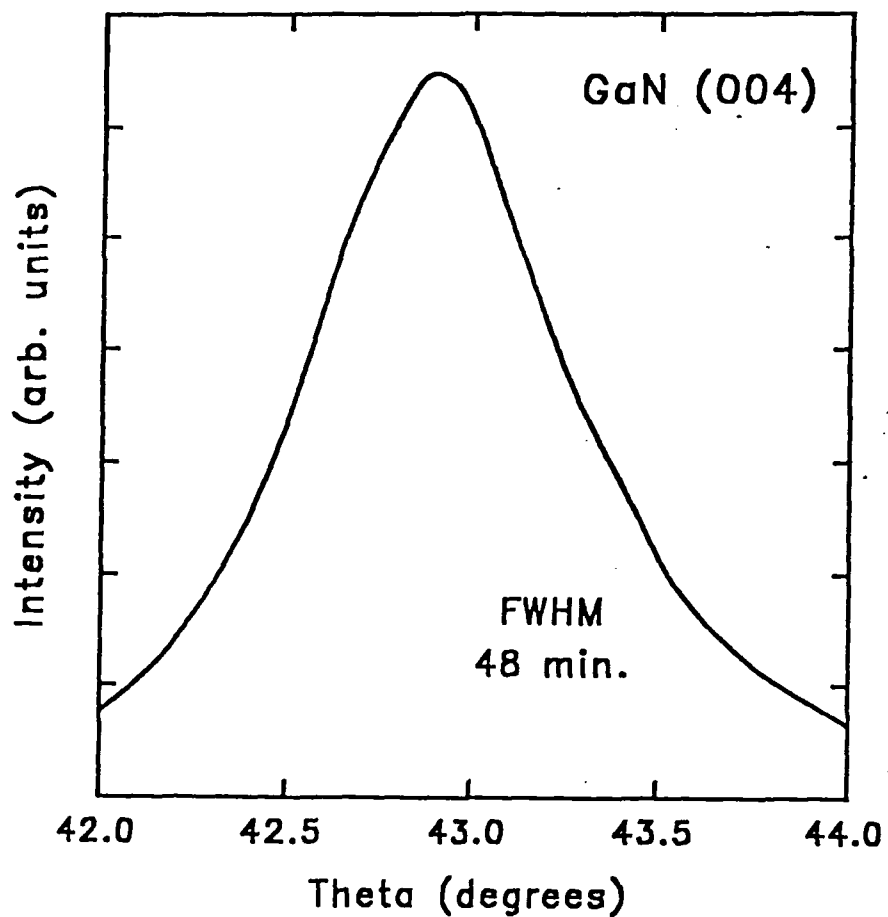
CL intensity recorded in-situ during the growth of p-type ZnSe:N epilayers as a function of nitrogen plasma emission intensity.

Figure I.6



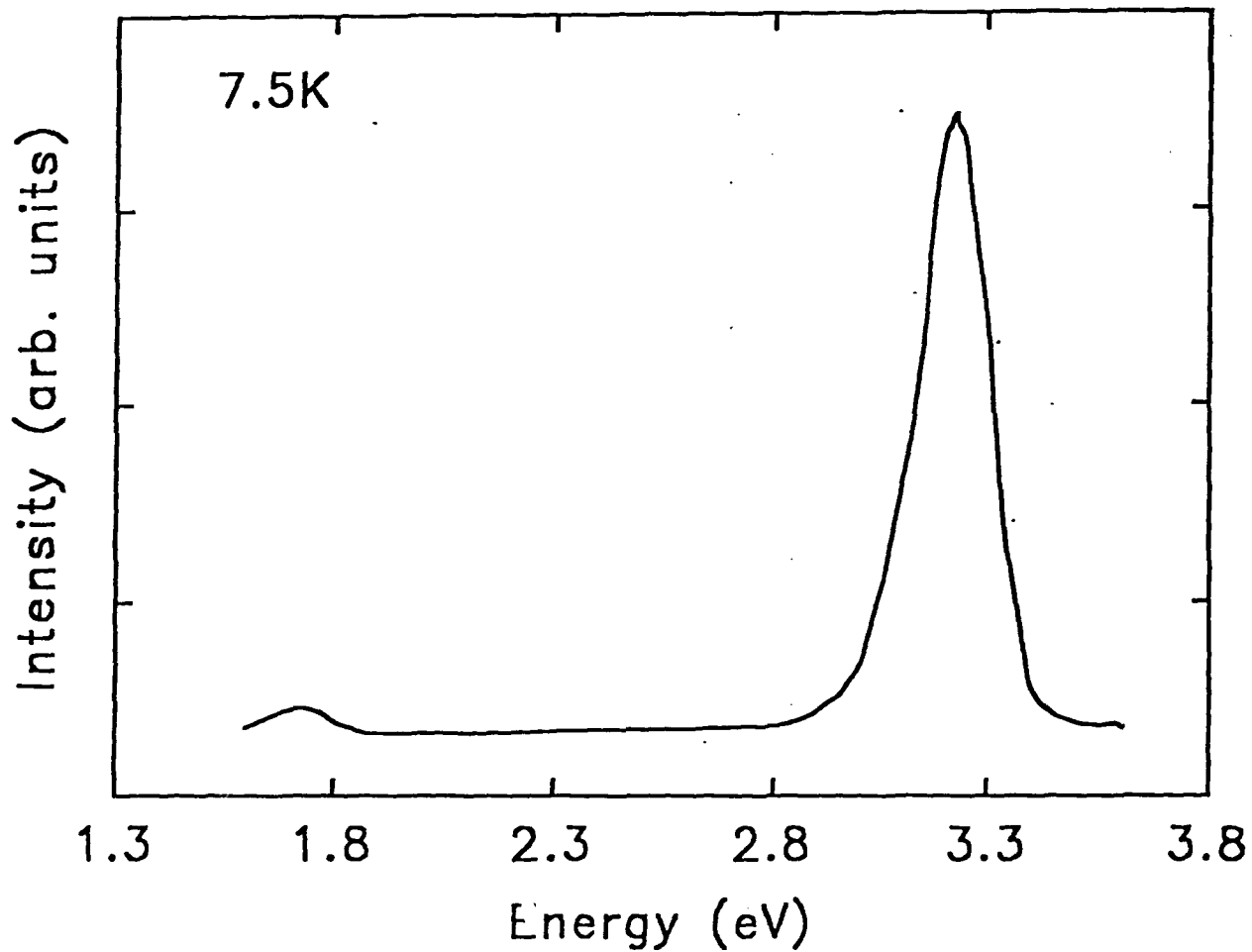
X-ray rocking curve spectrum recorded using a Phillips 5-crystal HR-XRD system (CuK α source) from a 1.4 μm thick zincblende-GaN film grown on β -SiC/(001)Si.

Figure I.7



High-resolution x-ray rocking curve spectrum showing zincblende-GaN (004) reflection.
 β -GaN lattice parameter = 4.50 Å

Figure I.8



PL spectrum recorded at 7.5K from a $1.4\mu\text{m}$ thick zincblende-GaN film grown on $\beta\text{-SiC}/(001)\text{Si}$.
(Spectrum courtesy of Prof. Pankov)

Figure I.9

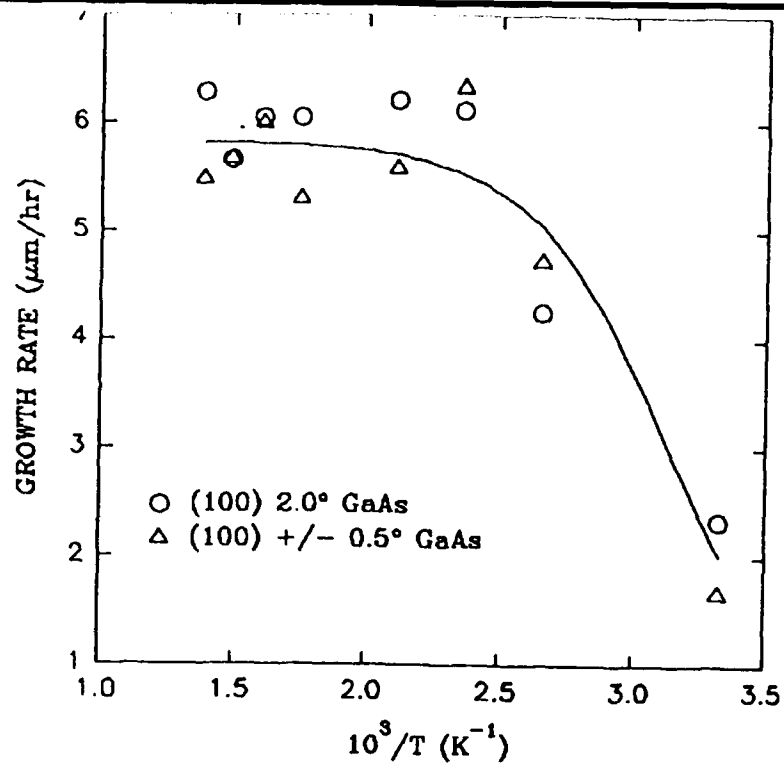


Figure II.1 Growth Rate as a function of substrate temperature.

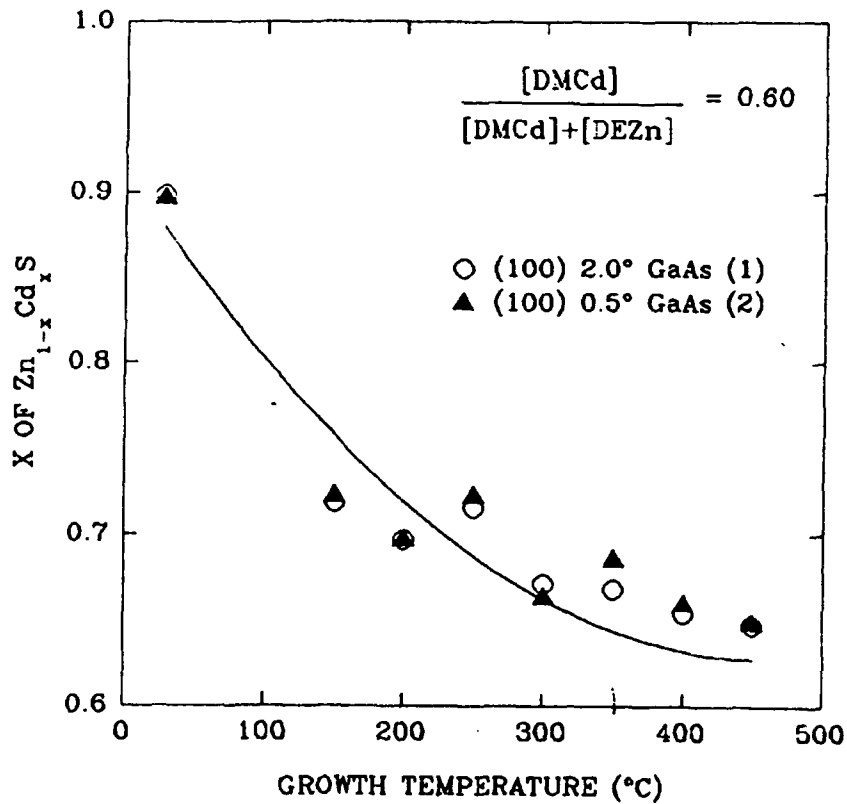


Figure II.2 Film Composition as a function of substrate temperature.

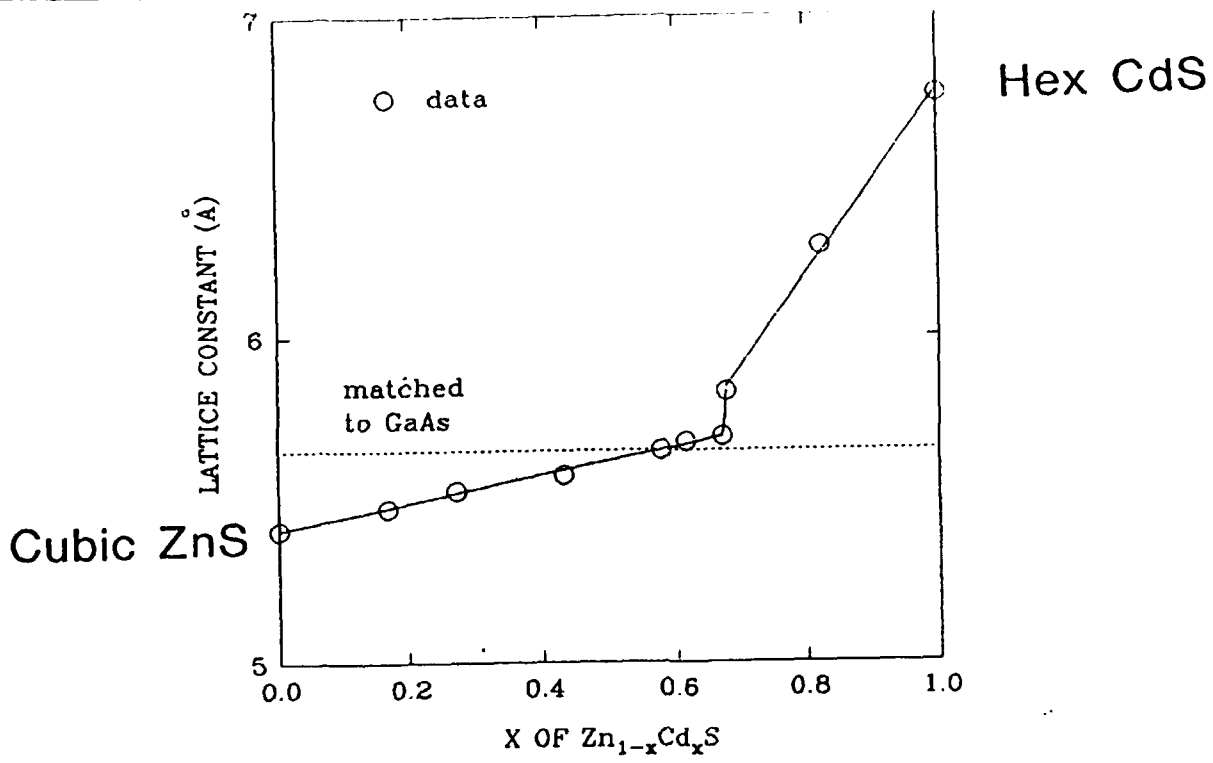


Figure II.3 Variation of film lattice constant (XRD) with film composition (EMPA).

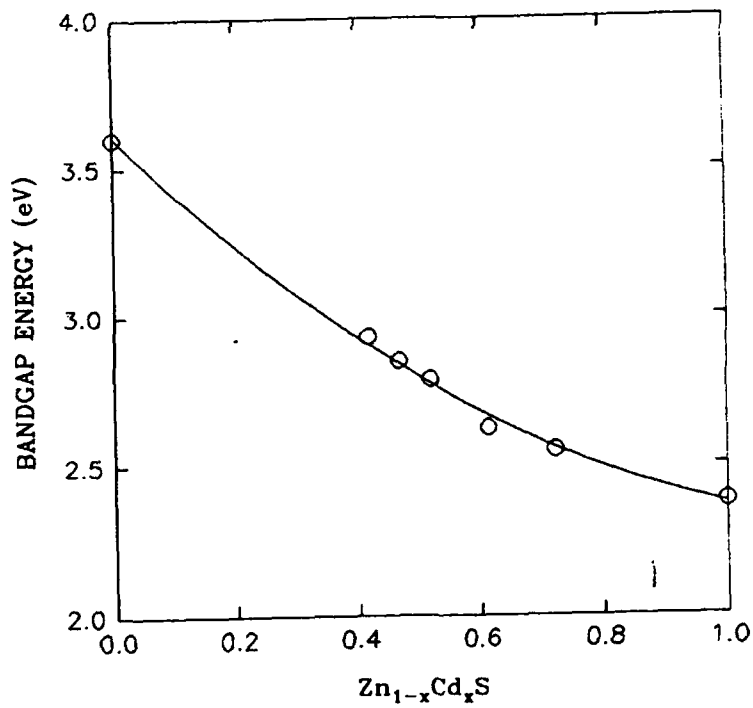
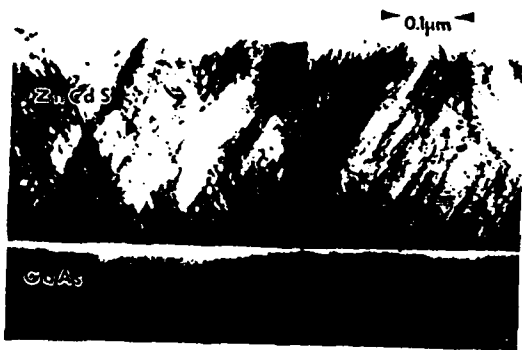
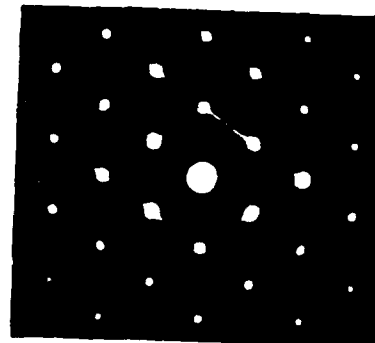


Figure II.4 Variation of bandgap energy (PL) with film composition (EMPA)



Cross Sectional
TEM Micrograph



Electron Diffraction Pattern

Figure II.5 Cross-sectional TEM and electron diffraction patterns for lattice-material film.

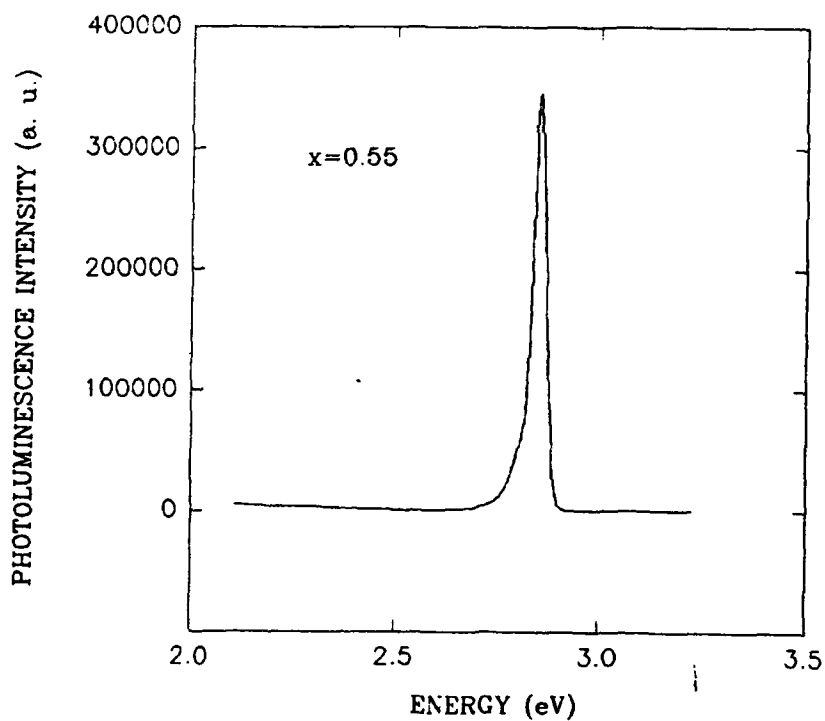


Figure II.6 40K PL spectrum for lattice matched film.

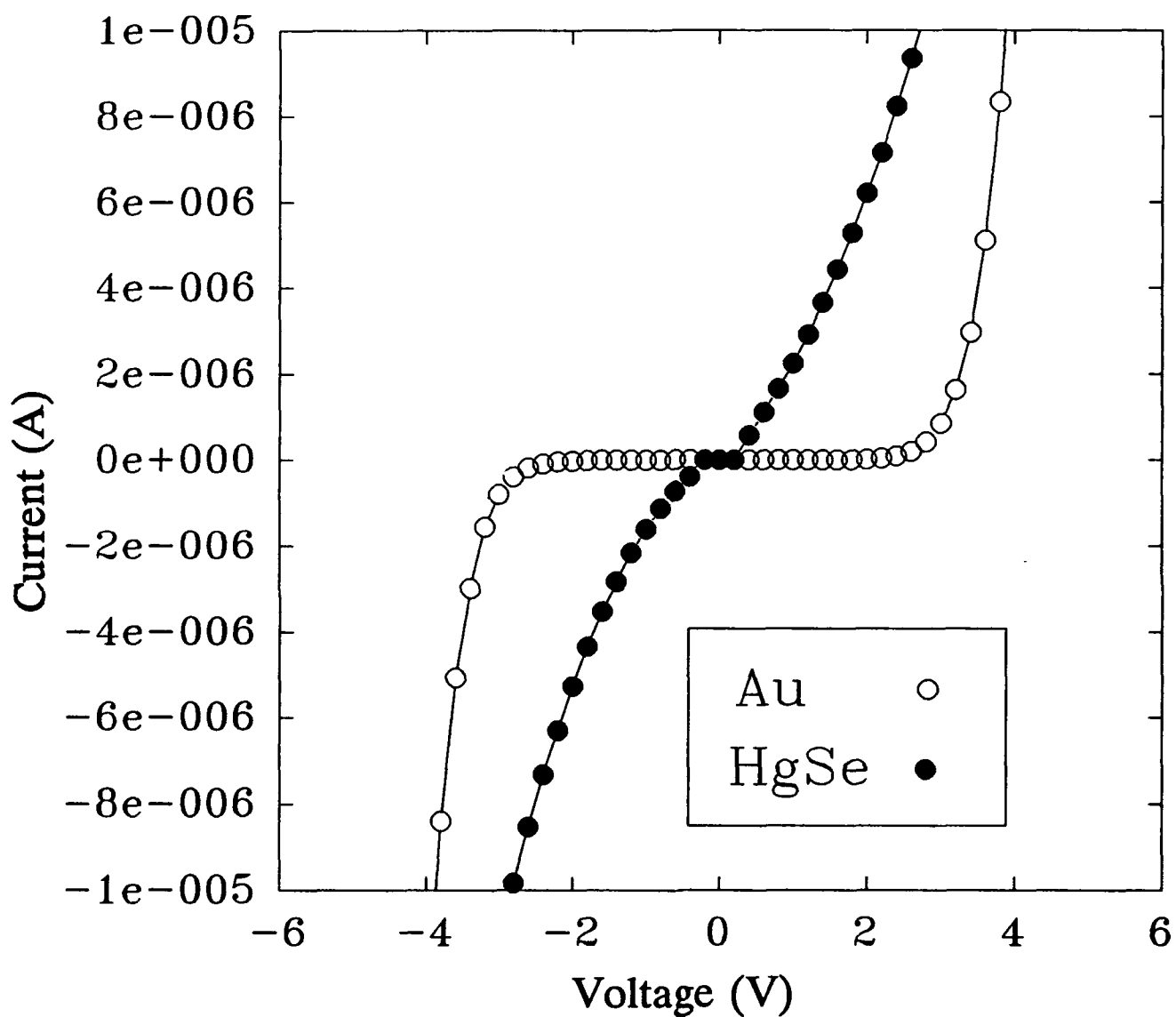


Figure III.1 Current versus voltage data from heat treated Au/p-ZnSe contacts and ex situ grown HgSe contacts.



1. SINGLE DONOR DEFECT STATE:

$$n_e = N_D \left[\frac{1}{1 + 2 \exp[(E_d - \Delta)/kT]} \right] - N_A$$

2. SINGLE DONOR WITH GROUND AND EXCITED STATES:

$$n_e = N_D \left[\frac{1}{1 + 2 \exp[(E_{d1} - \Delta)/kT] + 8 \exp[(E_{d2} - \Delta)/kT]} \right] - N_A$$

excited state energy $E_{d2} = (3.40/13.6) E_{d1}$

3. SINGLE DONOR WITH DOUBLY OCCUPIED STATE:

$$n_e = N_D \left[\frac{1 - \exp[2(E_{d2} - \Delta)/kT]}{1 + 2 \exp[(E_{d1} - \Delta)/kT] + \exp[2(E_{d2} - \Delta)/kT]} \right] - N_A$$

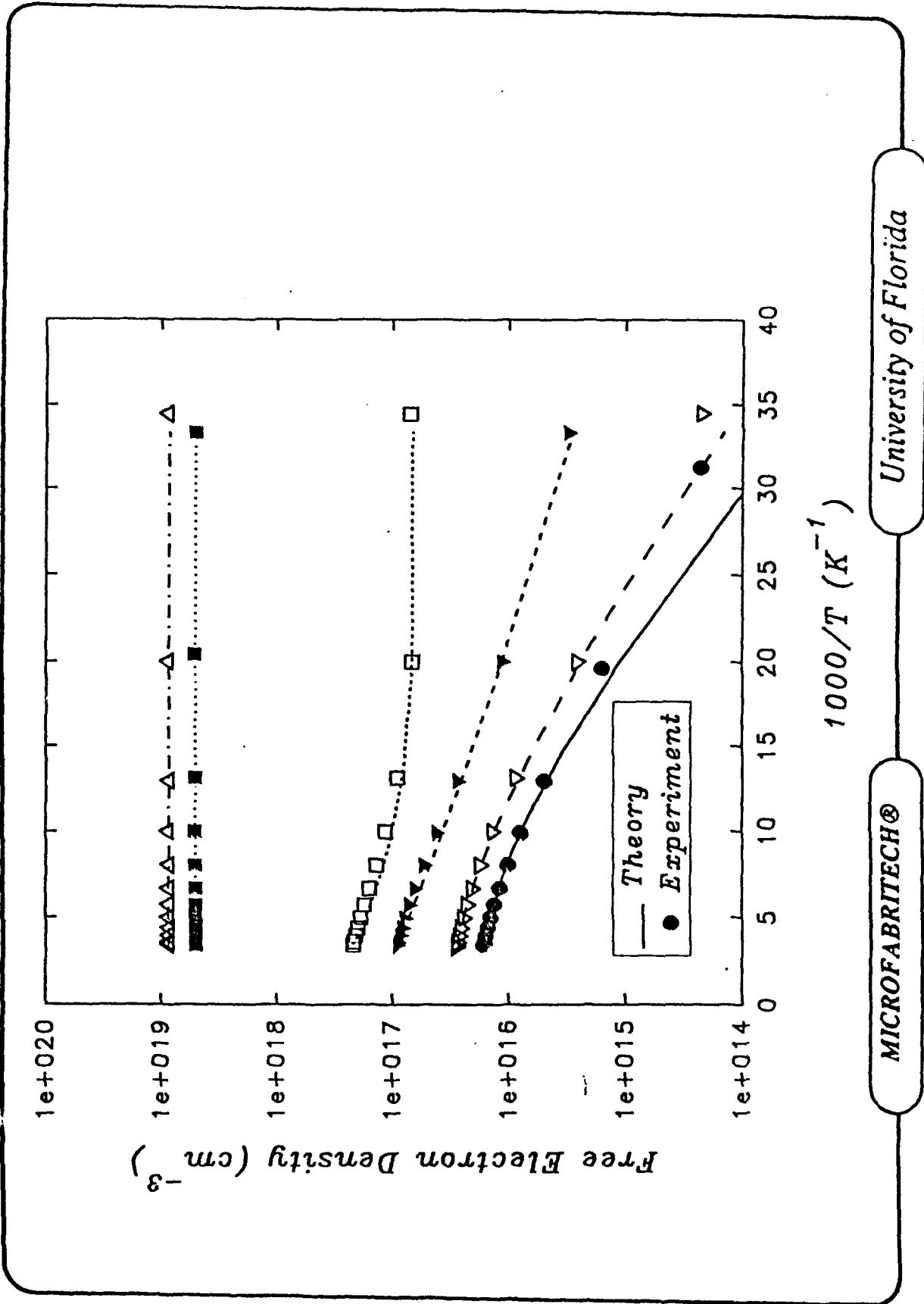
doubly occupied excited state energy $E_{d2} = (0.75/13.6) E_{d1}$

4. DOUBLE DONOR DEFECTS:

$$n_e = N_{D1} \left[\frac{1}{1 + 2 \exp[(E_{d1} - \Delta)/kT]} \right] + N_{D2} \left[\frac{1}{1 + 2 \exp[(E_{d2} - \Delta)/kT]} \right] - N_A$$

5. MOTT CONCENTRATION:

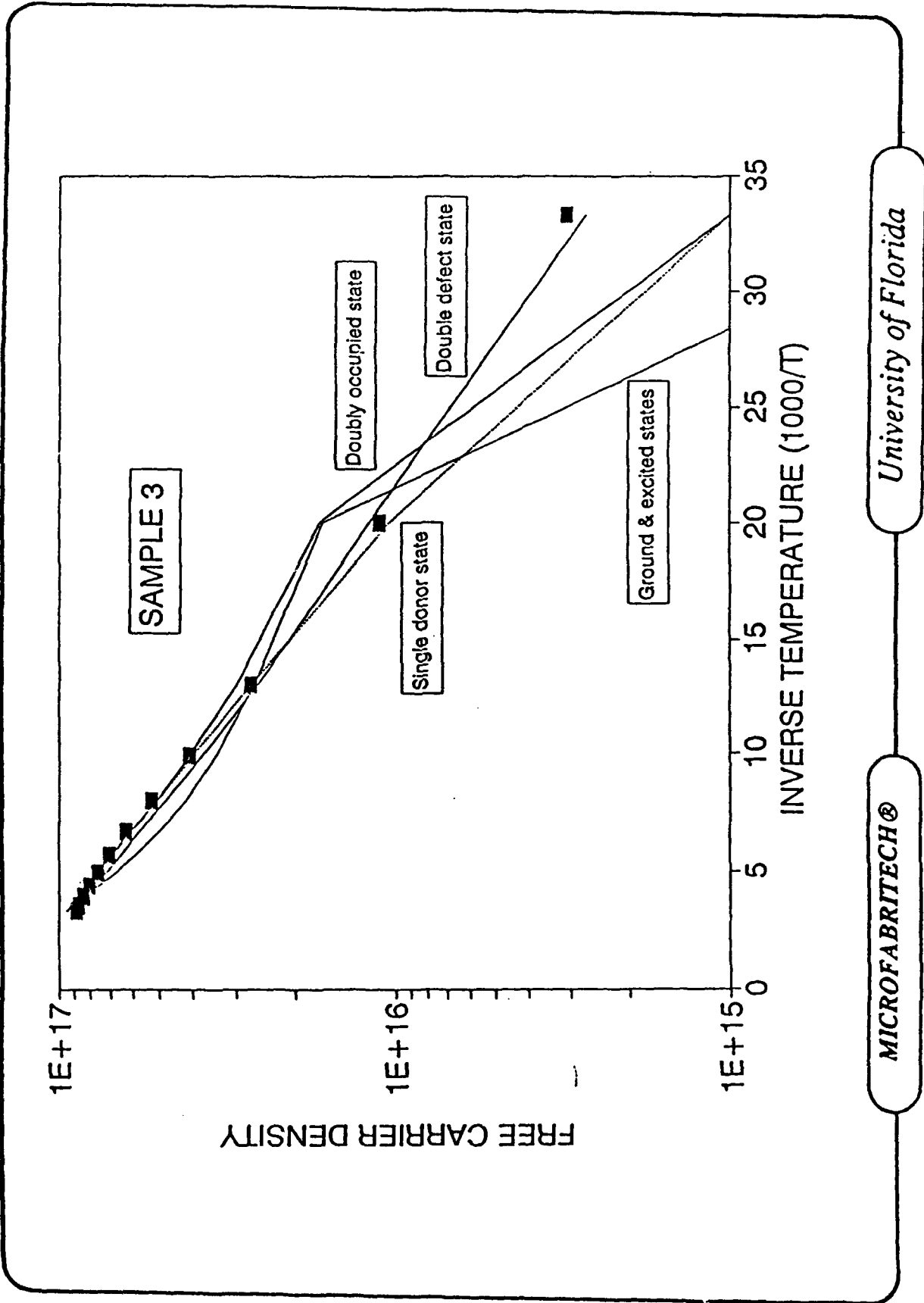
$$n_{Mott} = (0.25/a_H)^3 = 6.62 \times 10^{17} \text{ cm}^{-3}$$



MICROFABRITECH®

University of Florida

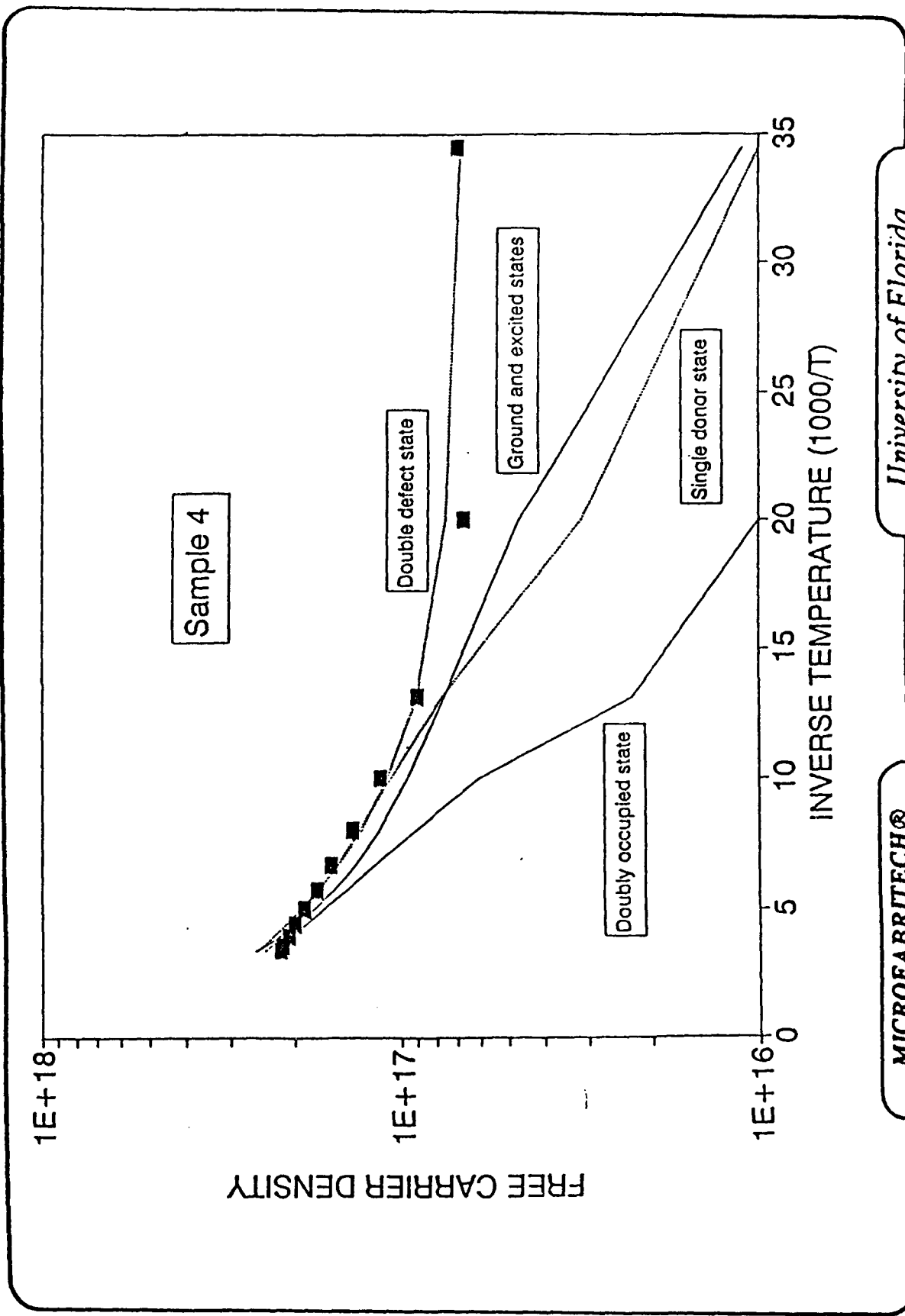
Figure VI.1



University of Florida

MICROFABRITECH®

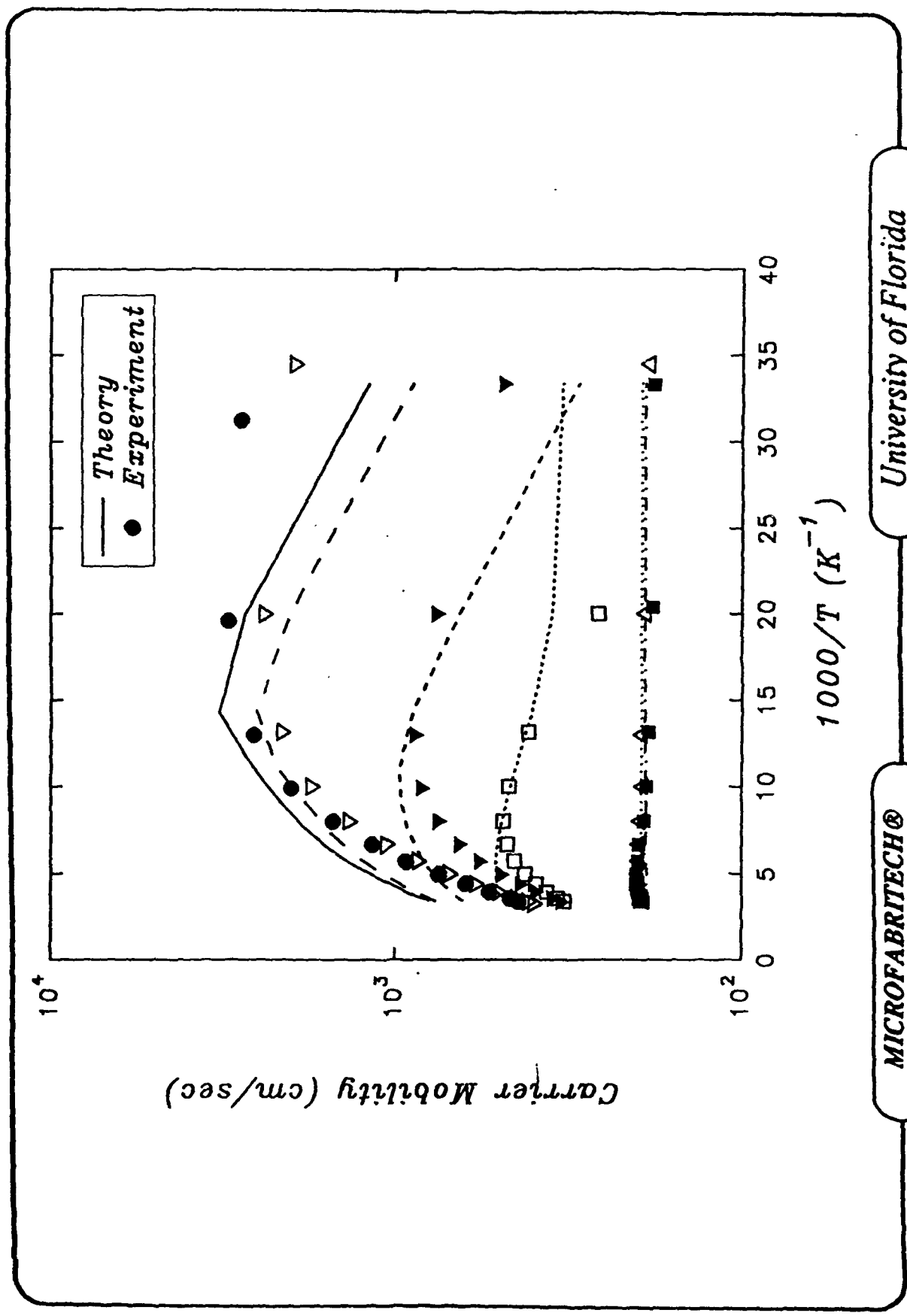
Figure VI.2



University of Florida

MICROFABRITECH®

Figure VI.3



University of Florida

MICROFABRITECH®

Figure VI.4

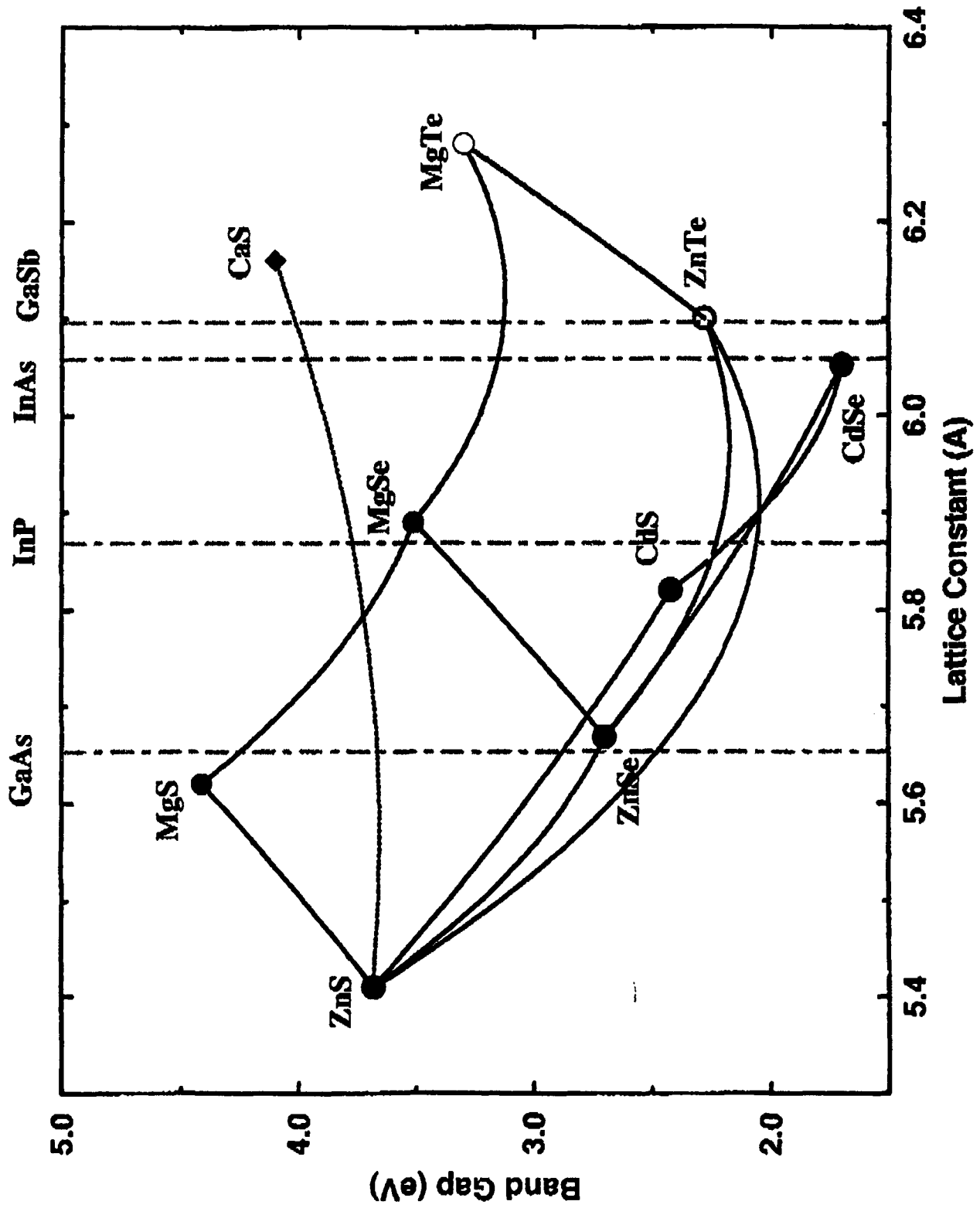


Figure IX.1

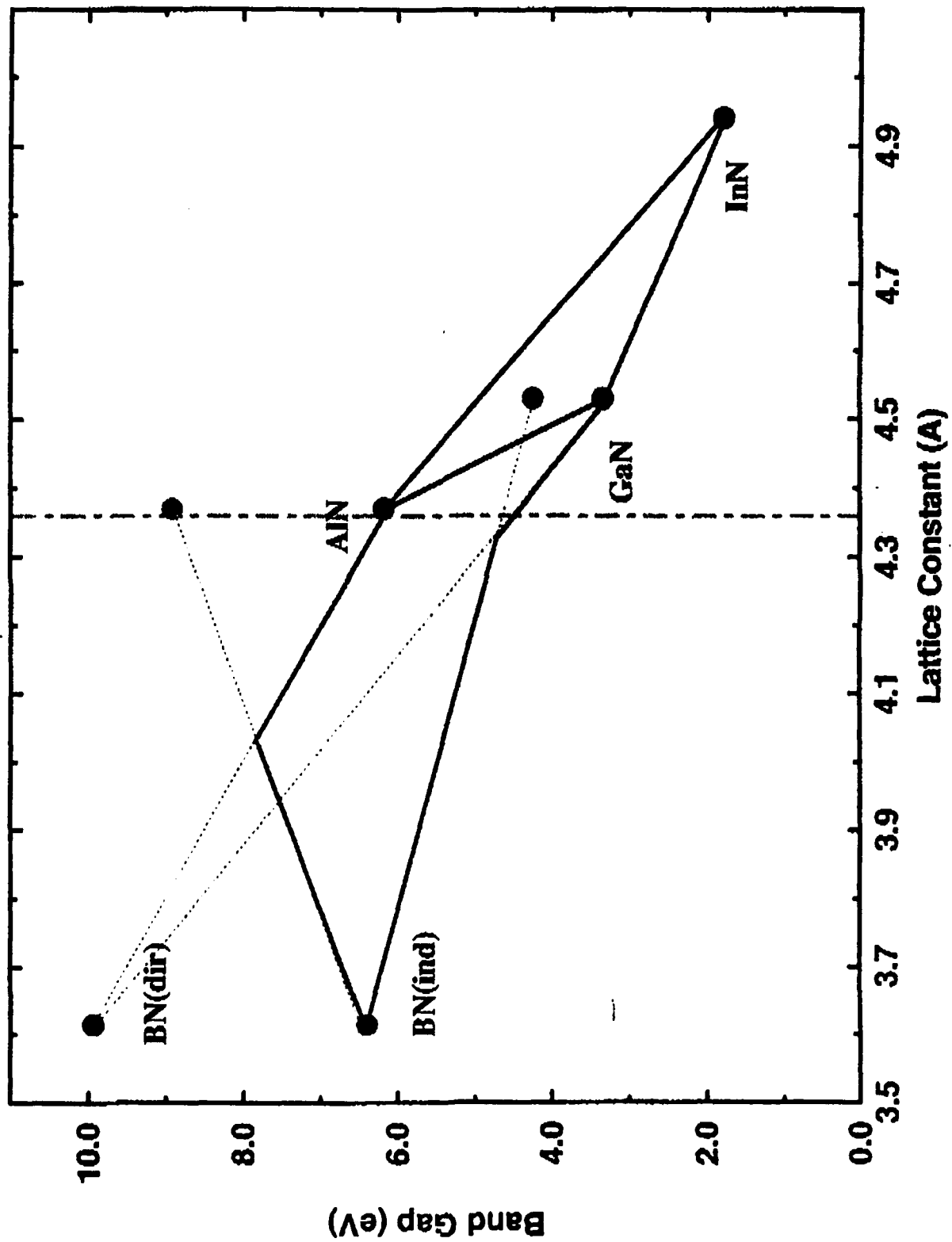


Figure IX.2

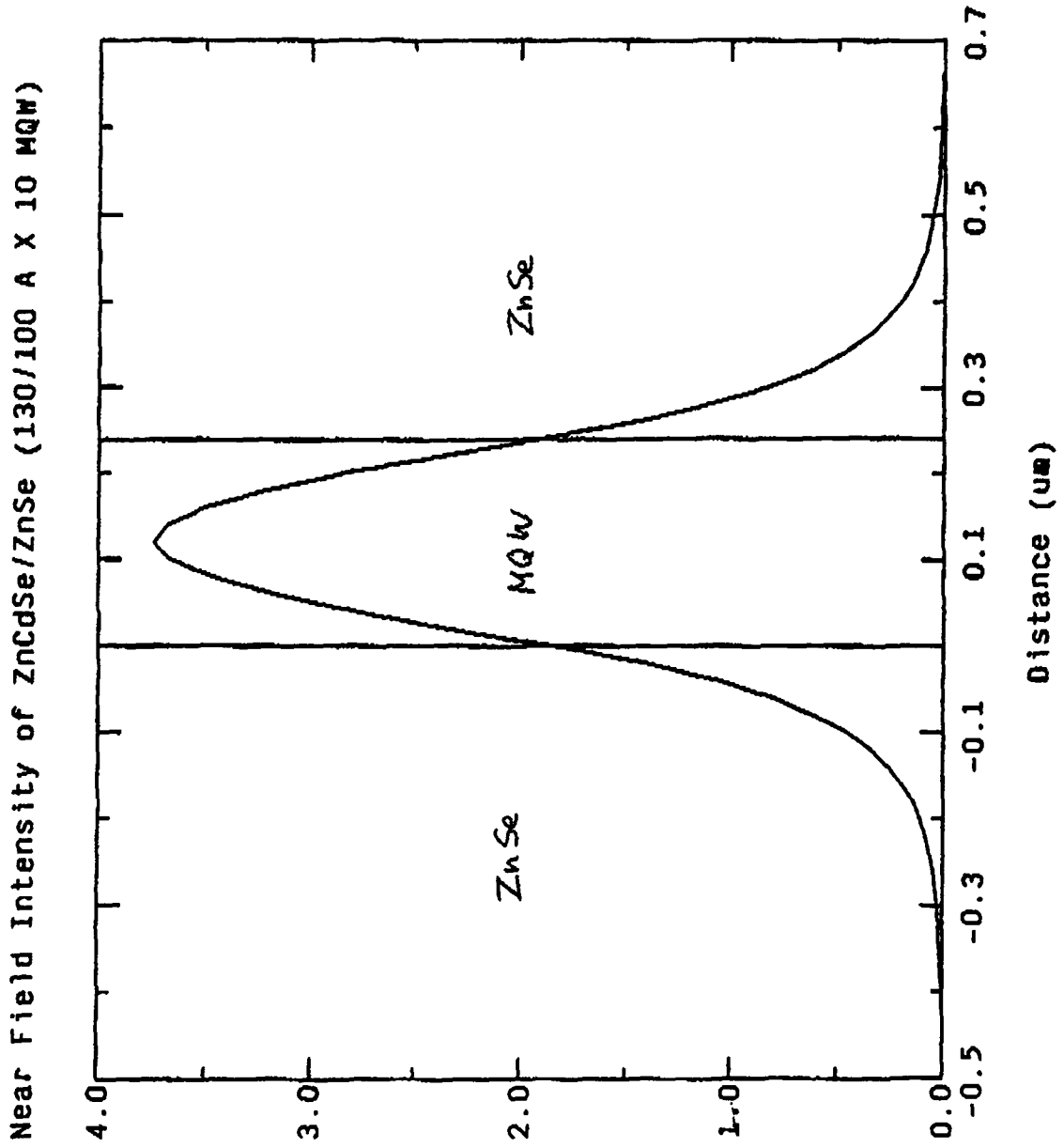


Figure IX.3

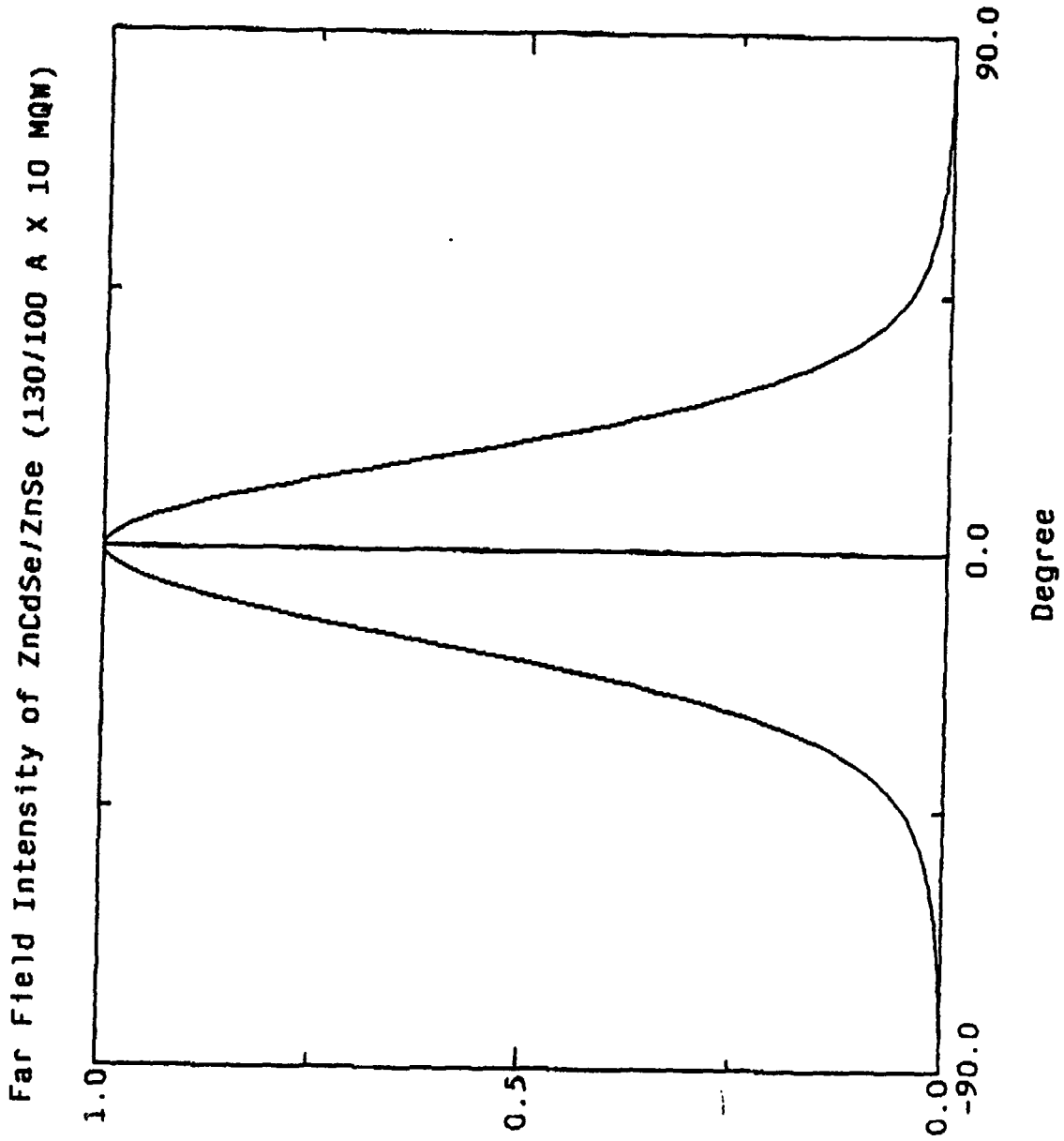
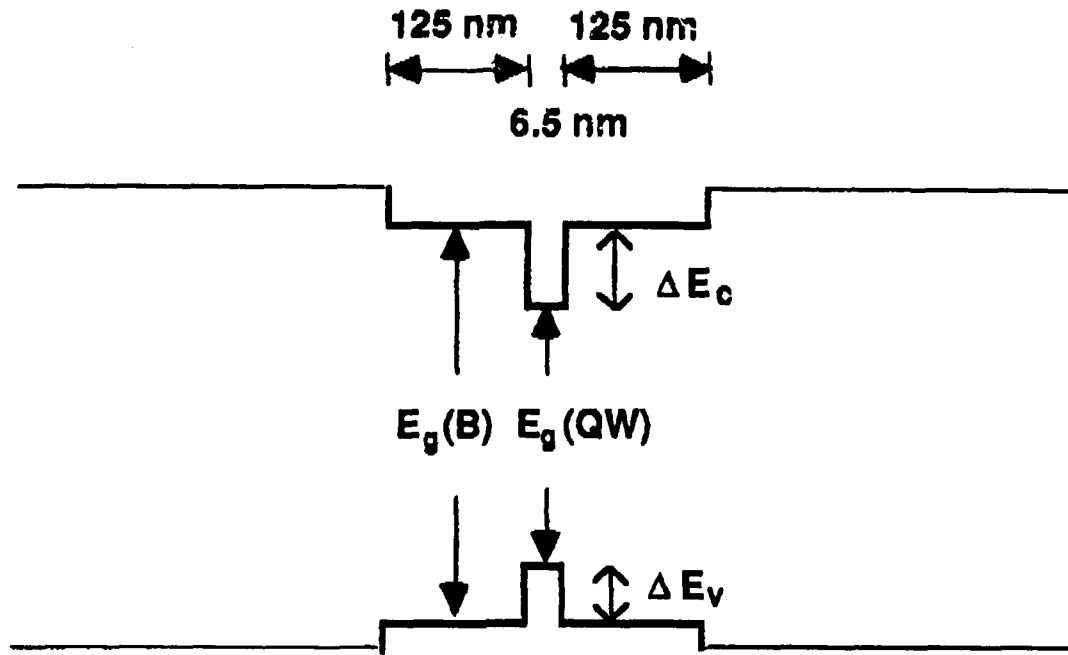


Figure IX.4

• Several SCH Structures with ZnCdSe QW



QW $Cd_{0.2}Zn_{0.8}Se$ $E_g(QW) = 2.46 \text{ eV}$	Barrier Material	Barrier Band Gap $E_g(B)$	Band offset ratio $Q_c = \Delta E_c / \Delta E_g$
SCH 1	ZnSe	2.70 eV	0.75
SCH 2	$ZnS_{0.06}Se_{0.95}$	2.73 eV	0.53
SCH 3	$Mg_{0.05}Zn_{0.95}S_{0.1}Se_{0.9}$	2.79 eV	0.50

Figure IX.5

Gain Spectra (TE) of 6.5 nm SQW at 300K Cd_{0.2}Zn_{0.8}Se/ZnSe

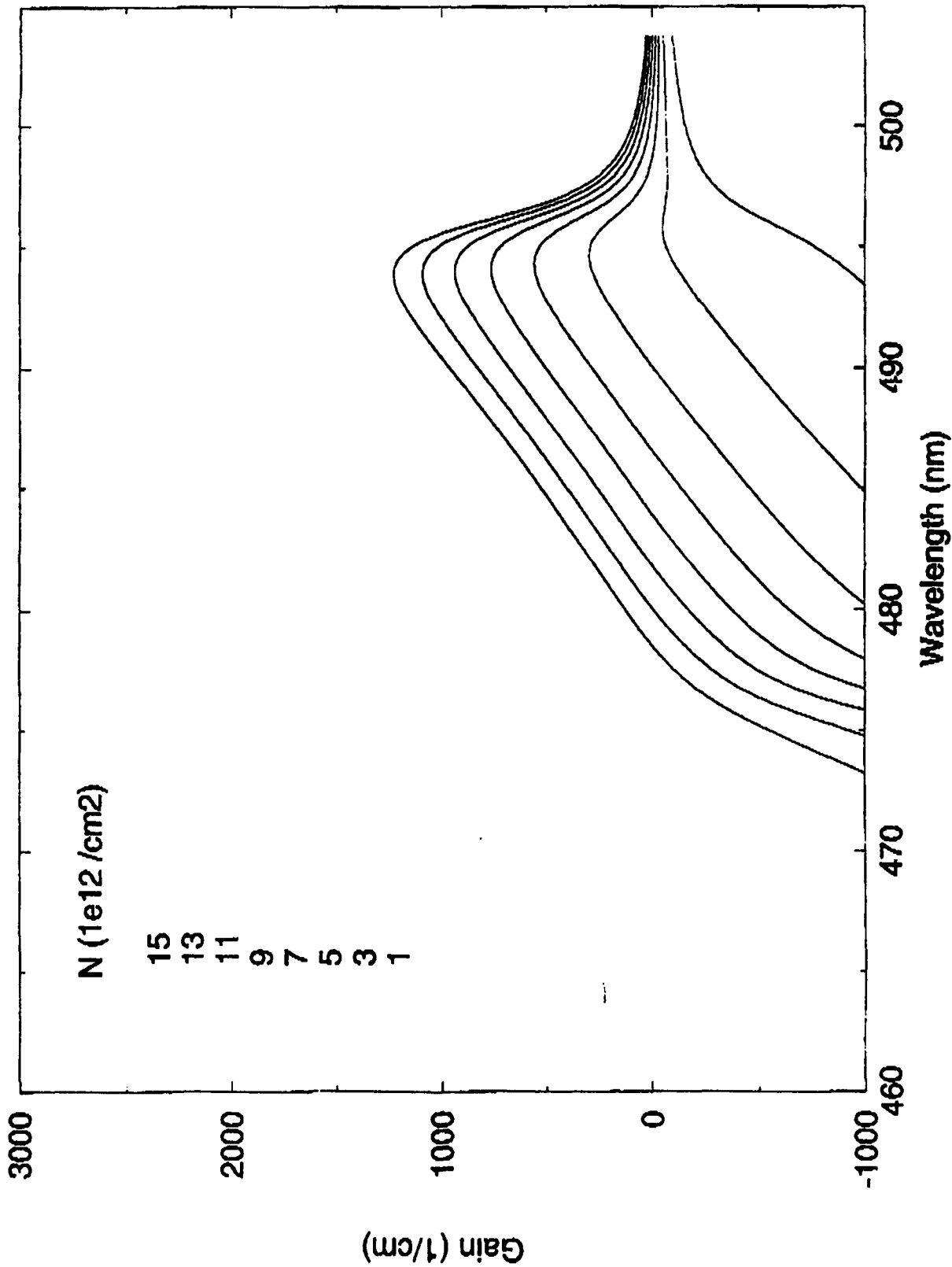


Figure IX.6

Gain Spectra (TE) of 6.5 nm SQW at 300K Cd_{0.2}Zn_{0.8}Se/ZnS_{0.06}Se_{0.94}

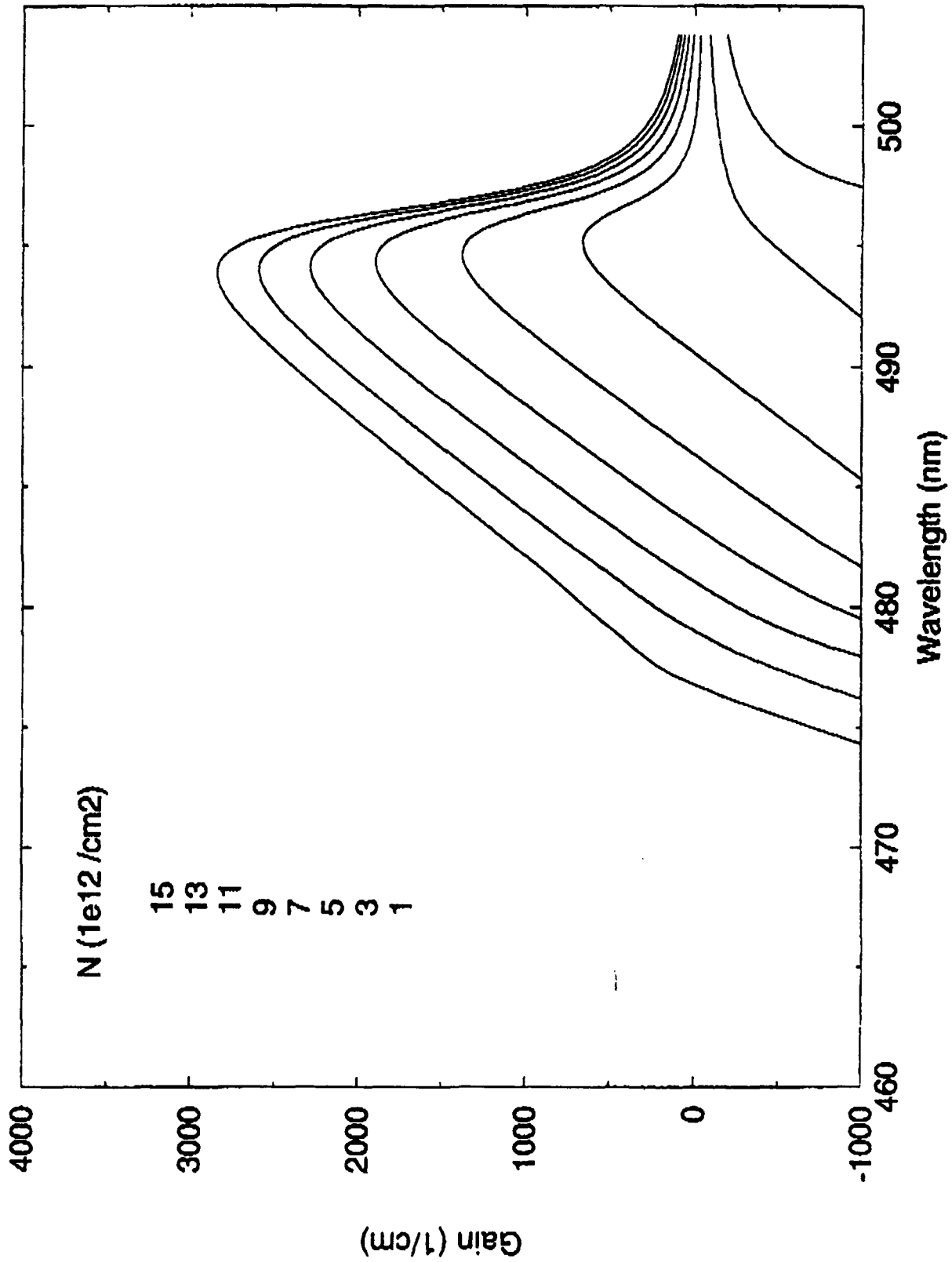


Figure IX.7

Gain Spectra (TE) of 6.5 nm SQW at 300K Cd_{0.2}Zn_{0.8}Se/Mg_{0.05}Zn_{0.95}S_{0.1}Se_{0.9}

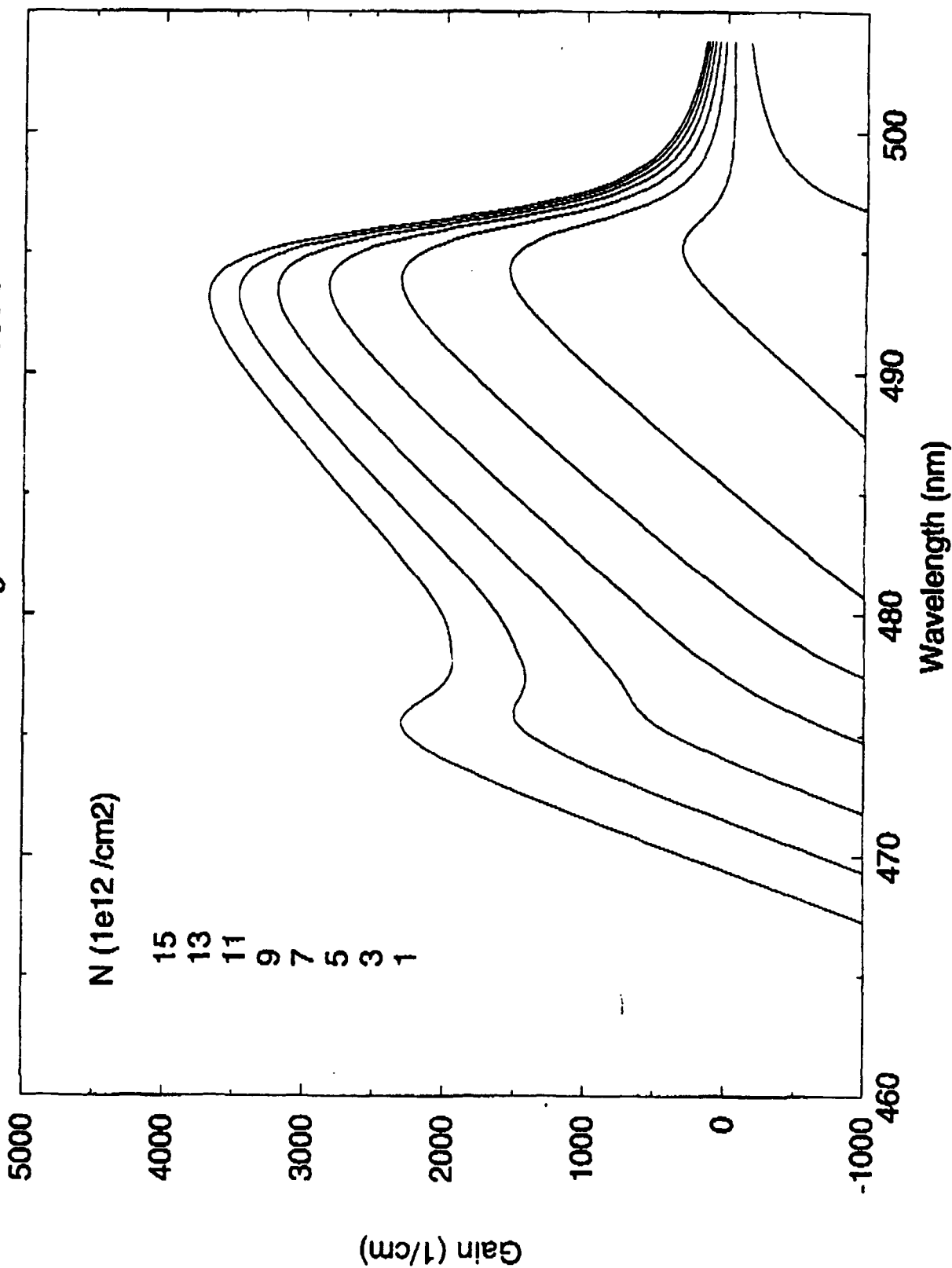


Figure IX.8

Maximum Local Gain vs. Carrier Density

6.5nm ZnCdSe SQW, TE polarization, T=300K

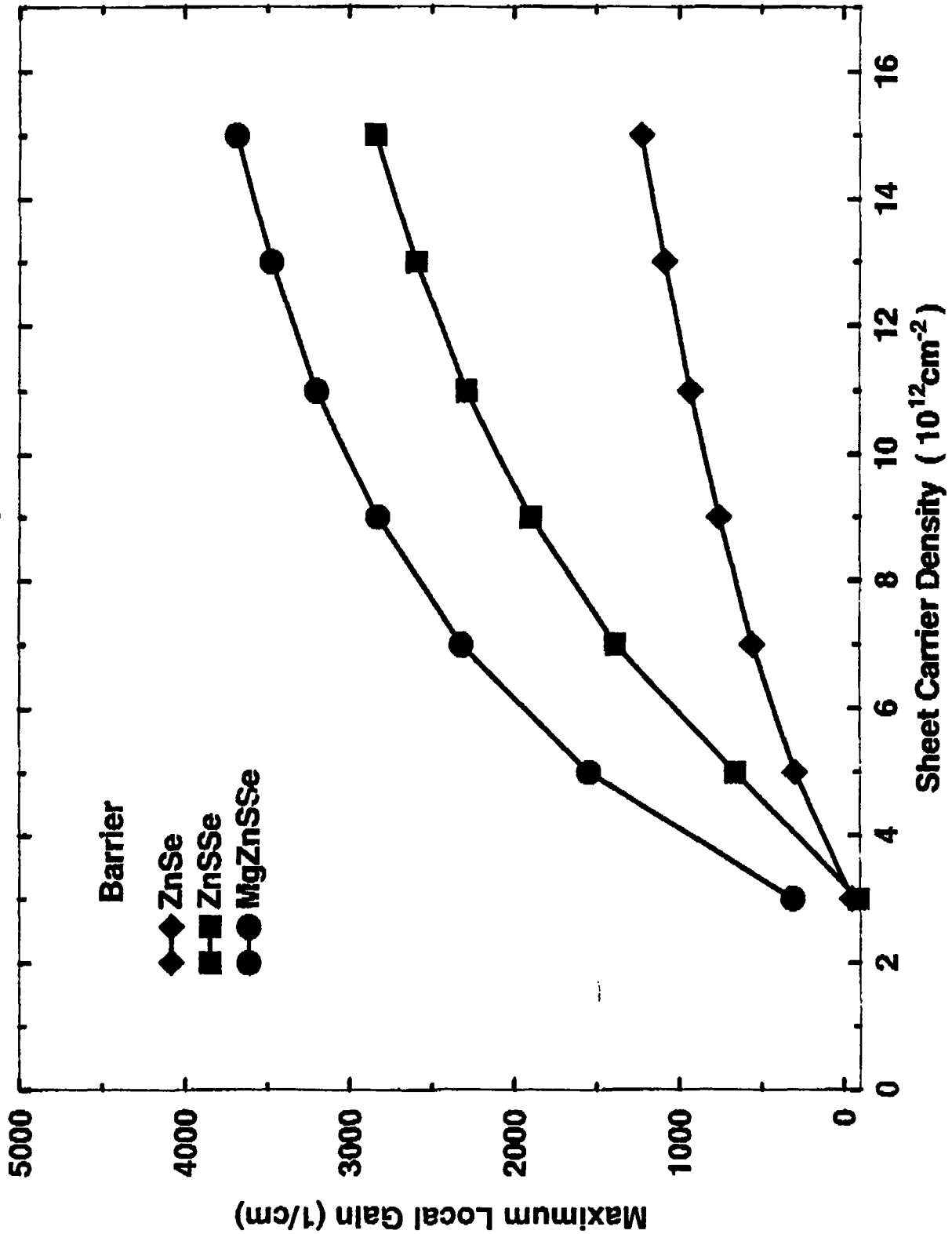


Figure IX.9

Carrier Distribution in QW and Barrier
Sch 1 : ZnCdSe/ZnSe, 6.5 nm QW, Qc=0.75

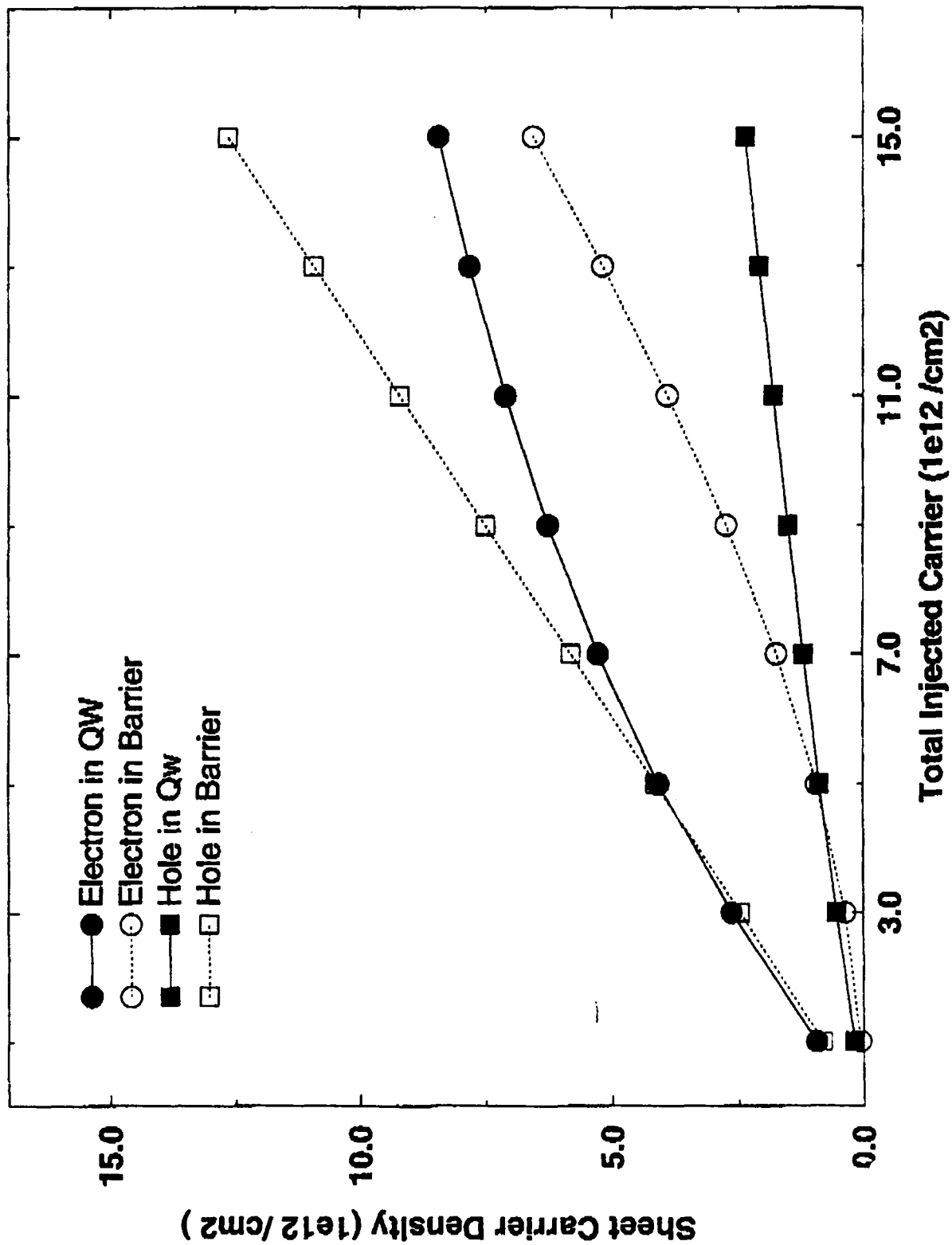


Figure IX.10

Carrier Distribution in QW and Barrier Sch 2 : ZnCdSe/ZnSSe, 6.5 nm QW, $Q_c=0.53$

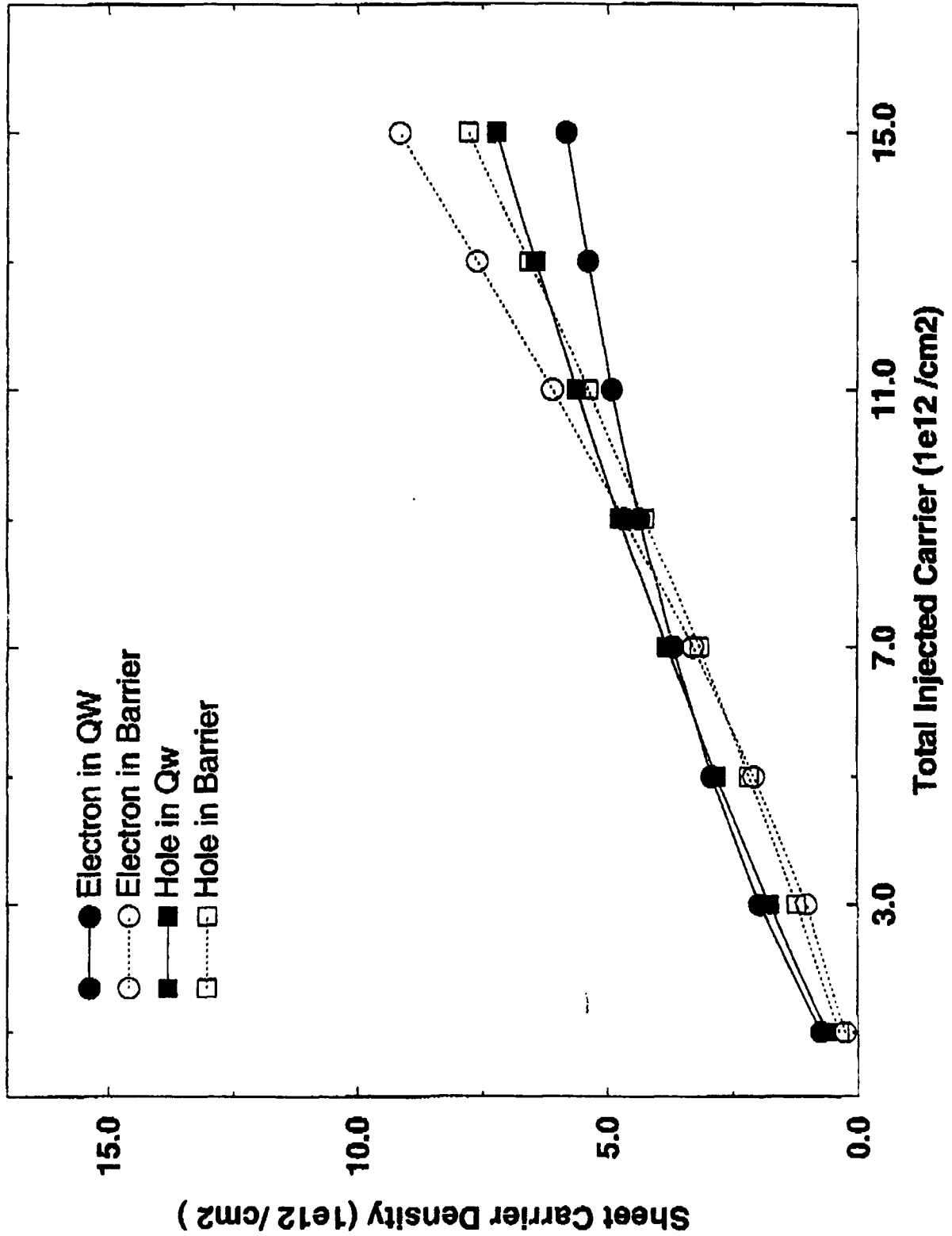


Figure IX.11

Carrier Distribution in QW and Barrier
Sch 3 : ZnCdSe/MgZnSse, 6.5 nm QW, Qc=0.5

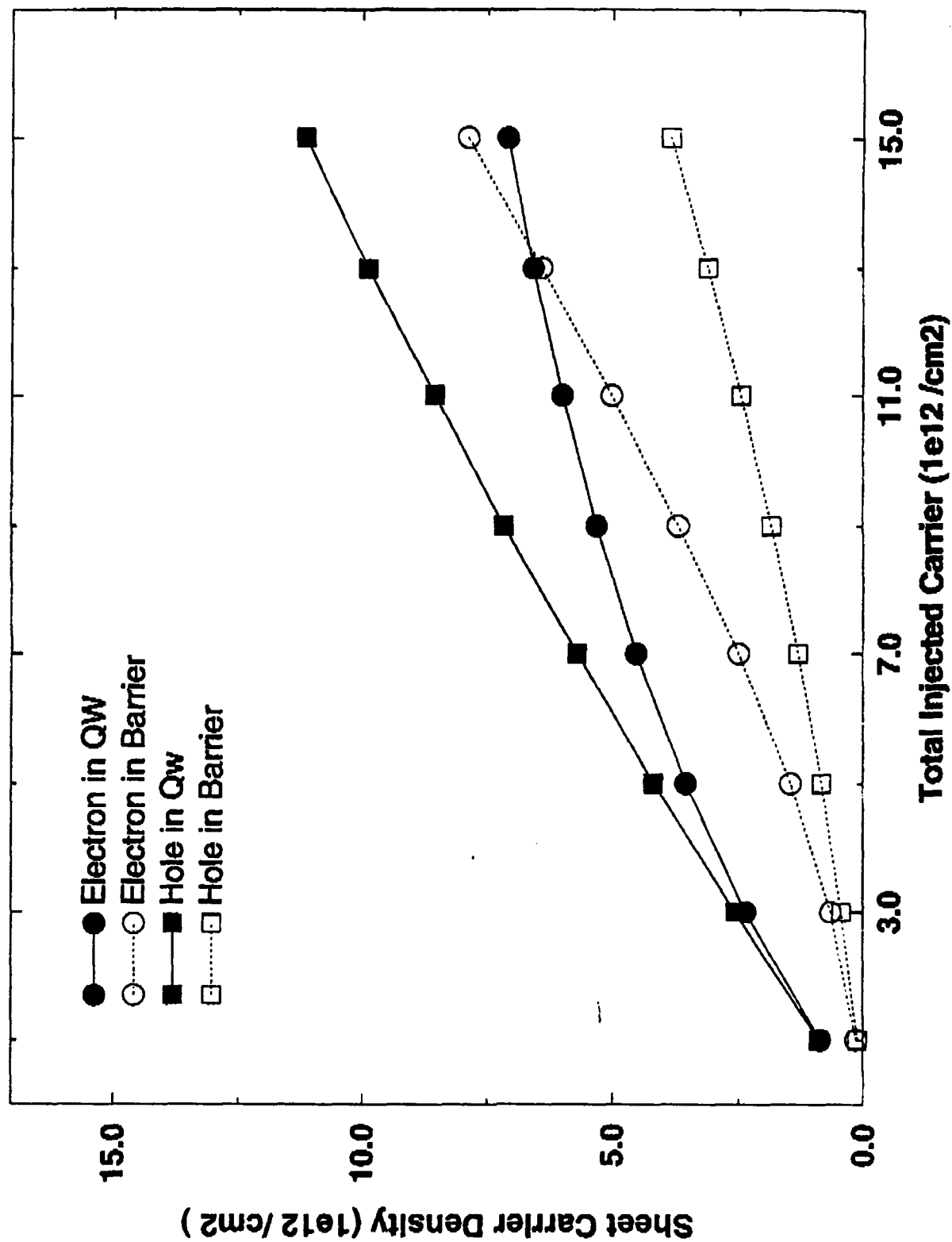


Figure IX.12

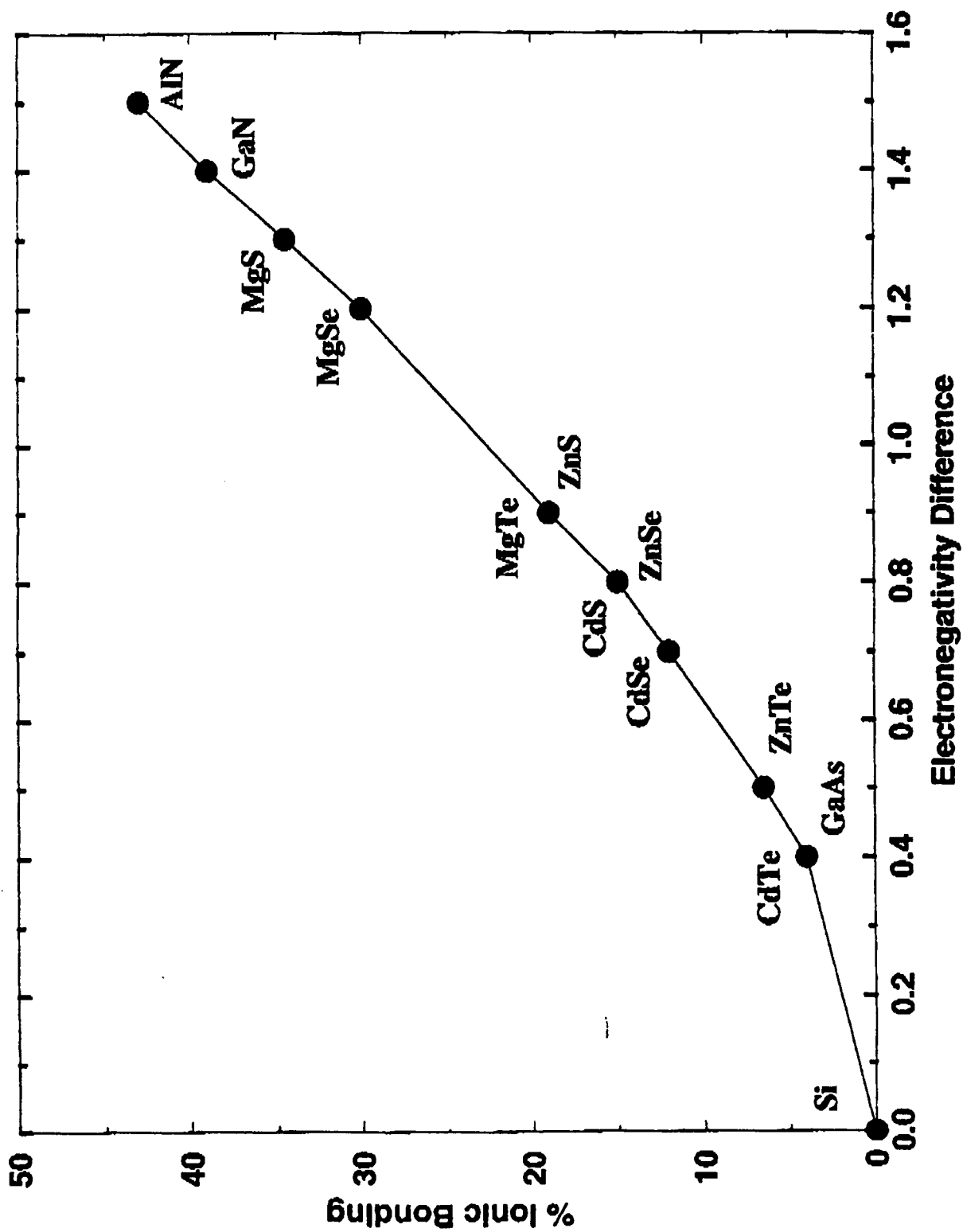


Figure IX.13

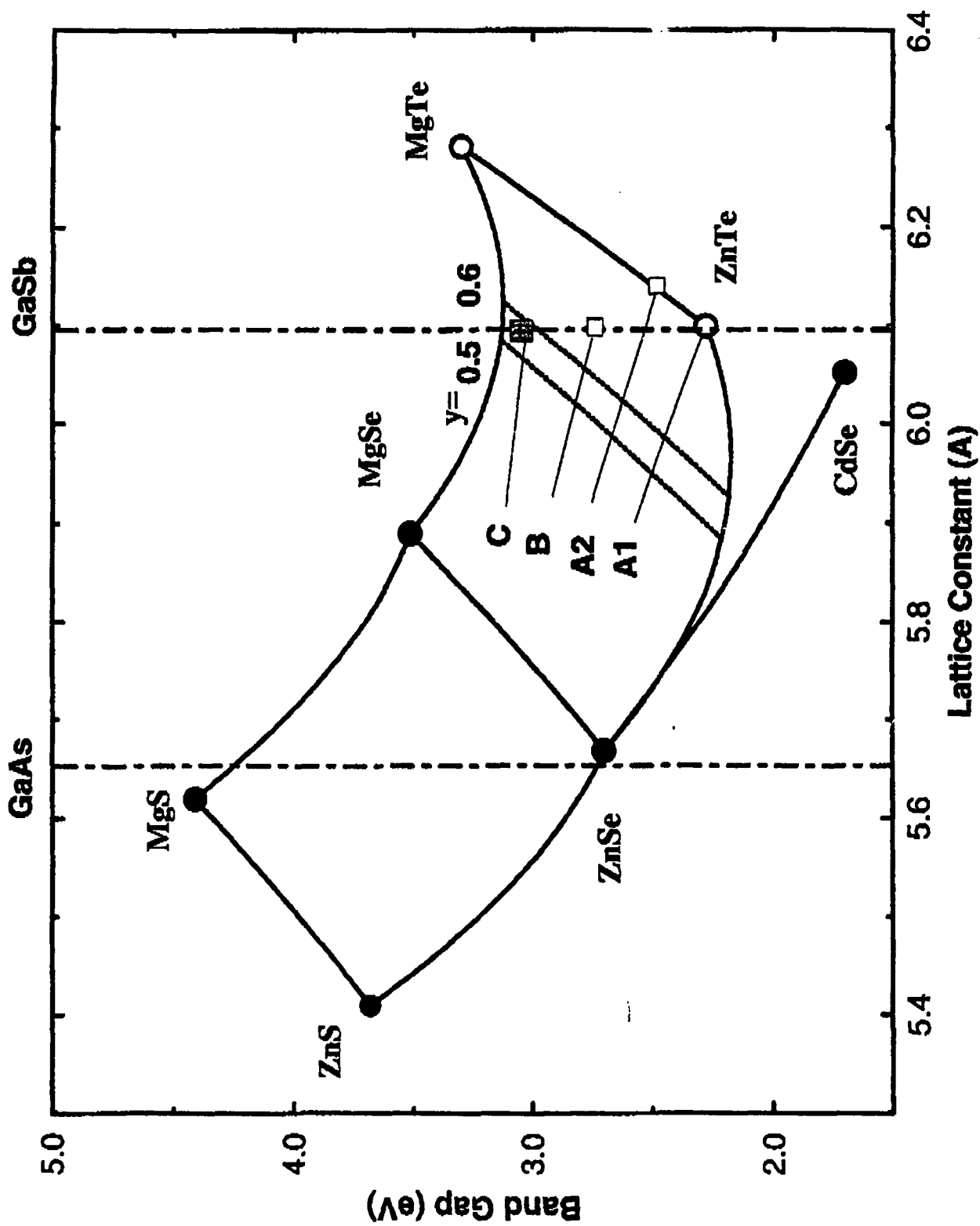


Figure IX.14

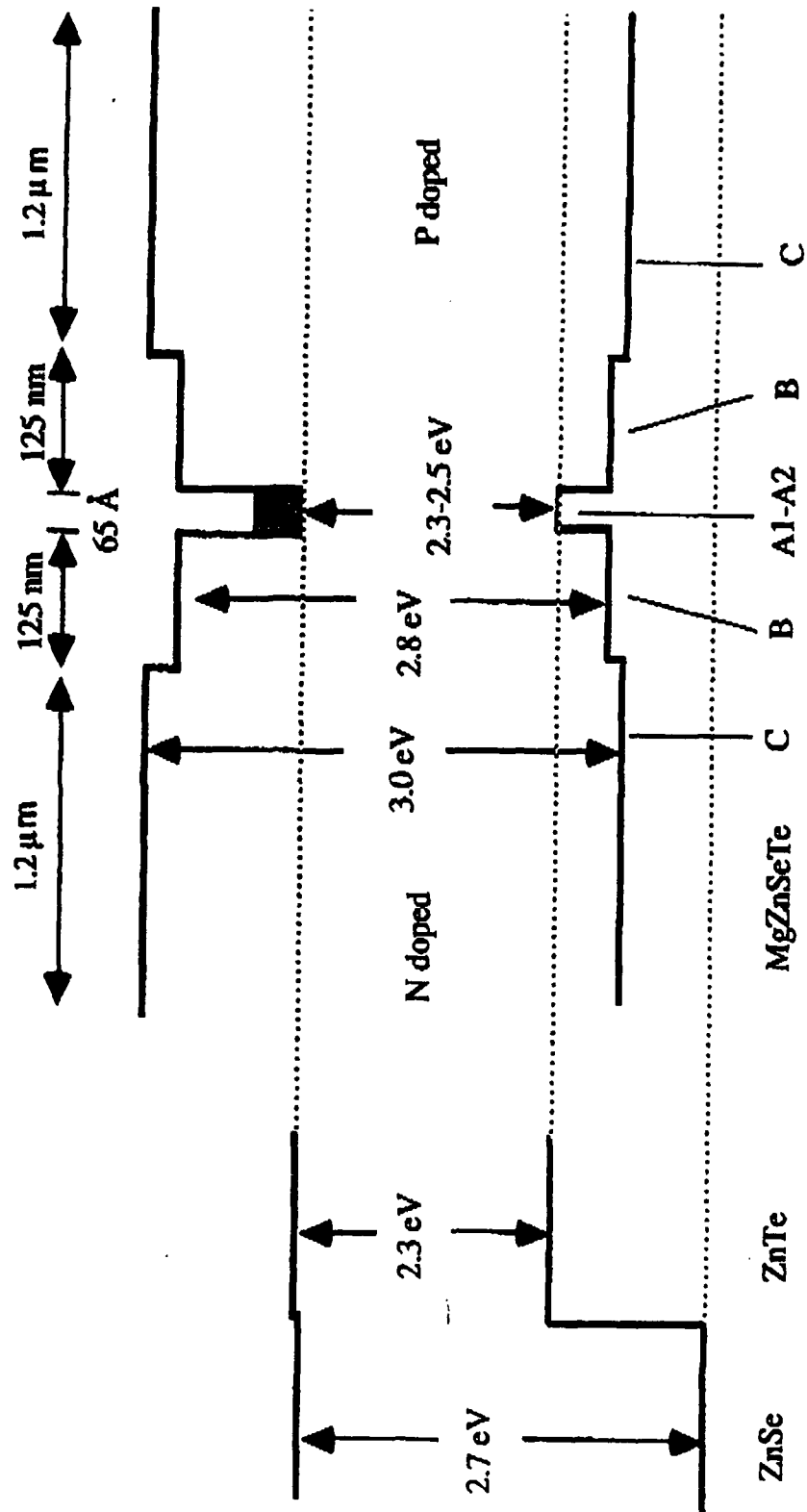


Figure IX.15

ZnSe based SCH QW Laser with ZnCaS Cladding
 (Lattice matched with GaAs except QW)

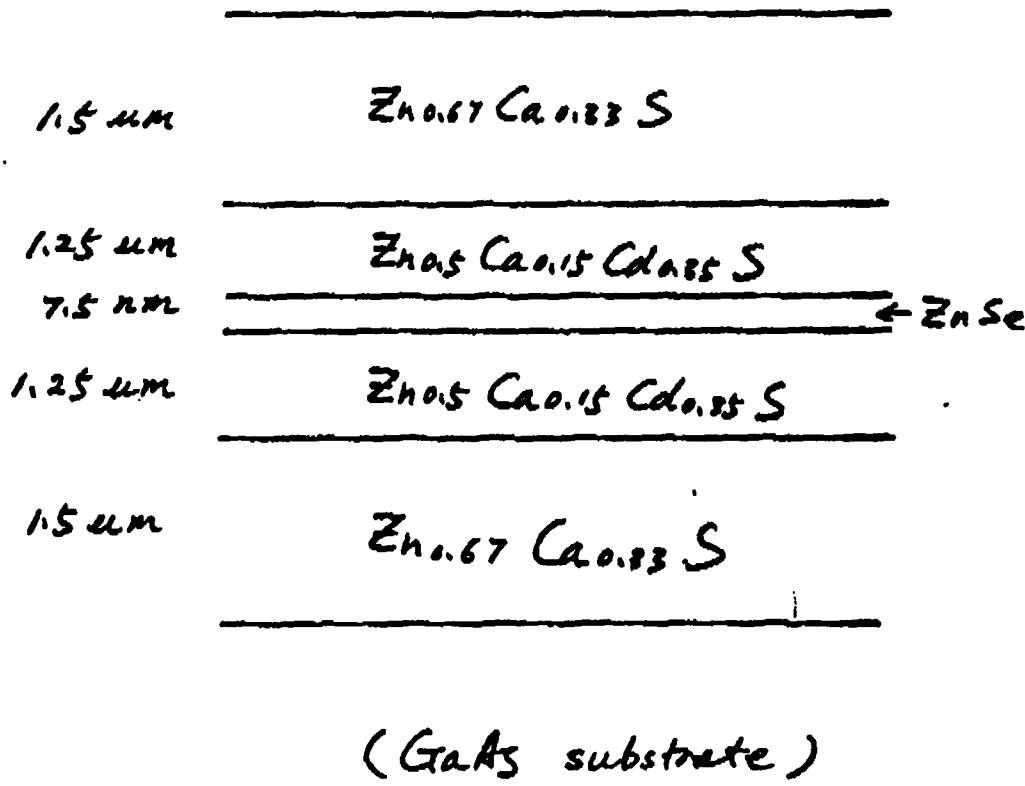
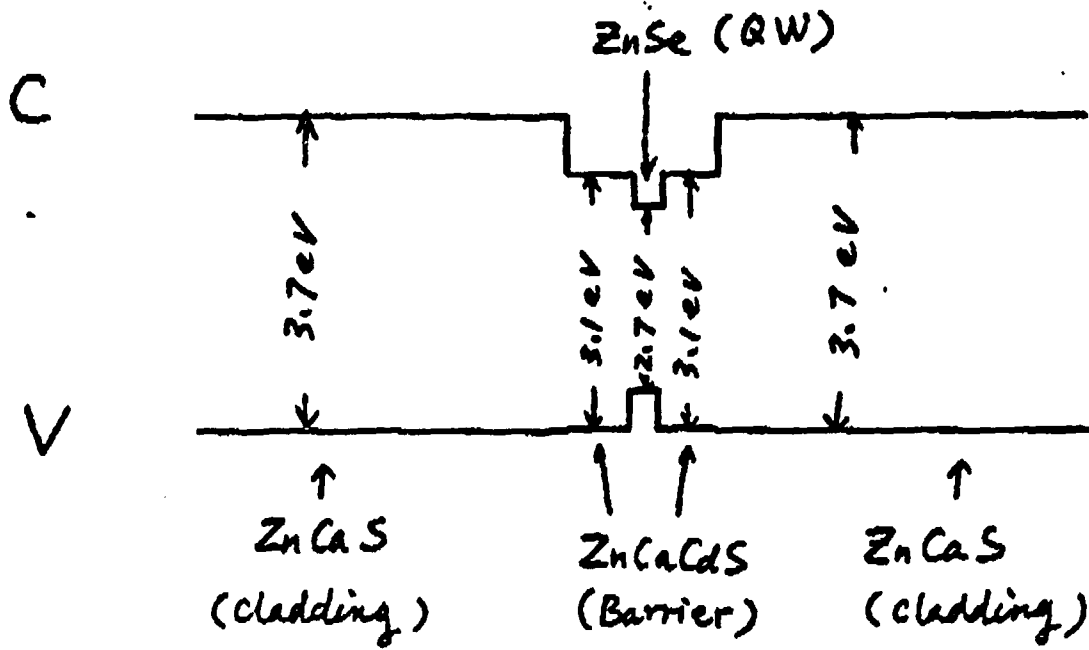


Figure IX.16

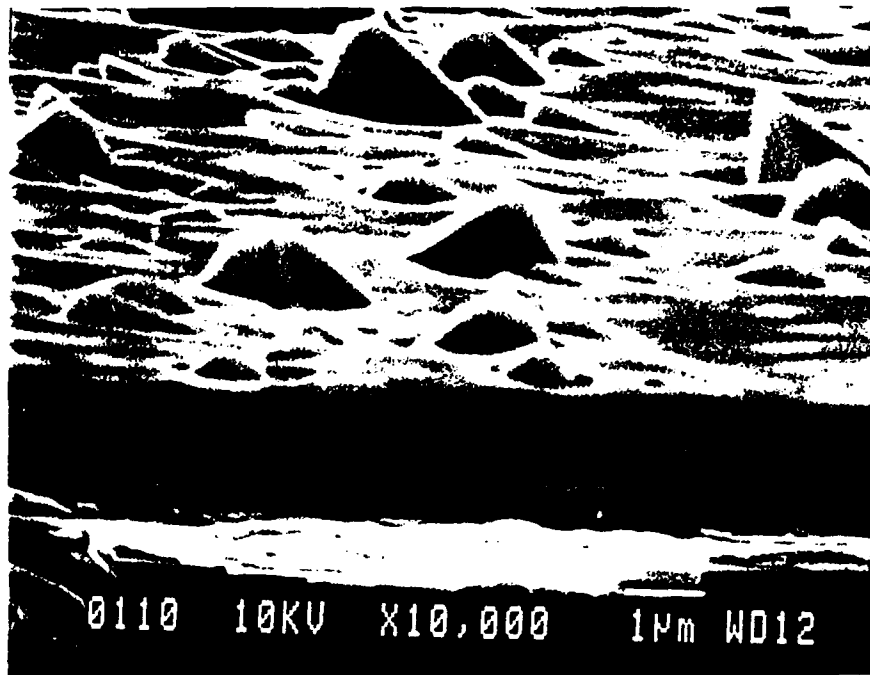


Figure X.1 SEM topograph of cleaved GaN on (1102) sapphire.

PROCESSED DATA

18 Jun 93 Cs

FILE: 30618P01

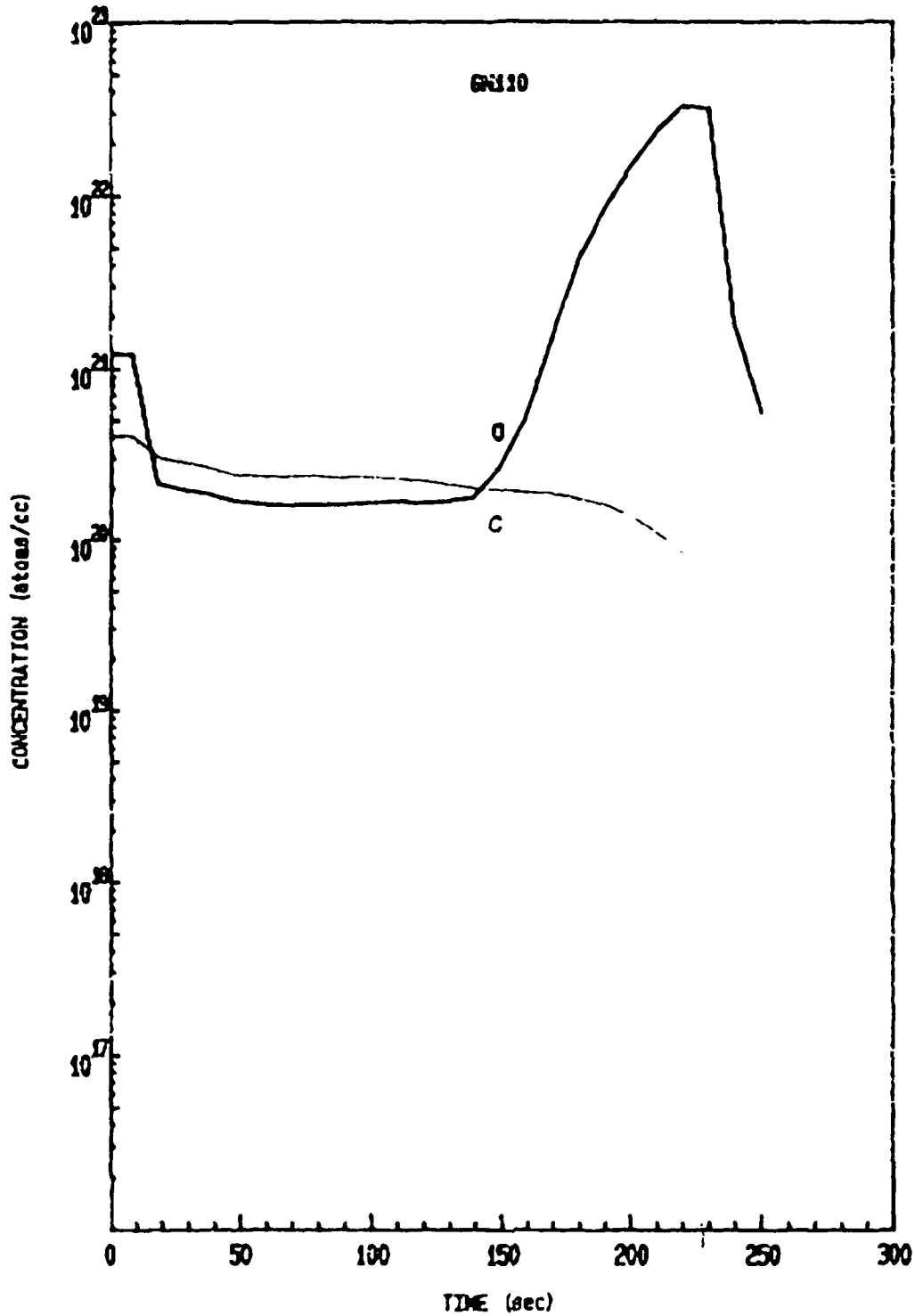


Figure X.2 SIMS profile of oxygen and carbon in a recent sample of GaN on sapphire.

PROCESSED DATA

EVANS EAST

13 Jan 93

FILE: 9303312

UColo/Pankova GaN48

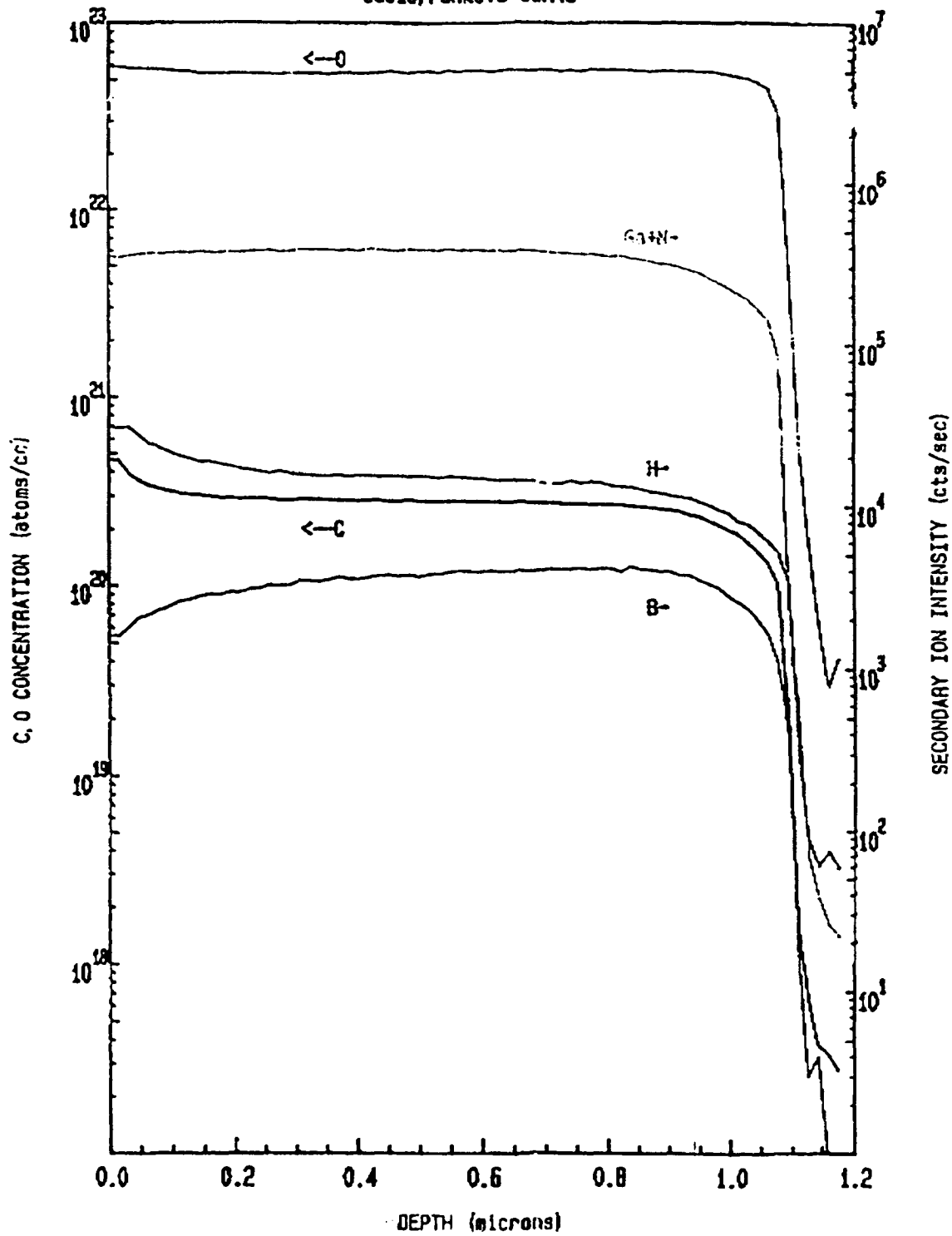


Figure x.3 SIMS profiles of oxygen and carbon (left scales) in an earlier sample of GaN on sapphire.

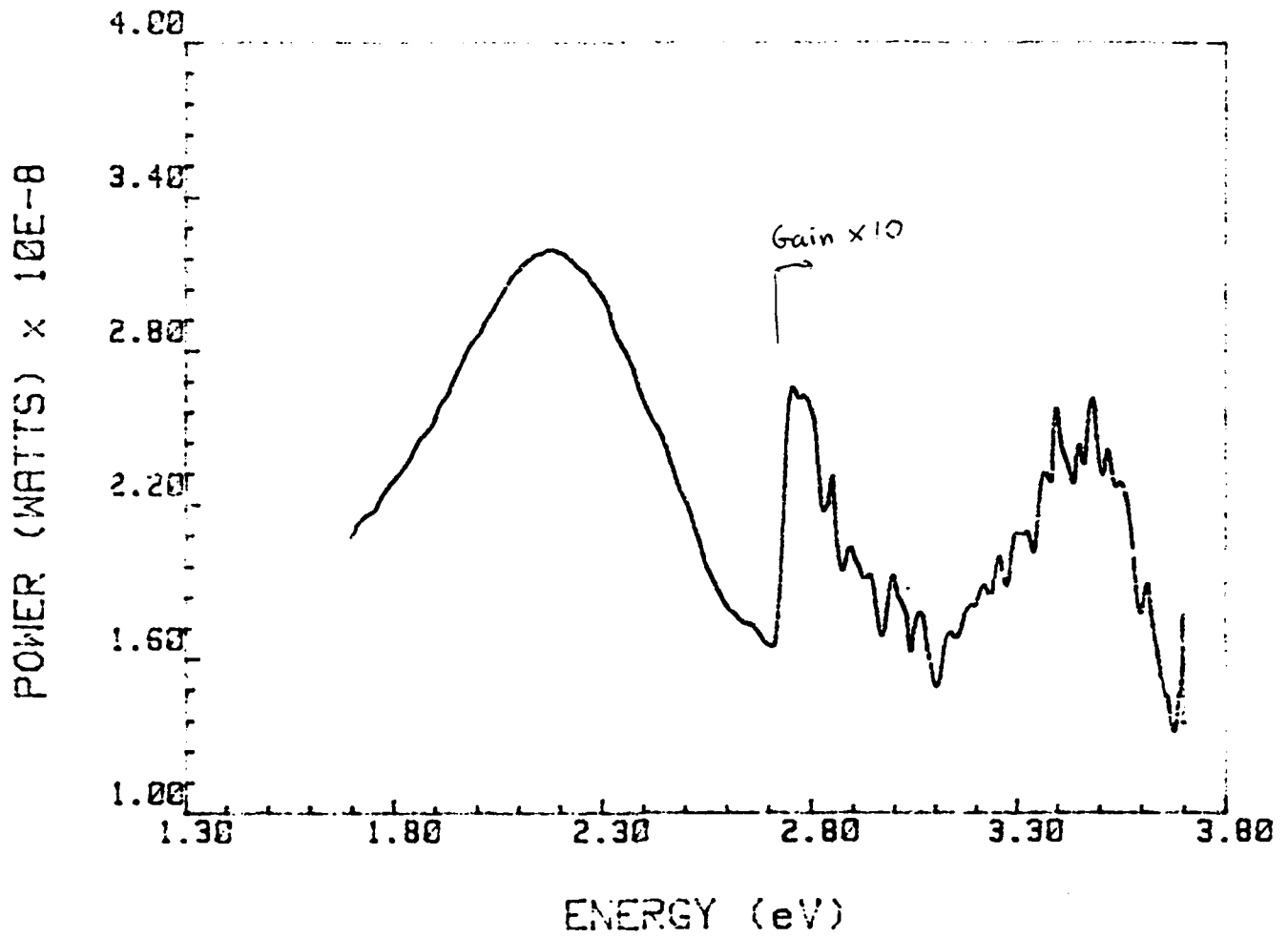


Figure X.4 Cathodoluminescence spectrum from recent sample of GaN on sapphire taken at 269 K.

gn73.w 3/18/93 S= .10 T= 2.0 GaN-#73

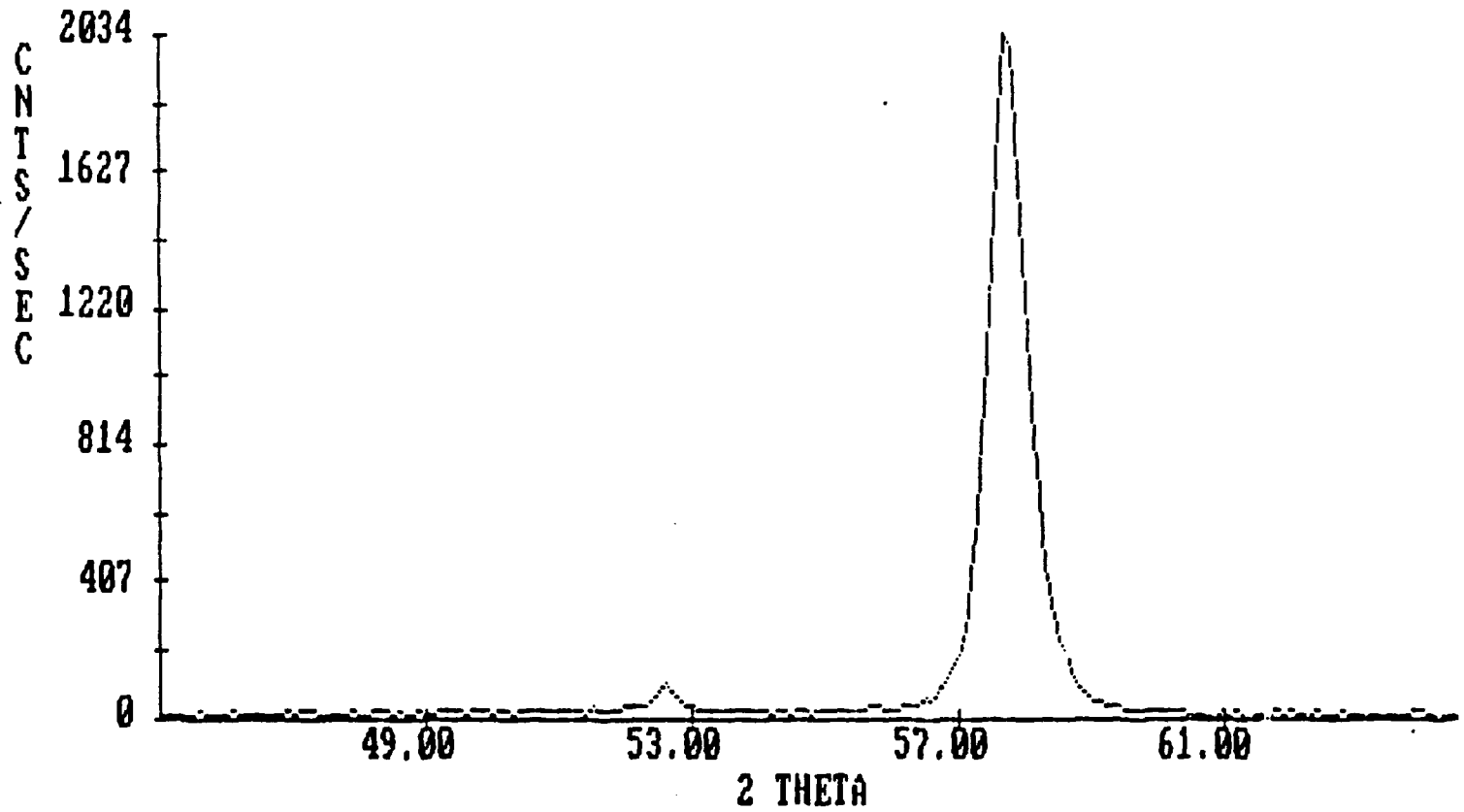


Figure x.5 $\theta/2\theta$ x-ray diffraction spectrum of GaN.